

Work Extraction from Pure Qubits in Ion Traps

Master Thesis by Bettina Meyer
meyerbe@student.ethz.ch
Department of Physics, ETH Zurich

March 2013

Supervised by:

Lídia del Rio, Prof. Renato Renner
Quantum Information Theory (QIT) Group
Institute for Theoretical Physics, ETH Zurich

In Collaboration with:

Prof. Dr. Jonathan Home, Dr. Ben Keitch
Group for trapped Ion Quantum Information, ETH Zurich

March 15, 2013

Abstract

This master thesis is embedded in a larger project, which aims to realise the extraction of work, using as only resources the thermal energy of the environment and a pure qubit as an entropy sink. The existence of such processes is stated by the Landauer Principle and mathematically described by a ‘work-extraction gate’.

In this thesis an experimental implementation of a specific work-extraction gate [26] in trapped ions is proposed. A successful implementation would serve as proof of principle of work extraction in trapped ions. The long-term goal of the project is, to develop efficient ‘information batteries’, combining a work-extraction protocol with reliable storage of information.

In Part I, the thesis contains a review about ion traps and the corresponding physical theory of two-level systems in quantum optics. In Part II, a specific work-extraction gate [26] is discussed and a proposal for its implementation, containing only six physical operations, is developed. There are still some open questions concerning the encoding of the systems, which are elaborated at the end of the thesis.

Acknowledgement

First of all I would like to thank Lídia del Rio, as a very dedicated supervisor, for all the explanations and discussions about the project. I want to thank Prof. Renato Renner for his inputs and critical considerations, which helped me to get a better understanding of the fundamentals of the project.

Special thanks also to Prof. Jonathan Home and Dr. Ben Keitch, who supported us with explanations and inputs about the experimental system. Their openness to our new and unconventional ideas allowed a very fruitful collaboration.

Contents

I Quantum Computation in Ion Traps	8
1 Quantum Optics for Two-Level Systems	9
1.1 Basic Hamiltonians for the two-level system	9
1.1.1 The ion	10
1.1.2 Many ions	11
1.1.3 Electromagnetic field (laser)	11
1.1.4 Interaction Hamiltonian	12
1.2 Driving transitions	14
1.2.1 Transitions	14
1.2.2 Rabi Oscillations	15
1.2.3 Direct transitions vs. two-photon transitions	15
1.3 Selectivity of induced transitions	17
2 Gates	19
2.1 Logical Gates	20
2.1.1 Single-Qubit Gates	20
2.1.2 Two-qubit gates	21
2.2 Elementary physical gates	23
2.2.1 Single-ion gates	23
2.2.2 Two-ion gates	24
2.3 Decomposition of unitaries into elementary <i>physical</i> gates	27
2.3.1 Decomposition of the CNOT gate	29
2.3.2 Decomposition of the CPhase gate	30
2.3.3 Universal decomposition of a two-qubit gate in an entangling <i>geometric phase</i> gate G and single-qubit rotations	31
2.3.4 Decomposition of arbitrary unitaries $U \in \mathrm{U}(n)$	32
3 Experimental Setup	33
3.1 The ion trap	33
3.2 Atomic Structure of the Ions	34
3.3 Qubit encoding	37
3.3.1 Degenerate qubit (Battery qubit)	37
3.3.2 Thermal Qubit	38
3.4 Tunable Quantities	40
II Work Extraction Gate	41
4 Theoretical concept	42
4.1 Work extraction protocols	42

4.2 Experimental implementation of a simplified gate	44
4.3 Decomposition of the work extraction Gate	47
4.3.1 Decomposition into CNOT gates:	47
5 Experimental Realisation	51
5.1 Implementation using the MS-gate	51
5.2 Encoding of the 3 systems	53
5.2.1 Different qubits in two Ca ions	54
5.2.2 Different ions	55
5.3 The MS-gate for two ions of different species	58
6 Outlook	59
6.1 Open questions	59
6.2 Different approaches for the gate implementation	60
6.2.1 Phase gate for degenerate σ_x -eigenstates	60
6.2.2 Controlled raising / lowering of the motional state by state-dependent forces	61
7 Conclusion	63
III Appendix	64
A Notation	65
B Variations of the MS-gate	66
C Additional Information	69
C.1 Geometric Phase gate	69
D Calculations	72
D.1 Derivation of the general qubit rotation matrix	72
D.2 Derivation of the interaction Hamiltonian for two-level systems	73
D.2.1 Rotating-wave approximation (RWA):	73
D.2.2 Interaction Picture:	73

Introduction

The project of this thesis is based on the Landauer principle. This principle states that to erase one bit of information, a minimal amount of $kT \ln 2$ work is needed, which is dissipated in form of heat into the environment. If this process is reversed, as suggested in [27], the same amount of energy ($kT \ln 2$) is transformed from heat into work, using one bit of information. The information loss in this process can be understood as an increase of the thermodynamic entropy of exactly $\Delta S = k \ln 2$.

Since we consider a fully quantum mechanical system, the one bit of information is provided as an initially pure qubit which is transformed into a fully mixed state. This transformation is accompanied by an increase of the von-Neumann entropy of $\Delta H = 1$. This is equivalent to a change of the thermodynamic entropy of $\Delta S = k \ln 2$. The Landauer principle would allow to extract work from pure qubits using the thermal energy from the environment. A scheme for this work extraction procedure was developed and theoretically stated in [27].

An optimal work extraction process transforms heat into $nkT \ln 2$ work by using exactly n pure qubits. The goal of this project is to find an experimental implementation of a non-optimal process, which transforms heat into $W \leq kT \ln 2$ work by using one pure qubit. During the process, this pure qubit is transformed into a mixed state, or, for a maximal gain of work, into a fully mixed state. In information theory language, this means a loss of part of the information originally stored in the qubit. From a thermodynamic point of view, this corresponds to the increase of entropy of the qubit by exactly the same amount as the work gain. For fully mixed final states, all the information is lost, i.e. a maximum increase in entropy $\Delta S = kT \ln 2$ occurs. In turn, the maximum amount of work $W = kT \ln 2$ could be extracted from the system.

This experiment should be a proof of principle, so adjustments in the concept are allowed. The following conditions must be met: the quantum states may be transformed using only *energy conserving operations* or *thermalisation*, by coupling the state to a thermal bath. This ensures that no other resource was used beside the heat energy of the environment and the entropy that is stored in the pure qubit.

The requirement of energy conservation appears to be a challenge in the experimental implementation.

We choose *trapped ions* as the physical system to implement the process. Ion traps revealed to be one of the most successful approaches to store and process quantum information in the last years. The ions are almost perfectly isolated from the environment by being kept in vacuum. This allows long coherence times. Well controlled computational operations have been implemented by laser pulses, manipulating the ion's state.

This thesis is structured as follows: Part I contains an overview about ion trap physics and the

possible manipulation schemes of the ion's degrees of freedom (Chapters 1 and 2). Therewith this part should serve as a toolbox, supporting the decomposition of an arbitrary (theoretical) gate into physically feasible implementations.

In Chapter 3, the experimental setup, which is used in the ion trap laboratory of J. Home at ETH Zurich, is presented. The inner structure of the ions used (Beryllium and Calcium) is explored and, based on this, the possible qubit encoding schemes and transitions between energy levels are discussed.

Part II deals with our specific work extraction gate and the corresponding three-part system. The gate is introduced and decomposed into physical gates. The theoretical constraints on the system need to be discussed in order to adapt them to the physical system, with reference to part I. Finally, a proposal for the gate implementation using the MS-gate is described. There are still some open questions about the experimental feasibility of some operations, used for the implementation. But the proposal seems to be very promising, since it allows to decompose the work extraction gate into only six physical gates.

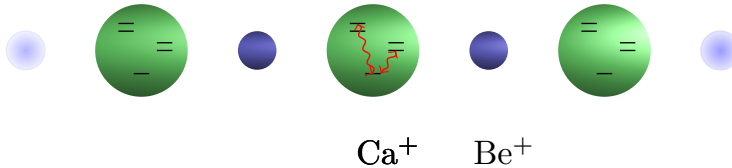
Part I

Quantum Computation in Ion Traps

Chapter 1

Quantum Optics for Two-Level Systems

In our experimental setup, ions will be aligned in a string within a *linear ion trap*. The information will be encoded as qubits in the internal or motional degrees of freedom (d.o.f.) of the ions, which are described below. Qubit operations are realised by manipulating the ions' states with electromagnetic (EM) fields, according to the laws of quantum optics. In the following we derive the theoretical description of an ion's physical state with its degrees of freedom and the interaction with an electromagnetic field. This description holds for arbitrary ions with one valence electron, spatially trapped in a potential that is harmonic in one direction. More details about the explicit experimental setup, used for our implementation, is given in Section 3.



1.1 Basic Hamiltonians for the two-level system

The joint system of ions, interacting with an electromagnetic field (laser or radio-frequency (RF) field), can be described in a *semi-classical model*. In such a model, the ion is treated as a quantum-mechanical system, whereas the EM field is assumed to consist of a high enough number of photons to be approximated by a classical field.

Atoms show a rich internal structure with many energy levels for the valence electron (we consider only ions with one valence electron). In Section 3, we will look at the internal energy structure of the ions used in more detail. To encode a *qubit* we choose two energy levels and treat the ion as a *two-level system*, while neglecting the other levels. This approximation is justified by the fact that *near-resonant interactions*, i.e. transitions that are induced by a laser tuned close to the energy difference of the two levels, are more likely to occur than nonresonant transitions ([4], Chapter 5.2).

1.1.1 The ion

(a) **Internal degrees of freedom (two-level system):**

We consider alkali-like ions with only one electron in the valence shell. The internal d.o.f. are given by two energy levels of the electron with energy difference $\hbar\omega_0$. The Hamiltonian is given by

$$H_{\text{internal}} = \hbar\omega_0 \hat{\sigma}^\dagger \hat{\sigma} = \hbar\omega_0 |e\rangle \langle e|$$

with the ground state $|g\rangle$, the excited state $|e\rangle$ and the lowering and raising operators $\hat{\sigma} = \hat{\sigma}_- = |g\rangle \langle e|$ and $\hat{\sigma}^\dagger = \hat{\sigma}_+ = |e\rangle \langle g|$.

(b) **Motional degrees of freedom (harmonic oscillator):**

The ions are trapped in a (quasi) perfect harmonic EM potential along the trap axis (z -direction). Therefore the motion in z -direction can be described by a harmonic oscillator. In the transverse xy -plane the ions are trapped by an RF potential. This leads to a circular motion (secular motion) of the ions around the trap axis. This way one distinguishes only between the axial and the transverse (or radial) motion.

Axial motion:

The trap potential can be chosen such that the oscillations transverse to the trap axis can be neglected. In the following, when considering single ion-motion and if not specified explicitly, the term ‘motional mode’ will be used for oscillations along the trap axis (z -direction). The creation and annihilation operators of this axial motional mode are denoted by \hat{a}^\dagger and \hat{a} with the corresponding frequency ω_z . This approach leads to the following motional Hamiltonian:

$$H_{\text{motional}} = \hbar\omega_z (\hat{a}^\dagger \hat{a} + 1/2).$$

The oscillation frequencies can be changed by tuning the trap frequency ω_z within a range of $\sim 100\text{kHz}$ up to $1 - 3\text{MHz}$. This allows us to adapt the separation of motional states (i.e. the energy of one phonon) to a required value within some regime.

Transverse/radial motional d.o.f.:

In general, the energy spectrum of the radial motion cannot be described by a simple harmonic oscillator. Only in a regime of small motions, the RF potential can be approximated by a h.o. If one wants to consider the motion in x - and y -direction separately, one has to lift the degeneracy of the directions. This can be achieved by adjusting the RF potential such that the ions move on an elliptic path.

There have been attempts to encode information in these d.o.f., but the control of it is more advanced. In our experiment we will use these d.o.f. only for the mediation of gates but not to encode information (c.f. Section 5.2).

The total state space and Hamiltonian of the ion are given by the tensor product of the different d.o.f. When neglecting the transverse motional modes, the last term in the sum below can be omitted.

$$\mathcal{H}_A = \mathcal{H}_{\text{internal}} \otimes \mathcal{H}_{\text{motional}} \simeq \mathbb{C}^2 \otimes \mathcal{H}_{\text{h.o.}}^z \otimes \mathcal{H}^{xy} \quad (1.1)$$

$$H_A = (\hbar\omega_0 \hat{\sigma}^\dagger \hat{\sigma} \otimes \mathbb{I}_{\text{motional}}) + (\mathbb{I}_{\text{internal}} \otimes \hbar\omega_z (\hat{a}^\dagger \hat{a} + 1/2) \otimes \mathbb{I}_{xy}) \quad (1.2)$$

$$+ (\mathbb{I}_{\text{internal}} \otimes \mathbb{I}_z \otimes H_{xy}) \quad (1.3)$$

1.1.2 Many ions

In ion trap experiments several ions are trapped in a linear chain. If the ions are close enough to each other, they are coupled by Coulomb interaction. The ions can be coupled and decoupled by changing their relative distance. When decoupled from the others, an ion moves like a single harmonic oscillator. When coupled, the ions move according to the collective motion of the whole string, which is described by the *normal modes*.

For a chain of identical ions, the overall potential of the ions can be expressed as a coupled harmonic oscillator ([3], Chap. 17.4)

$$H = \sum_{k=1}^N \frac{\hat{p}_k^2}{2M} + \frac{M\omega_z^2}{2} \sum_{k,l=1}^N A_{kl} \hat{q}_k \hat{q}_l$$

with the single ion-oscillation frequency ω_z and displacement q_k . M is the mass of a single ion and the coefficients A_{kl} represent the coupling of the ions (for explicit expressions of the coefficients c.f. [3]).

This Hamiltonian is diagonalised by the so-called *normal mode* coordinates Q_p , which describe the collective motion of the ions and are the eigenstates corresponding to energy eigenvalues μ_p . Each of the normal modes oscillates at a different frequency $\omega_p = \omega_z \sqrt{\mu_p}$ and represents a harmonic oscillator with ground state and excited states. For ions of identical mass, the first and second modes are the *center-of-mass* (COM) mode and the ‘breathing’ or ‘stretching’ mode. For $N = 3$ their frequencies are given by: $\omega_{\text{COM}} = \omega_z$ and $\omega_{\text{breathing}} = \sqrt{3}\omega_z$. When the masses are different (as in our setup with the alternating Ca and Be ions), the two modes (COM and breathing mode) appear in an asymmetric way [11]. As an example, the frequencies of a two-ion crystal with one Be^+ and one Mg^+ ion in the experimental setup of [11] are given by: $\omega_{\text{COM}} \approx 2.05\text{MHz}$, $\omega_{\text{breathing}} \approx 4.3\text{MHz}$.

Usually the ion string is cooled down to the motional state of lowest energy, which corresponds to the ground state of the COM mode. Controlled manipulations of the ions’ motion can then be performed by applying a laser with frequency resonant to a specific normal mode (normally the COM mode). Therewith collective motion can be used to perform multi-qubit quantum gates.

1.1.3 Electromagnetic field (laser)

We consider a classical electromagnetic field with frequency ω_L , phase ϕ_L and wavevector \vec{k} at the position \vec{r}_i of the interacting ion

$$\vec{E}(t, \vec{r}_i) = \hat{\epsilon} \frac{E_0}{2} \left(e^{-i(\omega_L t - \vec{k} \cdot \vec{r}_i - \phi_L)} + e^{i(\omega_L t - \vec{k} \cdot \vec{r}_i - \phi_L)} \right) = \vec{E}^{(+)}(t, \vec{r}_i) + \vec{E}^{(-)}(t, \vec{r}_i). \quad (1.4)$$

The EM field is taken as a constant value over the whole extent of the ion. This corresponds to the *long-wavelength approximation*, which is justified as following: The energy transitions in an ion, $\Delta E = \hbar\omega_0$, are in the optical range (or even lower frequency, like RF or microwave frequencies). We consider only near-resonance ion-laser interactions. These are induced by lasers of wavelength $\lambda = 2\pi/\omega_L \approx 2\pi/\omega_{\text{atom}} \approx 500\text{nm}$ (or even larger for RF/microwave range). Comparing this wavelength to the size of an ion (ca. 1\AA), the variation of the field over the extent of the ion is negligible.

1.1.4 Interaction Hamiltonian

To model the interaction between the atom and the EM field, the *dipole-interaction Hamiltonian* reveals to be a good approach in the *long-wavelength approximation* (also when considering a fully quantum mechanical model ([2], p. 434)),

$$H_{\text{AF}} = -\vec{d} \cdot \vec{E}, \quad \vec{d} = -e\vec{r}_e \quad (\text{atomic dipole}). \quad (1.5)$$

The vector \vec{r}_e denotes the relative distance of the valence-electron to the atomic nucleus. The dipole operator \vec{d} shows zero diagonal elements due to parity arguments:

$$\vec{d} = \langle g | \vec{d} | e \rangle (|e\rangle \langle g| + |g\rangle \langle e|) = \underbrace{\langle g | \vec{d} | e \rangle}_{deg=dge} (\hat{\sigma}^\dagger + \hat{\sigma}). \quad (1.6)$$

Rotating-wave approximation (RWA): The rotating-wave approximation (RWA) discards terms that are oscillating at high frequency (compared to the dominating terms) and replaces them by their zero time-average value [2] [5]. A heuristic derivation of the RWA is more intuitive in a fully quantum mechanical model, where the EM field is represented by an operator $\vec{E} = \vec{E}^{(+)} + \vec{E}^{(-)}$. The positive-rotating (or negative-rotating) field component is proportional to the annihilation (or creation) operator \hat{c} (\hat{c}^\dagger) of a photon mode: $\vec{E}^{(+)} \sim \hat{c}$, $\vec{E}^{(-)} \sim \hat{c}^\dagger$ [4]. The RWA takes into account only the terms that respect energy conservation: $\sim \hat{\sigma}_- \hat{c}^\dagger$ ($\sim \hat{\sigma}_+ \hat{c}$). These terms correspond to the lowering (raising) of the internal ion energy state accompanied by the creation (annihilation) of a photon.

The RWA discards some of the terms that arise in the multiplication of the dipole operator (1.6) with the EM field (1.4). This simplifies the interaction Hamiltonian to:

$$H_{\text{AF}} \approx -d_{eg} \left(|e\rangle \langle g| \cdot \vec{E}^{(+)} + |g\rangle \langle e| \cdot \vec{E}^{(-)} \right) = -d_{eg} \left(\hat{\sigma}^\dagger e^{-i(\omega_L t - \vec{k} \cdot \vec{r}_e - \phi_L)} + \text{h.c.} \right). \quad (1.7)$$

Lamb-Dicke parameter: In order to separate the internal and motional part of the interaction Hamiltonian, it is useful to consider the series expansion of the exponential factor. The motional d.o.f. are hidden in the position operator. In the direction of the trap axis (z -axis) the operator is given by: $r_z = \hat{z} = z_0 (\hat{a}_z + \hat{a}_z^\dagger)$, with $z_0 = \sqrt{\frac{\hbar}{2m\omega_z}}$ the equilibrium mode.

The *Lamb-Dicke parameter* is defined as $\eta := k z_0 \cos \theta$, where θ denotes the relative angle between the trap axis and the beam direction \hat{k} . Hence, $k \cos \theta$ stands for the projection of \vec{k} onto the z -axis. In the so-called *Lamb-Dicke regime*, where $\eta \ll 1$, the exponential factor of Equation 1.7 can be expanded in η as: $e^{\pm i(\omega_L t - \vec{k} \cdot \vec{r})} \approx e^{\pm i\omega_L t} (\mathbb{I} \mp i\eta(\hat{a} + \hat{a}^\dagger) + \mathcal{O}(\eta^2))$. One can interpret η as a coupling constant between the internal and motional d.o.f. If the coupling is too strong, the internal and motional d.o.f. can not be separated and the expansion is invalid.

For $\eta \ll 1$, H_{AF} (Equation 1.7) can be expanded as

$$\begin{aligned} H_{\text{AF}} &= \frac{\hbar\Omega}{2} \left(\hat{\sigma}^\dagger e^{-i(\omega_L t - \vec{k} \cdot \vec{r})} e^{i\phi_L} + \hat{\sigma} e^{i(\omega_L t - \vec{k} \cdot \vec{r})} e^{-i\phi_L} \right) \\ &\approx \frac{\hbar\Omega}{2} \left(\hat{\sigma}^\dagger e^{-i(\omega_L t - \phi_L)} + \hat{\sigma} e^{i(\omega_L t - \phi_L)} \right) \otimes \mathbb{I}_{\text{motional}} \\ &\quad + \frac{\hbar\Omega}{2} \left(\hat{\sigma}^\dagger \otimes i\eta e^{-i(\omega_L t - \phi_L)} (\hat{a}^\dagger + \hat{a}) + \text{h.c.} \right) + \mathcal{O}(\eta^2), \end{aligned} \quad (1.8)$$

1.1. BASIC HAMILTONIANS FOR THE TWO-LEVEL SYSTEM

where we defined the following parameters

$$\Omega := \frac{E_0}{\hbar} \langle g | \hat{\epsilon} \cdot \vec{d} | e \rangle \quad (\text{Rabi frequency}) \quad (1.9)$$

$$\eta := \eta_0 \cos \theta = kz_0 \cos \theta, \quad (\text{Lamb-Dicke parameter}) \quad (1.10)$$

$$z_0 = \sqrt{\frac{\hbar}{2m\omega_z}} \quad (\text{equilibrium position}). \quad (1.11)$$

By definition, the Lamb-Dicke parameter is a function of the ion mass m , the trap frequency ω_z , the beam geometry, i.e. the beam direction defined by θ , and the wavelength $|k| = \frac{2\pi}{\lambda}$. The condition for the Lamb-Dicke regime is fulfilled in most ion trap experiments, where the ion is confined to a spatial region that is much smaller than the wavelength of the exciting laser: $\eta_0 = kz_0 = 2\pi \frac{z_0}{\lambda} \ll 1$, for $z_0 \ll \lambda$. [3]

The Lamb-Dicke parameter η can also be interpreted in terms of the relative *recoil energy* E_{rec} of the ion per photon absorption or scattering ([5], Chap. 8):

$$\eta_0 = kz_0 = \sqrt{\frac{\hbar k^2}{2m\omega_z}} = \sqrt{\frac{E_{\text{rec}}}{\hbar\omega_z}}, \quad \text{with: } E_{\text{rec}} = \frac{(\hbar k)^2}{2m}. \quad (1.12)$$

The excitation of the ion's motional state, when the ion is addressed by an EM field, is often referred to as *heating* of the ion. The recoil energy depends on the ion's mass and the wave vector of the EM field ($E_{\text{rec}} \sim k^2/m$). As a consequence of the mass dependence, the motional state of a light ion is much more sensitive to photon absorption and emission. The wave vector is proportional to the momentum that is transferred from the absorbed ($p = +\hbar k$) or emitted ($p = -\hbar k$) photon to the atom. Hence the heating effect is more relevant for high-frequency EM fields, which means that lasers have a stronger effect than RF or microwave fields.

Transformation into the interaction picture: In order to achieve a convenient form of the interaction Hamiltonian, we change into the interaction picture w.r.t. the free atom Hamiltonian (1.3):

$$\begin{aligned} \tilde{H}_{\text{AF}} &= e^{iH_{\text{A}}t/\hbar} H_{\text{AF}} e^{-iH_{\text{A}}t/\hbar} \\ &= e^{i\omega_0 t |e\rangle\langle e|} e^{i\omega_z t (\hat{a}_z^\dagger \hat{a}_z + 1/2)} H_{\text{AF}} e^{-i\omega_0 t |e\rangle\langle e|} e^{-i\omega_z t (\hat{a}_z^\dagger \hat{a}_z + 1/2)} \\ &= \frac{\hbar\Omega}{2} \left(\hat{\sigma}^\dagger e^{-i((\omega_L - \omega_0)t - \phi_L)} e^{i\eta(\hat{a}_z^\dagger e^{i\omega_z t} + \hat{a}_z e^{-i\omega_z t})} + \text{h.c.} \right). \end{aligned}$$

This corresponds to a transformation into a reference frame, rotating at the atomic frequency ω_0 . To second order in η the above interaction Hamiltonian is given by (c.f. Appendix D.2 for detailed computations)

$$\begin{aligned} \tilde{H}_{\text{AF}} &\approx \frac{\hbar\Omega}{2} \left(\hat{\sigma}^\dagger e^{i(\omega_0 - \omega_L)t} e^{i\phi_L} + \hat{\sigma} e^{-i(\omega_0 - \omega_L)t} e^{-i\phi_L} \right) \otimes \mathbb{I}_{\text{motional}} \\ &+ \frac{\hbar\Omega}{2} [\hat{\sigma}^\dagger e^{i(\omega_0 - \omega_L)t} e^{i\phi_L} - \hat{\sigma} e^{-i(\omega_0 - \omega_L)t} e^{-i\phi_L}] \otimes i\eta (\hat{a}_z^\dagger e^{i\omega_z t} + \hat{a}_z e^{-i\omega_z t}) \\ &+ \mathcal{O}(\eta^2). \end{aligned} \quad (1.13)$$

1.2 Driving transitions

The interaction of the ions with the EM field is (with high probability) determined solely by the terms of the expanded interaction Hamiltonian \tilde{H}_{AF} (1.13) that are resonant with the frequency of the interacting field. The non-resonant terms are neglected since they occur with much lower probability. This becomes apparent when applying a second time the rotating-wave approximation (RWA), where time-dependent terms are discarded [9]. By choosing carefully the EM field's frequency, the ion can be manipulated in a well-controlled way (c.f. Section 2 about gates).

1.2.1 Transitions

The resonance condition, described above, leads to different induced transitions. One can distinguish two cases: (a) the field's frequency is exactly tuned to the transition of two internal states ($\omega_L = \omega_0$) or, (b) the field's frequency is detuned from such a transition ($\omega_L = \omega_0 + \Delta$).

(a) Resonance ($\omega_L \approx \omega_0$): **Carrier transition**

In the near-resonance approximation, this frequency picks out the *zeroth order* term of the interaction Hamiltonian (1.13), leading to the corresponding propagator

$$\begin{aligned}\tilde{H}_{\text{AF}}^{(0)} &= \frac{\hbar\Omega}{2}(\hat{\sigma}e^{-i\phi} + \hat{\sigma}^\dagger e^{i\phi}) \otimes \mathbb{I}_{\text{motional}} \\ U(t) &= e^{i\tilde{H}_{\text{AF}}^{(0)}t/\hbar} = e^{i\frac{\Omega t}{2}(\hat{\sigma}^\dagger e^{i\phi} + \hat{\sigma}e^{-i\phi})} \otimes \mathbb{I}_{\text{motional}}.\end{aligned}\quad (1.14)$$

To lowest order, only the internal state is excited and there occurs no coupling of the internal and motional d.o.f. This is called the *carrier transition*.

The population of the internal states undergo **Rabi oscillations** between the excited and the ground state at frequency equal to the Rabi frequency Ω .

(b) Non-zero detuning ($\omega_L \neq \omega_0$)

(i) *zeroth order term*:

For a nonzero detuning $\Delta = \omega_0 - \omega_L$ the Rabi flopping of the internal state occur at the *generalized Rabi frequency* $\tilde{\Omega} := \sqrt{\Omega^2 + \Delta^2}$.

In the near-resonance approximation these oscillations can be neglected.

(ii) *first order terms*: ($\omega_L = \omega_0 \pm s\omega_m$, $s \in \mathbb{N}$)

Red/Blue Sidebands (RSB/BSB): Field frequencies of $\omega_L = \omega_0 \pm s\omega_m$, $s \in \mathbb{N}$ excite the so-called *sidebands*, where ω_m denotes the frequency of the addressed motional mode. The resonant terms in the interaction Hamiltonian couple the internal and motional d.o.f. For single or uncoupled ions normally the axial motion is excited ($\omega_m = \omega_z$), whereas for a string of coupled ions a common motional mode ($\omega_m \in \{\omega_{\text{COM}}, \omega_{\text{stretch}}\}$) is addressed.

The first sidebands are given for $s = \pm 1$ and lead to oscillations at Rabi frequencies $\Omega_{n,n-1} = \sqrt{n}\eta\Omega$ ($s = -1$) or $\Omega_{n,n+1} = \sqrt{n+1}\eta\Omega$ ($s = +1$). The resonant Hamiltonian terms are:

- red sideband (RSB): $\omega_L = \omega_0 - \omega_m$:

$$\tilde{H}_{\text{AF}}^{(1)} \approx \frac{\hbar\Omega}{2}i\eta(\hat{a}^\dagger \hat{\sigma}e^{-i\phi_L} + \hat{a}\hat{\sigma}^\dagger e^{i\phi_L}) \quad (1.15)$$

- blue sideband (BSB): $\omega_L = \omega_0 + \omega_m$:

$$\tilde{H}_{\text{AF}}^{(1)} \approx \frac{\hbar\Omega}{2} i\eta (\hat{a}\hat{\sigma}e^{-i\phi_L} + \hat{a}^\dagger\hat{\sigma}^\dagger e^{i\phi_L}) \quad (1.16)$$

- (iii) *higher-order terms*: Higher-order terms of the interaction Hamiltonian are neglected within the Lamb-Dicke regime ($\eta \ll 1$).

1.2.2 Rabi Oscillations

When driving a transition of a two-level system, the time-evolution is determined by the propagator $U(t) \sim e^{iH_{\text{AF}}/\hbar t} \sim e^{i\Omega/2 t} = e^{i\theta/2}$. This leads to so-called *Rabi oscillations* of the state's population between the two levels. The frequency at which these oscillations occur, is equal to the Rabi frequency Ω , introduced in Section 1.1. The period of the oscillation is given $T = 2\pi/\Omega$. If the EM field (e.g. a laser) is applied for a finite time, the duration t of the pulse determines the final state. As an example, consider the oscillation between the excited and ground state of an internal two-level system, with its population initially in the ground state $|0\rangle$. For $t = T/4 = \frac{\pi}{2\Omega}$ (**$\pi/2$ -pulse**) the state after the field application corresponds to a superposition of the ground and the excited state: $|0\rangle \rightarrow \frac{1}{\sqrt{2}}(|0\rangle + |1\rangle)$. A pulse of duration $t = T/2 = \pi/\Omega$ (**π -pulse**) promotes the qubit to the excited state: $|0\rangle \rightarrow |1\rangle$. After a period $T = 2\pi/\Omega$ (**2π -pulse**) the state has returned back to its initial state.

$\pi/2$-pulse:	entanglement of the two states	$T = \frac{\pi}{2\Omega} \Rightarrow \theta = \pi/4$
π-pulse:	bit flip	$T = \frac{\pi}{\Omega} \Rightarrow \theta = \pi/2$
2π-pulse:	whole rotation	$T = \frac{2\pi}{\Omega} \Rightarrow \theta = \pi$

1.2.3 Direct transitions vs. two-photon transitions

The transitions, described in Section 1.2.1, can either be induced in *direct two-level transitions* with one resonant EM field or as *two-photon transitions*, where two EM fields drive a transition via an auxiliary intermediate level. The two possibilities are indicated in Figure 1.1.

In a two-photon transition, the two EM fields ω_1, ω_2 , taken individually, would drive the transition of one of the effective energy levels to the intermediate level. The difference of the laser's frequencies is tuned close to the energy gap of the effective two-level system, which should be driven (e.g. $\Delta\omega = \omega_1 - \omega_2 \approx \omega_0$). Therefore, in Section 1.2.1, the resonance condition has to be fulfilled for $\Delta\omega$, i.e. ω_L has to be replaced by $\Delta\omega$. With such a two-photon transition, gates on qubits outside the optical regime can be implemented by lasers instead of RF or microwave fields. Lasers allow a much better spatial selectivity than RF or microwave fields, due to the smaller wavelength.

A two-photon transition is driven via an auxiliary level. Since we want to drive transitions between an effective two-level system, it is important that this auxiliary level is populated only intermediate. Therefore one would have to chose an unstable level, which leads to incoherent scattering. To avoid this, so-called *Raman transitions* are applied, where the intermediate level is only "virtually" populated. This is achieved by detuning the lasers from the intermediate level and choosing two *coherent* laser beams.

For processes like state preparation or state detection, for which coherence is not required, also *incoherent* two-photon pulses, such as *optical pumping*, are applied.

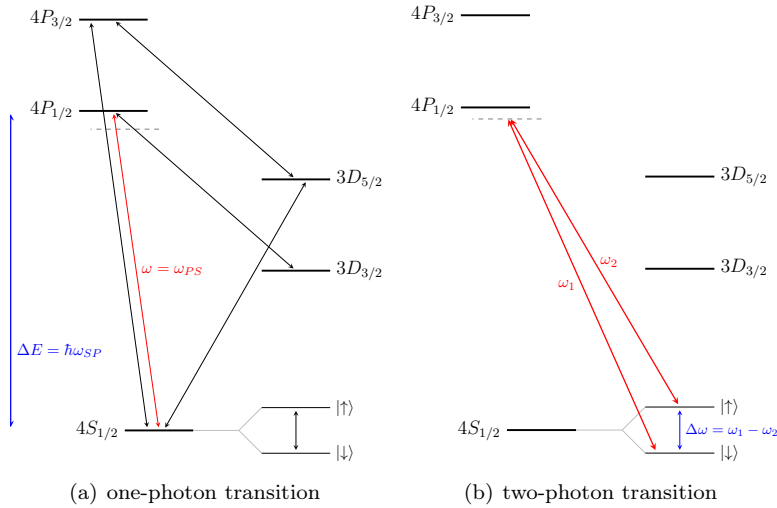


Figure 1.1: Transitions between internal atomic levels (of Calcium) are indicated: (a) *direct two-level transitions*, (b) *two-photon transitions* for the effective two-level system $|\uparrow\rangle, |\downarrow\rangle$

Raman transition:

A Raman transition is a coherent two-photon process that connects two states with narrow energy gap ($\sim 100\text{kHz} - 50\text{MHz}$) via a virtual auxiliary state. By Raman pulses, transitions between levels with a small energy gap (e.g. Hyperfine or Zeeman levels) can be addressed by lasers instead of RF pulses. The two lasers are detuned from the auxiliary level in order to keep the population on this level small. A smaller detuning means higher transition probability, which is desirable. On the other hand a smaller detuning increases the probability of populating the intermediate level. Depending on the chosen frequency difference $\Delta\omega := \omega_1 - \omega_2$ of the two lasers, a Raman transition either drives transitions of a single (internal or motional) qubit or it couples the internal and motional state by affecting both. Excitations with $|s| > 1$ are theoretically possible, but the experimental implementation is difficult due to a very low transition probability.

- (i) **Carrier transition:** $\Delta\omega = \omega_0: |g\rangle \otimes |n\rangle \leftrightarrow |e\rangle \otimes |n\rangle$
- (ii) **Excitation of the motional state:**
 $\Delta\omega = s\omega_m, s \in \mathbb{N}: |\Psi\rangle \otimes |n\rangle \leftrightarrow |\Psi\rangle \otimes |n+s\rangle, |\Psi\rangle \in \{e, g\}$
- (iii) **Sideband excitations:** $\Delta\omega = \omega_0 + s\omega_m, s \in \mathbb{N}: |g\rangle \otimes |n\rangle \leftrightarrow |e\rangle \otimes |n+s\rangle$

Such a two-photon transition via a *virtual* level only works for two coherent laser beams, i.e. they need to be produced by the same source. This is realised by splitting a laser into two beams, of which one is sent through an acousto-optic modifier (AOM) crystal. The AOM shifts the laser frequency by an amount f that is equal to the energy gap of the two connected levels ($f = \omega_0$). Frequency shifts are only feasible in a small range of $\sim 100\text{kHz} - 50\text{MHz}$. This sets a constraint on the frequency difference of a coherent laser pair and therewith on the energy gap of transitions that can be driven by Raman pulses. Typically Zeeman or Hyperfine transitions are addressed by Raman pulses.

Optical pumping:

An optical pumping process is depicted in Figure 1.2(a). Such a process consists of two subsequent steps: The population of a lower-energy level is lifted to an excited state by an induced transition (indicated by the red arrow). The excited state decays *spontaneously* to one or several lower-energy

levels (yellow curly arrows). This decay is visible as fluorescence.

A qubit can be prepared in a specific internal state of an ion by optical pumping. As an example, consider the preparation of Zeeman ground level-state in Calcium, described in Section 1.3 (i) corresponding to Figure 1.2(a).

Another application of optical pumping is state detection. Consider three internal levels: two qubit levels $|g\rangle, |e\rangle$ and an unstable, auxiliary level $|a\rangle$. An EM field, tuned close to the $|g\rangle \leftrightarrow |a\rangle$ transition, is applied to the ion. If the qubit is in the ground state $|g\rangle$, it is excited to the state $|a\rangle$, followed by spontaneous scattering, which can be detected as fluorescent light. No light detection means, that the qubit was in the excited state $|e\rangle$.

1.3 Selectivity of induced transitions

For quantum computation in trapped ions, it is important to be able to selectively drive specific transitions between internal states of a particular ion. Therefore spatial selectivity is required, i.e. we need to ensure that only the intended ion is addressed by the EM field. Additionally, when inducing a specific transition, we need to avoid that other transitions, which have a similar energy separation, are excited. An example of how to achieve this is given in the paragraph about polarised beams below.

Spatial selectivity: The spatial selectivity denotes the accuracy, with which an EM field can address a certain position in space. This is important if we want to manipulate single ions within an string.

A laser shows the better spatial selectivity than RF or microwave fields, due to its shorter wavelength, which allows a better spatial resolution

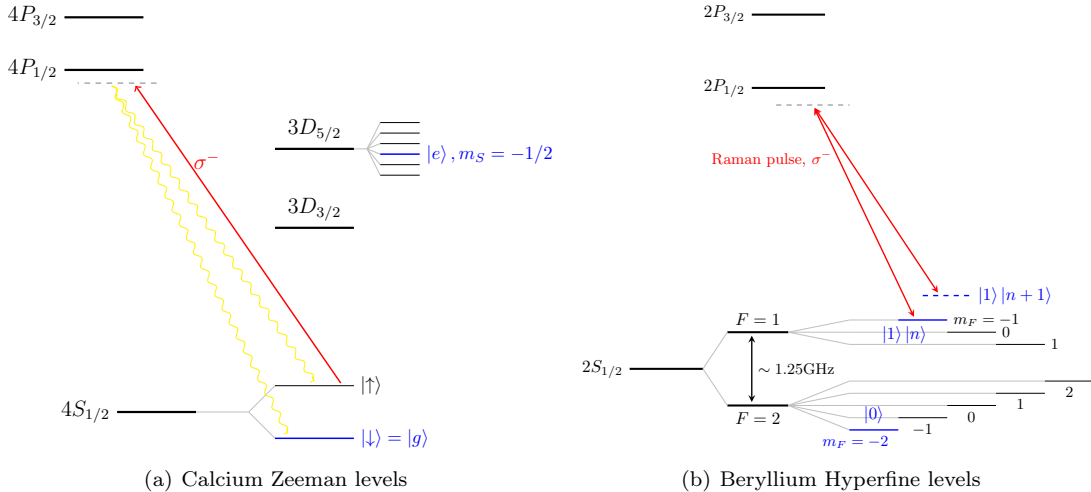


Figure 1.2: Two experimental implementations of selectively addressing a Zeeman or Hyperfine state.

Selectivity by polarised beams: For Zeeman or Hyperfine levels, the energy gap between different sub-levels lies in the RF or microwave frequency range and is therewith often smaller than the typical band width of a laser. When driving an optical transition from such a state, encoded in a Hyperfine or Zeeman sub-level, the laser excites not only the intended state but also

(with lower probability) the neighbouring sub-levels. This severely reduces the selectivity of the process.

To recover the selectivity of such a transition one can make use of the spin state of the levels. A circularly polarised laser drives only transitions between states with the corresponding difference in spin-states. As an example a laser with σ^+ -polarisation only drives transition between two states with $\Delta m_j = +1$, where j indicates for Zeeman levels the electron spin ($j = S$) and for Hyperfine levels the total angular momentum ($j = F$).

Several experimental applications of such processes can be found in literature:

- (i) *Preparation of a Zeeman ground level-state in Ca⁺* [5]: Initially the internal state of the Ca ion is in a superposition of the two Zeeman states $|\uparrow\rangle$ and $|\downarrow\rangle$. The initialisation of a $|\downarrow\rangle$ -state in the Zeeman ground levels can be realised by optical pumping process with a polarised laser beam as indicated in Figure 1.2(a). The state preparation is realised by an optical pumping process, where selectively the $|\uparrow\rangle$ -state is excited to the $P_{1/2}$ -level by a σ^- -polarised beam. This unstable level decays spontaneously into one of the Zeeman levels. After several such pumping cycles, the state is in the $|\downarrow\rangle$ -state.
- (ii) *State-dependent excitation of the motional mode for Hyperfine qubits in Be⁺* [17]: The qubit is encoded in two Hyperfine levels of Beryllium $|0\rangle = |F = 2; m_F = -2\rangle_{S_{1/2}}$, $|1\rangle = |F = 1; m_F = -1\rangle_{S_{1/2}}$ (c.f. Figure 1.2(b)). Depending on the qubit's state, the motional COM mode of the ion string should be excited. This is realised by the application of a Raman transition that selectively drives only the transition $|1\rangle|n\rangle \rightarrow |P_{1/2}; m_F = -2\rangle \rightarrow |1\rangle|n+1\rangle$. The selectivity is achieved by choosing a σ^- -polarised first Raman beam ω_1 . Angular momentum conservation allows only transitions with $m_F = -1$. Since there is no $|m_F = -3\rangle$ state in the $P_{1/2}$ -level, the qubit ground state $|0\rangle = |m_F = -2\rangle_S$ can not be excited. Only the excited qubit state $|1\rangle = |m_F = -1\rangle_S$ is excited to $|m_F = -2\rangle_P$.

Chapter 2

Gates

In order to implement arbitrary quantum computations, we need a *universal set of gates*, which has the property, that any gate can be approximated to arbitrary accuracy by a composition of operations of this set. There exist two discrete universal sets of gates [21]: Set one contains the Hadamard, phase and $\pi/8$ -gate, acting on a single qubit, and the CNOT gate as a two-qubit operation. Set two is spanned by the Hadamard, phase and CNOT gate plus the three-qubit Toffoli gate. It is important to state, that even though it can be proven, that there exist discrete sets of gates that are universal, most unitary transformations can only be implemented very inefficiently [21].

Since any single-qubit gate can be expressed in terms of rotations, the discrete single-qubit gates can be replaced by the continuous rotation group. For trapped ions, a physical realisation of single-qubit rotations is directly given by the carrier transition of the interaction Hamiltonian (1.14).

It is important to distinguish between *logical gates* and *physical gates*. Logical gates are abstract mathematical operations and do not contain any information about their experimental implementation on a specific physical system. For some of these gates, it might even not be possible to implement them in one step, i.e. the experimental implementation can only be realised by a sequence of several physical operations (e.g. as for the CNOT-gate, which is realised by a composition of the MS-gate, five rotations plus two Hadamard gates, as shown in Section 2.2.2). Physical gates denote operations that can directly be implemented in a physical system. These gates differ for different physical systems.

The gates are implemented by addressing the ions with an external EM field (lasers, RF or microwave fields). The EM fields interact with the ion, inducing Rabi oscillations on the addressed two-level system. The gate operators are at first order given by the resonant terms of the interaction Hamiltonian H_{AF} (1.13). For a given initial state, the final state is determined by the laser's frequency ω_L (or $\Delta\omega$ for two-photon transitions), phase ϕ ($\Delta\phi$) and pulse length t . In the following two equivalent notations for the qubit energy difference are used: $\omega_0 \equiv \omega_{eg}$.

2.1 Logical Gates

In this section some of the most important logical one- and two-qubit gates are listed. Special focus lies on controlled gates, since they are important for the implementation of the intended work extraction gate.

The gates are represented as matrices in the computational basis $\{|0\rangle = (1, 0)^\top, |1\rangle = (0, 1)^\top\}$.

2.1.1 Single-Qubit Gates

a) **Rotation:**

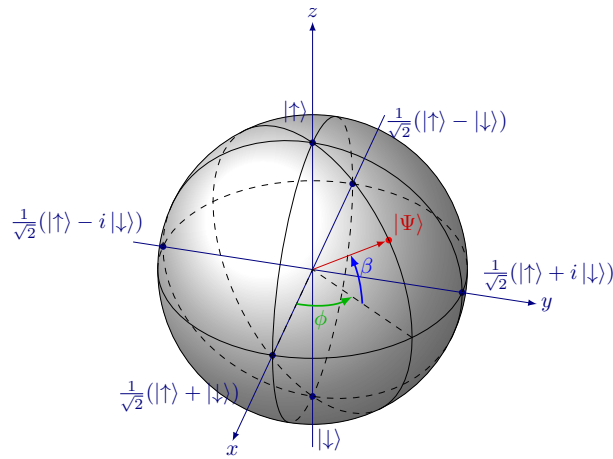


Figure 2.1: An arbitrary pure state $|\Psi\rangle$ of a single qubit can be described by a three-dimensional unity vector \hat{n} on the "Bloch sphere", determined by the two angles $\beta \in [-\frac{\pi}{2}, \frac{\pi}{2}]$ and $\phi \in [0, 2\pi]$: $\hat{n} = (\cos \beta \cos \phi, \cos \beta \sin \phi, \sin \beta)$. On the intersections of the axes with the sphere, the eigenvectors of the corresponding Pauli matrices lie: e.g. $\frac{1}{\sqrt{2}}(|\uparrow\rangle \pm |\downarrow\rangle)$ are the eigenvectors of σ_x .

In the canonical two-dimensional Hilbert space of a single qubit, rotations are represented by $SU[2]$ operators. A qubit can also be represented as a threedimensional Bloch vector, as visualised in Figure 2.1. In this *Bloch sphere picture*, all possible single-qubit operations can be described by rotations in three dimensions. Such a general rotation of a qubit about an angle θ around an axis $\hat{n} \in \mathbb{R}^3$ is given by $R_{\hat{n}}(\theta) = e^{-i\frac{\theta}{2}\hat{n} \cdot \vec{\sigma}}$ with $\vec{\sigma}_i$ the Pauli-matrices

$$R_{\hat{n}}(\theta) = \begin{pmatrix} \cos \theta/2 - i n_z \sin \theta/2 & -i \sin \theta/2(n_x - i n_y) \\ i \sin \theta/2(n_x + i n_y) & \cos \theta/2 + i n_z \sin \theta/2 \end{pmatrix}. \quad (2.1)$$

The rotation axis \hat{n} can be chosen such that it coincides with the x -, y - or z -axis. For special rotation angles we recover elementary gates like a *bit flip* or *phase flip*: An x -rotation about an angle $\theta = \pi$ is (up to a global phase factor) equal to a bit flip operation $R_x(\pi) = -i\sigma_x$. Similar, a z -rotation about $\theta = \pi$ denotes a phase flip operation $R_z(\pi) = -i\sigma_z$.

$$\begin{aligned} R_x(\theta) &= \begin{pmatrix} \cos \frac{\theta}{2} & -i \sin \frac{\theta}{2} \\ -i \sin \frac{\theta}{2} & \cos \frac{\theta}{2} \end{pmatrix}, & R_y(\theta) &= \begin{pmatrix} \cos \frac{\theta}{2} & \sin \frac{\theta}{2} \\ -\sin \frac{\theta}{2} & \cos \frac{\theta}{2} \end{pmatrix}, & R_z(\theta) &= \begin{pmatrix} e^{-i\frac{\theta}{2}} & 0 \\ 0 & e^{i\frac{\theta}{2}} \end{pmatrix} \\ R_x(\pi) &= -i\sigma_x = -i \begin{pmatrix} 1 & 1 \\ 1 & -1 \end{pmatrix}, & R_z(\pi) &= -i\sigma_z = -i \begin{pmatrix} 1 & 0 \\ 0 & -1 \end{pmatrix} \end{aligned} \quad (2.2)$$

In trapped ions, only qubit rotations around an axis in the xy -plane are elementary physical gates, that can be implemented in a single operation. A rotation about an angle θ around an axis in the xy -plane is described by the matrix $R(\theta, \phi)$. It is straightforward to derive it from the general rotation matrix. The rotation axis is specified by the angle ϕ between the x -axis and the rotation axis itself (c.f. Figure 2.1). In the experimental realisation ϕ corresponds to the relative phase of the EM field and the qubit state. We can recover $R_x(\theta)$ by setting $\phi = 0$ and $R_y(\theta)$ by $\phi = \pi/2$.

$$R(\theta, \phi) = \begin{pmatrix} \cos \theta/2 & -ie^{-i\phi} \sin \theta/2 \\ ie^{i\phi} \sin \theta/2 & \cos \theta/2 \end{pmatrix} : \begin{cases} |g\rangle \rightarrow \cos\left(\frac{\theta}{2}\right)|g\rangle - ie^{-i\phi} \sin\left(\frac{\theta}{2}\right)|e\rangle \\ |e\rangle \rightarrow \cos\left(\frac{\theta}{2}\right)|e\rangle + ie^{i\phi} \sin\left(\frac{\theta}{2}\right)|g\rangle \end{cases}. \quad (2.3)$$

- b) **Hadamard Gate:** The Hadamard gate maps the computational basis $\{|0\rangle, |1\rangle\}$ to the “rotational basis” $\{|\pm\rangle = \frac{1}{\sqrt{2}}(|0\rangle \pm |1\rangle)\}$. Since the computational and rotational bases are the eigenbases of the Pauli Z-operator and X-operator respectively, this mapping corresponds to the identities $H\sigma_xH = \sigma_z$ and $H\sigma_zH = \sigma_x$.

$$H = \frac{1}{\sqrt{2}} \begin{pmatrix} 1 & 1 \\ 1 & -1 \end{pmatrix} : \begin{cases} |0\rangle \rightarrow |+\rangle \\ |1\rangle \rightarrow |-\rangle \end{cases} \quad (2.4)$$

The Hadamard gate is a hermitian, unipotent operation: $H^\dagger = H$, $H^2 = \mathbb{I}$. Like any single-qubit gate it can be decomposed into single-qubit rotations plus a global phase factor:

$$H = e^{i\pi} R_z(-\pi) R_x(\pi/2) R_z(-\pi). \quad (2.5)$$

2.1.2 Two-qubit gates

Two-qubit gates act on a joint system of two qubits. In conditioned or *controlled gates*, the two qubits are referred to as the *target qubit* and *control qubit*. This indicates that the gate is applied to the target qubit only if the control qubit is in state $|1\rangle$. In the computational basis for a two-qubit state this can be expressed as:

$$U = \begin{pmatrix} \mathbb{I}_2 & 0 \\ 0 & \tilde{U} \end{pmatrix} : |\Psi\rangle \rightarrow \begin{pmatrix} \alpha \\ \beta \end{pmatrix} \oplus \tilde{U} \begin{pmatrix} \gamma \\ \delta \end{pmatrix}$$

with: $|\Psi\rangle = \alpha|00\rangle + \beta|01\rangle + \gamma|10\rangle + \delta|11\rangle = \begin{pmatrix} \alpha \\ \beta \\ \gamma \\ \delta \end{pmatrix}$ (2.6)

For the special case of separable states, this simplifies to:

$$U|\Psi\rangle = U(|\Psi_c\rangle \otimes |\Psi_t\rangle) = |\Psi_c\rangle \otimes \tilde{U}^c |\Psi_t\rangle, \quad \text{with } c = \begin{cases} 0, & \text{for } |\Psi_c\rangle = |0\rangle \\ 1, & \text{for } |\Psi_c\rangle = |1\rangle \end{cases}$$

- a) **CNOT-gate:** The CNOT-gate is a controlled two-qubit gate, corresponding to a controlled bit flip: the target qubit $|\Psi_t\rangle$ is flipped if the control qubit is in the excited state $|\Psi\rangle_c = |1\rangle$.

$$U_{\text{CNOT}} = \begin{pmatrix} 1 & 0 & 0 & 0 \\ 0 & 1 & 0 & 0 \\ 0 & 0 & 0 & 1 \\ 0 & 0 & 1 & 0 \end{pmatrix} : \begin{cases} |00\rangle \rightarrow |00\rangle \\ |01\rangle \rightarrow |01\rangle \\ |10\rangle \rightarrow |11\rangle \\ |11\rangle \rightarrow |10\rangle \end{cases} \quad (2.7)$$

The implementation of the gate requires the physical distinction between the target and the control qubit. An implementation is realised in the Cirac&Zoller gate or MS-gate (Section 2.2.2).

- b) **CPhase gate:** In the controlled phase gate (denoted by CPhase or CZ-gate) the common system of control and target qubit acquires a phase factor $e^{i\phi}$ (usually $e^{i\pi} = -1$).

$$U_{\text{CPhase}} = \begin{pmatrix} 1 & 0 & 0 & 0 \\ 0 & 1 & 0 & 0 \\ 0 & 0 & 1 & 0 \\ 0 & 0 & 0 & -1 \end{pmatrix} : \begin{cases} |00\rangle \rightarrow |00\rangle \\ |01\rangle \rightarrow |01\rangle \\ |10\rangle \rightarrow |10\rangle \\ |11\rangle \rightarrow -|11\rangle \end{cases} \quad (2.8)$$

For trapped ions, such a gate can be realised as a geometric phase gate by driving a cyclic motion of the ion's motional d.o.f. in state space. After a closed cycle, the ion returns to its initial motional state, but the qubit acquired a phase factor [17].

The CNOT and CPhase are connected to each other by single-qubit Hadamard gates. By further decomposing the Hadamard gate into rotations (c.f. Equation 2.5), the CNOT and CPhase gates can be expressed in terms of each other plus single-qubit rotations.

$$\text{CNOT} = (\mathbb{I} \otimes H) \circ \text{CPhase} \circ (\mathbb{I} \otimes H) \quad (2.9)$$

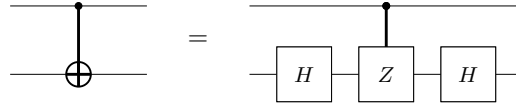


Figure 2.2: Expressing the CNOT gate in terms of the CPhase and single-qubit Hadamard gates.

2.2 Elementary physical gates

With “elementary physical gates” we denote gates, that can directly be implemented in an ion trap setup, without a further decomposition into simpler gates. It is important to note, that both two-qubit gates, which form together with the single-qubit rotations a universal set of gates (CNOT and CPhase), are *no* elementary physical gates. Both of them need to be implemented as a composition of several gates (c.f. Section 2.3). But since it could be shown, that the physical two-qubit MS-gate together with single-qubit rotations is sufficient to construct a CNOT gate [15], we may conclude, that the elementary physical gates, described in this section, span a universal set of gates.

In theory, one could add elementary gates that couple three (or more) systems, given by the 2nd order sideband excitations. But these transitions occur at very low probability and are badly resolved.

2.2.1 Single-ion gates

Single-ion gates act only on one ion with its internal and motional d.o.f. We distinguish between (a) gates that act on a single internal qubit, realised by *rotations*, (b) gates that raise or lower the motional state and (c) gates that couple an internal and a motional state, denoted by *sideband transitions*. If we consider multiple ions in a string we always refer to the collective motion of the string as motional state.

(a) **Rotation:** *Carrier transition on an internal qubit*

$$R(\theta, \phi) = \begin{pmatrix} \cos \theta / 2 & -ie^{-i\phi} \sin \theta / 2 \\ ie^{i\phi} \sin \theta / 2 & \cos \theta / 2 \end{pmatrix} : \begin{cases} |g\rangle & \rightarrow \cos\left(\frac{\theta}{2}\right)|g\rangle - ie^{-i\phi} \sin\left(\frac{\theta}{2}\right)|e\rangle \\ |e\rangle & \rightarrow \cos\left(\frac{\theta}{2}\right)|e\rangle + ie^{i\phi} \sin\left(\frac{\theta}{2}\right)|g\rangle \end{cases}. \quad (2.10)$$

The carrier transition acts only on the internal d.o.f., the motional state is unchanged. This corresponds to a rotation in the Bloch sphere picture $R(\theta, \phi)$.

The gate operator is given by the zeroth-order term of the interaction Hamiltonian (1.14): $R(\theta, \phi) = e^{iH_{\text{AF}}^{(0)}t/\hbar} = e^{i\theta/2(\hat{\sigma}^\dagger e^{i\phi} + \hat{\sigma} e^{-i\phi})}$, with $\theta = t\Omega$. The carrier transition can either be excited by a direct transition or a two-photon process, as described in Section 1.2. For both implementations, an EM field with zero detuning ($\omega_L = \omega_0$ or $\Delta\omega = \omega_0$) is required.

(b) **Motional state:** *Raman transitions*

$$R_R: |\Psi\rangle |n\rangle \leftrightarrow |\Psi\rangle |n+s\rangle$$

The frequency difference of the Raman beams is chosen such that only the motional state is excited: $\Delta\omega := \omega_1 - \omega_2 = s\omega_m$, $s \in \mathbb{Z}$. The ion’s internal state is unchanged.

(c) **Red/Blue Sideband (RSB/BSB) transitions:** *Coupling of the internal and the motional state*

The sideband transitions couple the internal and the motional d.o.f. The gates are implemented by an EM field, detuned such that the raising of a qubit state is accompanied by the creation/annihilation of one (or several) h.o. phonons: $\omega_L = \omega_0 \pm s\omega_m$, $s \in \mathbb{N}$.

The gate operators are given by the higher order terms of the interaction Hamiltonian (c.f. Equations 1.15, 1.16). The transition probability decreases rapidly for higher order sidebands. The *first sideband transitions* are given by:

- **red sideband (RSB):** $|g\rangle \otimes |n\rangle \leftrightarrow |e\rangle \otimes |n-1\rangle$

$$R^-(\theta, \phi) = \exp(i\theta/2(\hat{\sigma}\hat{a}^\dagger e^{-i\phi} + \hat{\sigma}^\dagger \hat{a} e^{i\phi})) , \quad \text{with } \theta = t\Omega_{n,n-1} \quad (2.11)$$

and Rabi frequency $\Omega_{n,n-1} = \sqrt{n}\eta\Omega$

- **blue sideband (BSB):** $|g\rangle \otimes |n\rangle \leftrightarrow |e\rangle \otimes |n+1\rangle$

$$R^+(\theta, \phi) = \exp(i\theta/2(\hat{\sigma}^\dagger \hat{a}^\dagger e^{i\phi} + \hat{\sigma} \hat{a} e^{-i\phi})) , \quad \text{with } \theta = t\Omega_{n,n+1} \quad (2.12)$$

and Rabi frequency $\Omega_{n,n+1} = \sqrt{n+1}\eta\Omega$

The sideband transitions can either be excited by a direct resonant transition or a Raman process, as described in Section 1.2.

2.2.2 Two-ion gates

a) Geometric Phase Gate:

The geometric phase gate can be used to implement either a normal *phase gate* on an internal qubit of a single ion, or a *controlled phase gate* on two qubits encoded in the internal states of two ions. The ions' motional mode can be in an arbitrary state within the Lamb-Dicke regime (Section 1.1.4).

The following gates have been implemented experimentally. More information about the experiments can be found in the Appendix C.1.

(i) Version 1: *Hyperfine qubits*

$$G^{(1)} = \begin{pmatrix} 1 & 0 & 0 & 0 \\ 0 & e^{i\phi} & 0 & 0 \\ 0 & 0 & e^{i\phi} & 0 \\ 0 & 0 & 0 & 1 \end{pmatrix} : \begin{cases} |gg\rangle \rightarrow |gg\rangle \\ |ge\rangle \rightarrow e^{i\phi} |ge\rangle \\ |eg\rangle \rightarrow e^{i\phi} |eg\rangle \\ |ee\rangle \rightarrow |ee\rangle \end{cases} \quad (2.13)$$

The gate was implemented for a phase factor $\phi = \pi/2$ on *Hyperfine qubits* in Be^+ ions [17]. The frequency difference of the Raman beams, establishing the periodic force, was chosen close to the common motional stretching mode: $\Delta\omega = \omega_{\text{stretch}} + \delta$.

(ii) Version 2: *Optical qubits*

$$G^{(2)} = \begin{pmatrix} e^{i\phi} & 0 & 0 & 0 \\ 0 & 1 & 0 & 0 \\ 0 & 0 & 1 & 0 \\ 0 & 0 & 0 & e^{i\phi} \end{pmatrix} : \begin{cases} |gg\rangle \rightarrow e^{i\phi} |gg\rangle \\ |ge\rangle \rightarrow |ge\rangle \\ |eg\rangle \rightarrow |eg\rangle \\ |ee\rangle \rightarrow e^{i\phi} |ee\rangle \end{cases} \quad (2.14)$$

The gate was applied for a phase factor $\phi = \pi/2$ on *optical qubits* encoded in two Ca^+ ions. The frequency difference of the Raman beams, establishing the periodic force, was chosen close to the common motional center-of-mass mode $\Delta\omega = \omega_{\text{COM}} + \delta$.

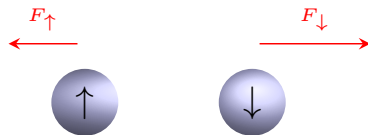
In contrary to most of the gates, the pulse length can not be varied for the geometric phase gate. It has to be chosen equal to the period $T = 2\pi/\delta$, where δ is the detuning of the EM

field from the motional mode frequency. The phase ϕ can be adjusted by adapting the laser intensity and detuning.

The implementation of the gate basically uses three concepts, for which a heuristic explanation is given in the following. A more extended mathematical description can be found in the Appendix C.1 and in literature [5], [10], [7].

(i) **State-dependent force:**

A state-dependent force acts on the motional mode of the ion (i.e. it has a mechanical



effect on the ion). Its strength (and direction) is different, depending on the internal states $|\uparrow\rangle, |\downarrow\rangle$ of the ion:

$$F_\downarrow = -a, \quad F_\uparrow, \quad a > 0.$$

Such a field can be established by two Raman laser beams, illuminating the ions and interfering at the ions' position. The superposed field oscillates at frequency equal to the difference of the frequencies of the individual beams: $\Delta\omega := \omega_1 - \omega_2$. For more details, please refer to [7], Chapter 4.3.

If the force points in opposite direction for the two states, one would expect that either the COM mode (for two ions in the same internal state) or the stretch mode (for two ions in different internal state) of the ion string is excited.

- (ii) **Oscillating state-dependent force:** In a linear trap, the ions are confined in a harmonic potential, such that their motional state can be described as a harmonic oscillator. An oscillating force, acting on the ions, drives this harmonic oscillator if it is close to resonance with its frequency. If the field and motional mode are far off-resonant, the field has no perceivable effect on the ions.

We consider an EM field like above, which acts as a state-dependent force on the ions. The frequency of the field is tuned close to the frequency of a motional mode of the ion string:

$$\Delta\omega = \omega_m + \delta, \quad \text{with: } \omega_m \in \{\omega_{\text{COM}}, \omega_{\text{stretch}}\}, \quad \delta \ll \omega_m$$

Due to the resonance condition, only specific two-qubit states lead to an excitation of the ions' motional state:

$$\omega_m = \omega_{\text{COM}} : \begin{cases} |\uparrow\uparrow\rangle, |\downarrow\downarrow\rangle : \text{COM mode excited} \\ |\downarrow\uparrow\rangle, |\uparrow\downarrow\rangle : \text{nothing happens} \end{cases} \quad (2.15)$$

$$\omega_m = \omega_{\text{stretch}} : \begin{cases} |\uparrow\uparrow\rangle, |\downarrow\downarrow\rangle : \text{nothing happens} \\ |\downarrow\uparrow\rangle, |\uparrow\downarrow\rangle : \text{stretch mode excited} \end{cases} \quad (2.16)$$

- (iii) **Driven Harmonic oscillator:** The application of a periodic force with slightly off-resonant frequency (detuning δ) on a classical harmonic oscillator leads to a *driven harmonic oscillator*. Such a h.o. is periodically damped and accelerated by the force. After a period $T = \frac{2\pi}{\delta}$ the h.o. has returned back to its initial state in phase space.

The same holds for a quantum mechanical h.o., like the motional state of the ions. Within

a period $T = \frac{2\pi}{\delta}$ the h.o. state describes a *closed path in phase space*. After the gate was applied, the motional mode has returned to its initial state, up to an *acquired phase factor*. This phase distinguishes the quantum mechanical from the classical case. It arises due to the non-commutative characteristics of the time-evolution operator, generated by the force.

b) **Mølmer-Sørensen (MS) Gate**

The MS gate drives a *collective spin flip* of two ions ($|ee\rangle \leftrightarrow |gg\rangle$ and $|eg\rangle \leftrightarrow |ge\rangle$) using a two-photon transition. The transitions are indicated in Figure 2.3. The gate is a *symmetric* two-qubit gate, i.e. it is *not* a controlled gate.

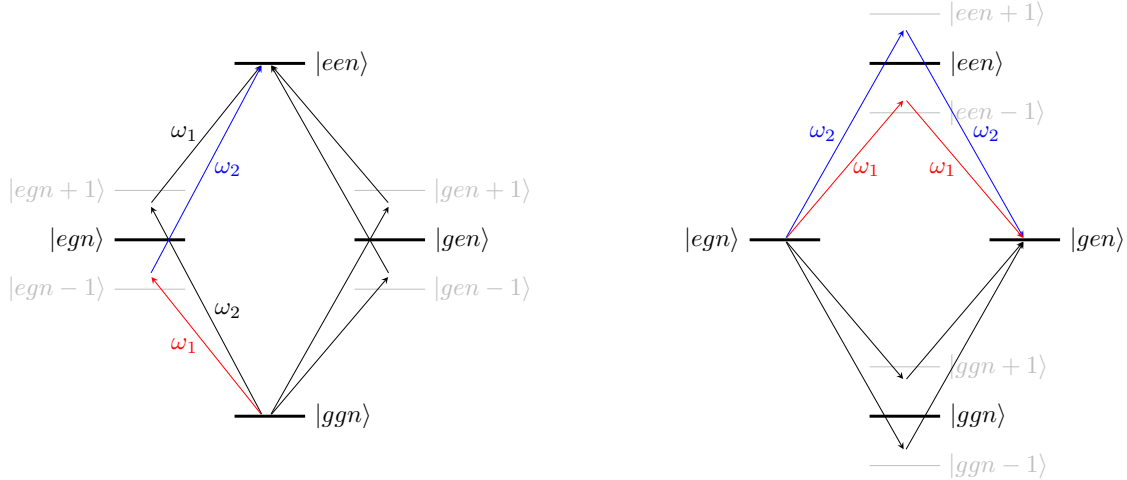


Figure 2.3: Scheme of the initial/final states and the virtual intermediate states in the two transitions induced by the MS gate [14].

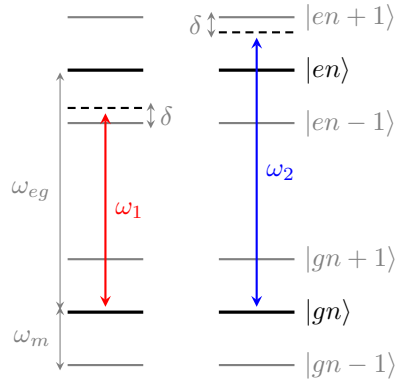


Figure 2.4: Comparison of the ions' energy levels and frequencies of the laser beams, used in an MS gate.

Implementation: Two lasers of different frequencies (bichromatic field) drive this two-ion gate. Each laser addresses both ions. The lasers are detuned by $\pm\delta \ll \omega_m$ from a sideband (c.f. Figure 2.4): the first laser is close to the RSB $\omega_1 = \omega_{eg} - \omega_m + \delta$, the second laser is close

2.3. DECOMPOSITION OF UNITARIES INTO ELEMENTARY PHYSICAL GATES

to the BSB $\omega_2 = \omega_{eg} + \omega_m - \delta$. Assume in a first step, that ion i is only addressed by the laser ω_i . This induces one of the four ‘excitation paths’, indicated by colours in the left graph of Figure 2.3:

$$\begin{aligned} \text{Ion 1: RSB with } \omega_1 = \omega_{eg} - \omega_m + \delta : & \quad |g_1\rangle|n\rangle \xrightarrow{\omega_1} |e_1\rangle|n-1\rangle \\ \text{Ion 2: BSB with } \omega_2 = \omega_{eg} + \omega_m - \delta : & \quad |g_2\rangle|n\rangle \xrightarrow{\omega_2} |e_2\rangle|n+1\rangle. \end{aligned}$$

The detuning is chosen large enough, such that the intermediate levels can be considered as virtual levels, i.e. they are never populated. But since the detuning of the first laser is chosen to be the negative of the detuning of the second laser, the composition of the two processes leads to a transition between “physical” states with: $\omega_1 + \omega_2 = 2\omega_{eg}$.

$$\text{Two-ion transitions: } \begin{cases} |g_1g_2\rangle|n\rangle \xleftrightarrow{\omega_1, \omega_2} \{|e_1g_2\rangle|n\pm1\rangle, |g_1e_2\rangle|n\pm1\rangle\} \xleftrightarrow{\omega_1, \omega_2} |e_1e_2\rangle|n\rangle \\ |e_1g_2\rangle|n\rangle \xleftrightarrow{\omega_1, \omega_2} \{|g_1g_2\rangle|n\pm1\rangle, |e_1e_2\rangle|n\pm1\rangle\} \xleftrightarrow{\omega_1, \omega_2} |g_1e_2\rangle|n\rangle \end{cases}$$

A general pulse of length t mixes the states in Rabi oscillations with Rabi frequency $\tilde{\Omega} \sim \Omega_1\Omega_2$, which depends on the detuning δ .

$$U_t^{\text{MS}} : \begin{cases} |gg\rangle & \rightarrow \cos\left(\frac{\tilde{\Omega}t}{2}\right)|gg\rangle + i \sin\left(\frac{\tilde{\Omega}t}{2}\right)|ee\rangle \\ |ee\rangle & \rightarrow \cos\left(\frac{\tilde{\Omega}t}{2}\right)|ee\rangle + i \sin\left(\frac{\tilde{\Omega}t}{2}\right)|gg\rangle \\ |ge\rangle & \rightarrow \cos\left(\frac{\tilde{\Omega}t}{2}\right)|ge\rangle - i \sin\left(\frac{\tilde{\Omega}t}{2}\right)|eg\rangle \\ |eg\rangle & \rightarrow \cos\left(\frac{\tilde{\Omega}t}{2}\right)|eg\rangle - i \sin\left(\frac{\tilde{\Omega}t}{2}\right)|ge\rangle. \end{cases} \quad (2.17)$$

A **π -pulse** ($t = \pi/\tilde{\Omega}$) gives the *collective bit flip*, whereas a **$\pi/2$ -pulse** can be used to entangle the ion’s internal states in *maximally entangled EPR states*.

$$\pi\text{-pulse: } U_{t=\pi/\tilde{\Omega}}^{\text{MS}} = i \begin{pmatrix} 0 & 0 & 0 & 1 \\ 0 & 0 & -1 & 0 \\ 0 & -1 & 0 & 0 \\ 1 & 0 & 0 & 0 \end{pmatrix}.$$

2.3 Decomposition of unitaries into elementary *physical* gates

In this section, we describe decompositions of n -dimensional unitary operations into lower-dimensional, elementary physical gates. As a special case, circuits for the CNOT and CPhase gate are listed.

Given an n -dimensional unitary gate $U \in \text{U}(n)$, we aim to find a circuit for ion traps that approximates U efficiently. The efficiency of the circuit is important due to practical reasons: Each gate can be implemented with fidelity smaller than one. Hence, in the subsequent implementation of several gates, the fidelity decreases with the number of gates. Furthermore, the qubits, encoded in the internal state of trapped ions, have a finite coherence time. For a high number of gates, the time for implementing the circuit could be critical compared to this coherence time. This strongly restricts the length of our circuit.

There are two approaches to find a decomposition circuit, starting at different ‘ends’. Both approaches correspond to an optimisation problem over a different set of variables with different advantages and disadvantages:

- a) We define a *universal set of logical gates* and decompose our unitary into these gates. As universal set we chose single-qubit rotations and a two-qubit operation (CNOT or CPhase). Since the CNOT and CPhase gate can be expressed in terms of each other, the choice of the two-qubit gate is insignificant. We chose the CNOT gate, since it is easier to think in terms of bit flips than phase flips.
- ⊕ The gates do not depend on the physical setup.
 - ⊕ The application of purely mathematical decomposition algorithms is possible.
 - ⊕ A resulting circuit could easily be translated to different physical systems.
 - ⊖ Logical two-qubit gates need to be further decomposed into several physical gates, e.g. the CNOT gate corresponds to three rotations and two side-band transformations.
- b) We start with the set of *elementary physical operations* as described in Section 2.2 and try to combine them in a way that they approximate our unitary U .
- ⊕ One can take advantage of special properties of the physical system, as for example direct interactions between two internal qubits or the internal and the motional d.o.f., given by the higher-order terms of the interaction Hamiltonian H_{AF} . An example for the increased efficiency is given below for the implementation of the Toffoli gate.
 - ⊕ All gates can directly be implemented.
 - ⊖ No universal decomposition algorithm exists.

Example: Decomposition of the Toffoli gate

As an example for more efficiency by using the special properties of the physical system, we consider the decomposition of the Toffoli gate. The decomposition into a universal set of logical gates, given by the CNOT gate and the single-qubit Hadamard gate H , non-Clifford gate T and phase gate S requires *six* CNOT gates (c.f. Figure 2.5, [24]). In contrast, a Toffoli gate can easily be expressed by a single CNOT gate and two MS gates, if an additional ancilla qubit is added.

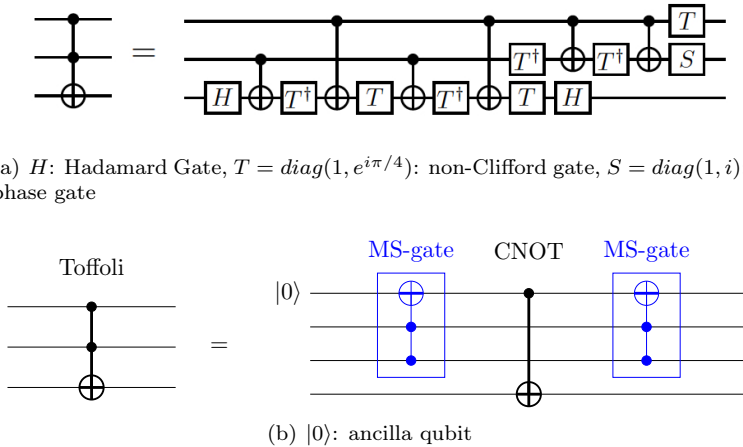


Figure 2.5: Decomposition of the Toffoli gate a) in terms of *six* CNOT gates and single-qubit gates or b) in terms of two MS gates and *one* CNOT gate with an ancilla qubit $|0\rangle$.

2.3.1 Decomposition of the CNOT gate

a) MS-gate:

A CNOT-gate is implemented by the following sequence of operations

$$U_{\text{CNOT}} = R_{z,2}(\pi) U_T^{\text{MS}} R_{z,1}^{-1}(\pi) H_1 R_{z,1}(\pi) U_T^{\text{MS}} H_2 R_{z,2}(\pi) R_{z,1}(\pi) \quad (2.18)$$

With rotations $R_{z,i}$ giving a $\pi/2$ -phase change on the excited state of ion i , Hadamard gates H_i , and the MS-gate U_T^{MS} with pulse time $T = \frac{\pi}{2\Omega}$ (corresponding to the entangling gate).

b) Cirac&Zoller gate: [12] [13]

The Cirac&Zoller gate performs a CNOT-*gate* on two qubits, encoded in the *internal states* of a control and a target ion. The idea of the gate is, to use the common motional state of the ion string as ‘bus mode’ to communicate between the control qubit $|\Psi\rangle_c$ and the target qubit $|\Psi\rangle_t$. This allows the application of the two-qubit gate even on non-neighbouring ions.

Idea: We consider a string of ions ($N \geq 2$), cooled down to the ground state of their collective motional mode. The qubits are encoded in internal states of a control and a target ion ($\{|g\rangle_{c,t}, |e\rangle_{c,t}\}$). A sideband transition, performed on the control ion, changes the ion’s internal state and the collective motional state of the whole ion string. Therefore all ions will be in the same new motional state after the transition. Due to the coupling of the internal and the motional states in sideband transitions, this state depends on the initial state of the control qubit. This way, the initial state $|\Psi\rangle_c$ of the control qubit is mapped onto the collective motional state of the string and all ions, including the target ion, “know” about it.

The controlled gate on the target qubit can then be performed controlled on the motional mode. In the end the control qubit and the motional mode have to be reset to their initial state by a “reverse” sideband transformation.

Implementation: Cirac and Zoller originally implemented the gate as follows [12]:

- (i) The *control qubit* is mapped onto the motional mode by a π -pulse on the red sideband (RSB) with phase $\phi = 0$:

$$R_c^-(\pi, 0) \otimes \mathbb{I}_t : |g\rangle_c |1\rangle \leftrightarrow |e\rangle_c |0\rangle$$

All other two states are unchanged.

- (ii) A *controlled phase gate* on the *target qubit* with the motional state as control qubit is realised by a full rotation on an auxiliary transition ($|\tilde{e}\rangle$ is an auxiliary internal state of the ion)

$$\tilde{R}_t(2\pi, 0) \otimes \mathbb{I}_c \otimes \mathbb{I}_{\text{motional}} : |g\rangle_t |1\rangle \leftrightarrow |\tilde{e}\rangle_t |0\rangle .$$

By a full rotation the state $|\tilde{e}\rangle_t |0\rangle$ acquires a phase of (-1) , whereas all other states are unaltered.

- (iii) By another π -pulse on the RSB $R_c^+(\pi, 0) \otimes \mathbb{I}_t$ the control and motional qubit are reset to their initial state.

On the basis $\{|g\rangle_t, |e\rangle_t\}$ the composite gate $\tilde{U} := R_c^+(\pi, 0)\tilde{R}_t(2\pi, 0)R_c^+(-\pi, 0)$ acts as a *controlled phase gate*.

$$\begin{aligned} |g\rangle_c |g\rangle_t |0\rangle &\xrightarrow{R_c^-} |g\rangle_c |g\rangle_t |0\rangle \xrightarrow{\tilde{R}_t} |g\rangle_c |g\rangle_t |0\rangle \xrightarrow{R_c^-} +|g\rangle_c |g\rangle_t |0\rangle \\ |g\rangle_c |e\rangle_t |0\rangle &\longrightarrow |g\rangle_c |e\rangle_t |0\rangle \longrightarrow |g\rangle_c |e\rangle_t |0\rangle \longrightarrow +|g\rangle_c |e\rangle_t |0\rangle \\ |e\rangle_c |g\rangle_t |0\rangle &\longrightarrow -i|g\rangle_c |g\rangle_t |1\rangle \longrightarrow i|g\rangle_c |g\rangle_t |1\rangle \longrightarrow +|e\rangle_c |g\rangle_t |0\rangle \\ |e\rangle_c |e\rangle_t |0\rangle &\longrightarrow -i|g\rangle_c |e\rangle_t |1\rangle \longrightarrow -i|g\rangle_c |e\rangle_t |1\rangle \longrightarrow -|e\rangle_c |e\rangle_t |0\rangle. \end{aligned}$$

But in the rotational basis $\{|\pm\rangle_t = \frac{1}{\sqrt{2}}(|g\rangle_t \pm |e\rangle_t)\}$, the same operation has the effect of a CNOT-gate. So with an additional basis transformation, given by the $\pi/2$ -rotations V, V^\dagger we find the CNOT-gate operator $U_{\text{CNOT}} = V\tilde{U}V^\dagger$.

Since the ion string is cooled to its motional ground state, we only consider the action of U_{CNOT} on the initial motional states $|0\rangle$.

$$\begin{aligned} |g\rangle_c |g\rangle_t |0\rangle &\xrightarrow{V^\dagger} |g\rangle_c |+\rangle_t |0\rangle \xrightarrow{\tilde{U}} |g\rangle_c |+\rangle_t |0\rangle \xrightarrow{V} |g\rangle_c |g\rangle_t |0\rangle \\ |g\rangle_c |e\rangle_t |0\rangle &\longrightarrow |g\rangle_c |-\rangle_t |0\rangle \rightarrow |g\rangle_c |-\rangle_t |0\rangle \rightarrow |g\rangle_c |e\rangle_t |0\rangle \\ |e\rangle_c |\mathbf{g}\rangle_t |0\rangle &\longrightarrow |e\rangle_c |+\rangle_t |0\rangle \rightarrow |g\rangle_c |-\rangle_t |1\rangle \rightarrow |e\rangle_c |\mathbf{e}\rangle_t |0\rangle \\ |e\rangle_c |\mathbf{e}\rangle_t |0\rangle &\longrightarrow |e\rangle_c |-\rangle_t |0\rangle \rightarrow |g\rangle_c |+\rangle_t |1\rangle \rightarrow |e\rangle_c |\mathbf{g}\rangle_t |0\rangle \end{aligned}$$

$$U_{\text{CNOT}} = V\tilde{U}V^\dagger,$$

with $\tilde{U} := R_c^+(\pi, 0)\tilde{R}_t(2\pi, 0)R_c^+(-\pi, 0)$

$$V = R_t\left(\frac{\pi}{2}, \frac{\pi}{2}\right) \otimes \mathbb{I}_c \otimes \mathbb{I}_{\text{motional}}, \quad (2.19)$$

$$V^\dagger = R_t\left(-\frac{\pi}{2}, \frac{\pi}{2}\right) \otimes \mathbb{I}_c \otimes \mathbb{I}_{\text{motional}}.$$

2.3.2 Decomposition of the CPhase gate

a) Geometric Phase gate:

A geometric phase gate can be decomposed into a CPhase gate and a global phase factor. This phase factor can be corrected by single-ion operations. In the experiment with Hyperfine qubits in Be⁺-ions [17], this leads to the following gate:

$$G^{(1)} = \begin{pmatrix} 1 & 0 & 0 & 0 \\ 0 & e^{i\pi/2} & 0 & 0 \\ 0 & 0 & e^{i\pi/2} & 0 \\ 0 & 0 & 0 & e^{i\pi} \end{pmatrix} \underbrace{\begin{pmatrix} 1 & 0 & 0 & 0 \\ 0 & 1 & 0 & 0 \\ 0 & 0 & 1 & 0 \\ 0 & 0 & 0 & e^{-i\pi} \end{pmatrix}}_{U_{\text{CPhase}}} : \begin{cases} |gg\rangle &\rightarrow |gg\rangle \\ |ge\rangle &\rightarrow e^{i\pi/2}|ge\rangle \\ |eg\rangle &\rightarrow e^{i\pi/2}|eg\rangle \\ |ee\rangle &\rightarrow e^{-i\pi}(e^{i\pi/2}|e\rangle)(e^{i\pi/2}|e\rangle) \end{cases} \quad (2.20)$$

b) **Cirac&Zoller gate:** [12] [13] Without the additional basis transformations V , V^\dagger , the composite gate \tilde{U} acts as a *controlled phase gate* on the basis $\{|g\rangle_t, |e\rangle_t\}$.

$$U_{\text{CPhase}} = \tilde{U} := R_c^+(\pi, 0) \tilde{R}_t(2\pi, 0) R_c^+(-\pi, 0) \quad (2.21)$$

2.3.3 Universal decomposition of a two-qubit gate in an entangling geometric phase gate G and single-qubit rotations

This scheme chooses a universal set of gates, consisting of the *geometric phase gate* and *single-qubit rotations*. The algorithm provides a decomposition of arbitrary *two-qubit unitaries* $U \in U(2)$ into these elementary gates [23].

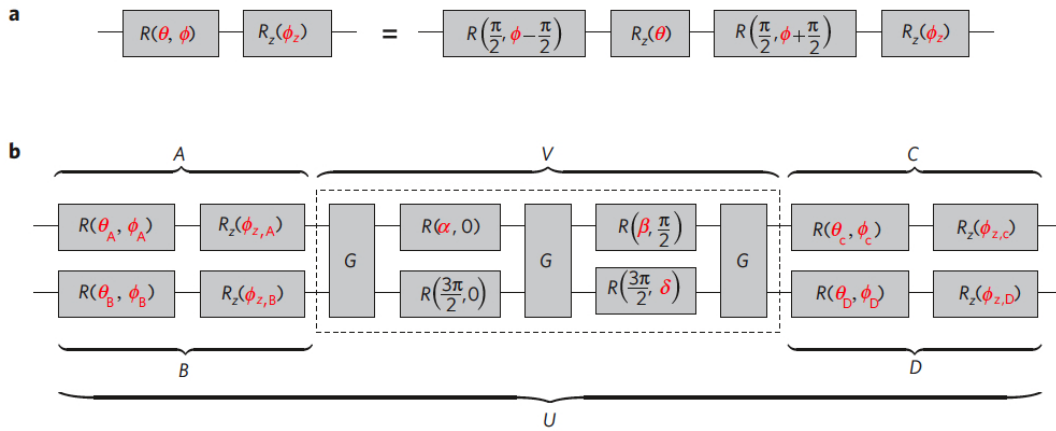


Figure 2.6: Universal decomposition of an arbitrary two-qubit unitary into geometric phase gates and single-qubit rotations [23].

For the decomposition, a special equivalence class of two-qubit gates, where all gates are equivalent that are connected by single-qubit operations, is considered. Any single-qubit unitary can be decomposed, up to a global phase, into qubit rotations. Hence the equivalence class can be represented as $[U] = \{V \in U(2) | AVB = U \text{ with } A, B \in SO(3)\}$. V is in a special form that requires fewer operations for its decomposition. This leads to following decomposition

$$\begin{aligned} U &= (C \otimes D) \cdot V \cdot (A \otimes B) \\ A, C &\text{: single-qubit rotations on ion 1} \\ B, D &\text{: single-qubit rotations on ion 2} \\ V &\in [U] \cap SU(2) \end{aligned} \quad (2.22)$$

The final decomposition is sketched in Figure 2.6. The phase gate G is implemented as a geometric phase gate, which changes the phase of the two states $|01\rangle, |10\rangle$. It is implemented for a phase

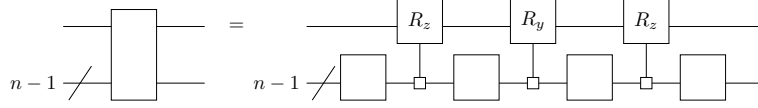


Figure 2.7: Quantum Shannon decomposition of a general unitary gate into lower-dimensional gates and multiplexed rotations.

$\phi = \pi/2$, leading to the entangling gate

$$G(\phi) = e^{-i\phi/2} \cdot e^{i\phi/2(\sigma_z \otimes \sigma_z)} = \begin{pmatrix} 1 & e^{-i\phi} & \\ & e^{-i\phi} & \\ & & 1 \end{pmatrix}, \quad G\left(\frac{\pi}{2}\right) = \begin{pmatrix} 1 & -i & \\ & -i & \\ & & 1 \end{pmatrix}.$$

2.3.4 Decomposition of arbitrary unitaries $U \in \mathbf{U}(n)$

a) Cosine-Sine decomposition of multiplexed gates:

A controlled gate is a special case of a multiplexed gate $A = A_0 \oplus A_1$. An arbitrary multiplexed $2n$ -dimensional unitary U can be “demultiplexed” by the Cosine-Sine Decomposition into lower-dimensional unitaries plus rotations [25]. This corresponds to the mathematical *Singular Value Decomposition*

$$U = U_0 \oplus U_1 = (\mathbb{I} \otimes V)(D \oplus D^\dagger)(\mathbb{I} \otimes W)$$

$$\begin{pmatrix} U_0 & \\ & U_1 \end{pmatrix} = \begin{pmatrix} V & \\ & V \end{pmatrix} \begin{pmatrix} D & \\ & D^\dagger \end{pmatrix} \begin{pmatrix} W & \\ & W \end{pmatrix}$$

with D a diagonal matrix. V and W are $(n-1)$ -qubit gates. Since any diagonal matrix can be rewritten as an R_z -rotation, the matrix $(D \oplus D^\dagger)$ is in fact a multiplexed R_z -rotation.

- b) **Quantum Shannon Decomposition:** By this decomposition, an arbitrary n -qubit gate can be decomposed into a circuit of $(n-1)$ -qubit gates plus multiplexed rotations, as indicated in Figure 2.7. A proof can be found in [25]. This decomposition implies an upper bound on the number of CNOT gates (c_n), used to implement a general n -qubit gate:

$$c_n \leq \frac{23}{48}4^n - \frac{3}{2}2^n + \frac{4}{3}$$

A lower bound on the number of CNOTs is given by:

$$c_n \geq \frac{1}{4}(4^n - 3n - 1)$$

Chapter 3

Experimental Setup

For the experimental implementation we collaborate with the group of Jonathan Home at ETH Zurich. J. Home's laboratory for trapped ion quantum information was started in 2010. At the moment (February 2013), the experiment is still in its assembling and testing phase. A first single ion was trapped before Christmas 2012. In the final setup one may expect up to six or seven ions. Higher numbers might be possible but demand more advanced control.

In the following a brief overview of the proposed experimental setup is given.

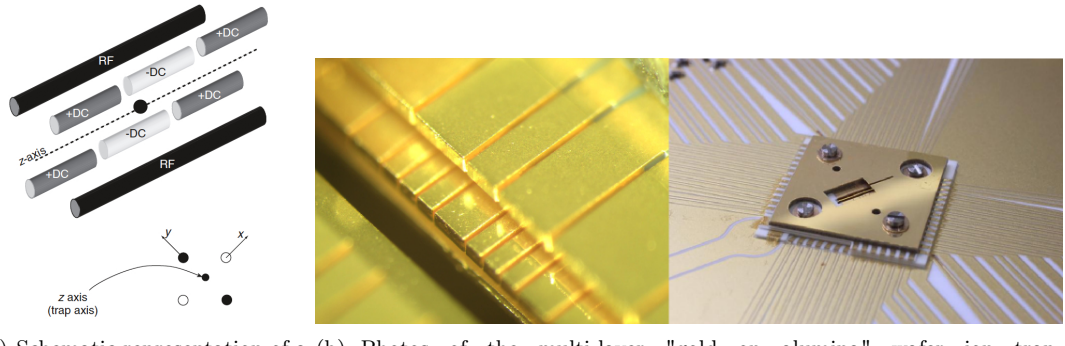
3.1 The ion trap

Figure 3.1(a) shows a schematic representation of a linear radio frequency ion trap with its DC and RF electrodes. The DC electrodes trap the ions in a harmonic potential along the trap axis (z -axis). The RF potential restricts the ions' transverse motion on a circular path around the origin.

The exact physical background of the trap is not very important for this project. Of importance is the understanding that the energy spectra of the ions' motional d.o.f. are determined by the trapping potential. By tuning the harmonic DC trapping potential, the frequency ω_z of the axial motional d.o.f. can be changed within a range of $\sim 100\text{kHz}$ up to $1 - 3\text{MHz}$.

Ion string: The system will include two different types of ions: $^{40}\text{Ca}^+$ and $^9\text{Be}^+$. In the trap, the Ca and Be ions will be aligned alternately in a string as pictured in Figure 3.2. Due to the different energy level structure of the two ion types, this alignment improves the spatial selectivity of the driving lasers: A laser, tuned to a specific transition frequency and directed to the position of an ion, does not affect the adjacent ions even if the laser width is broader than the spatial separation of the ions.

The two ion species show totally different mass: $m_{\text{Be}} \approx 9.01\mu$, $m_{\text{Ca}} \approx 40.078\mu \sim 4.5m_{\text{Be}}$. This has a big effect on the recoil energy and therewith vibrational behaviour of the two ion species. The motional mode of a Be ion reacts much more sensitively on photon recoil (e.g. from photon scattering) and one has to be very careful in order to keep the ion's motional modes cool (c.f. Section 1.1.4). The mass difference also affects the common motional modes of the ion string, which can only be described approximately in COM and stretching mode.



(a) Schematic representation of a linear radio frequency ion trap. (b) Photos of the multi-layer "gold on alumina" wafer ion trap. (www.tiqi.ethz.ch, 05.02.2013)
([3] Chap. 17)

Figure 3.1: Schematic representation and photos of a linear radio frequency trap. The photos show the multi-layer "gold on alumina" wafer ion trap of J. Home's group at ETH Zurich. The picture on the left shows the laser-machined and electroplated electrode structure (smallest electrodes 100 micron wide), while on the right hand side you see the trap assembly mounted on the filter board. There are 58 independent electrode connections in total.

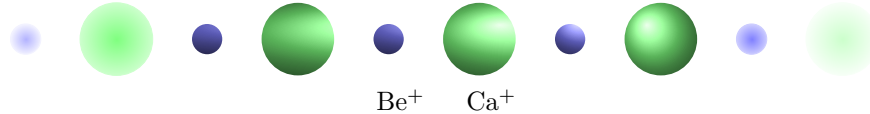


Figure 3.2: Ion string, consisting of an alternating alignment of Be^+ and Ca^+ ions.

3.2 Atomic Structure of the Ions

Figure 3.3 depicts the internal energy levels for the valence electrons of the two ions. The arrows indicate transitions between two energy levels that can be realised in our setup (i.e. for which a resonant EM field is provided). It is convention to specify optical transitions by the wavelength λ of the resonant laser, whereas for RF or microwave transition the frequency ω is stated.

The energy levels are characterised by their different stability. The life times and decay rates always correspond to a specific transition of one level to a second level of lower energy. The life times for different transitions of the same upper level may differ depending on the energy gap and the electric characteristics of the transition (e.g. dipole or quadrupole transition). Depending on its energy gap, a transition needs to be addressed by lasers, microwave or radio-frequency (RF) waves (c.f. Table 3.2). A transition in the radio frequency (RF) range can either be induced by a single radio wave field or by two lasers in a Raman two-photon transition (c.f. Section 1.2). Some properties of different transitions are listed in Table 3.1 .

3.2. ATOMIC STRUCTURE OF THE IONS

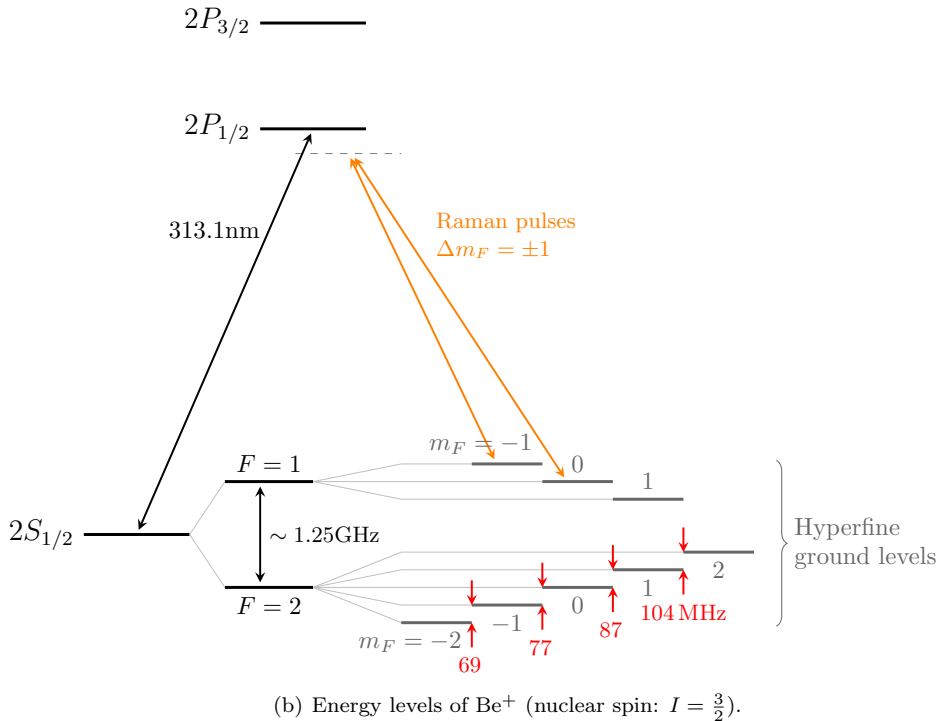
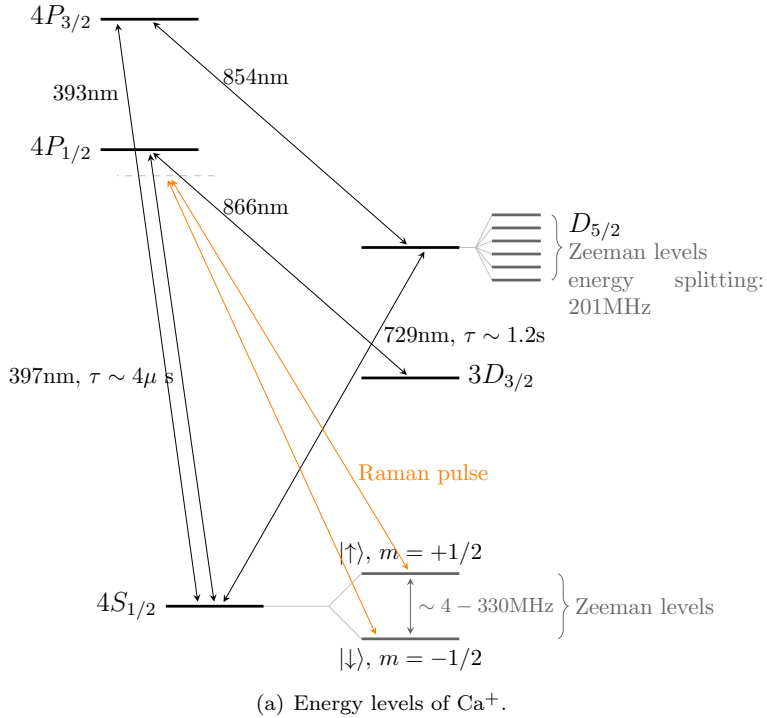


Figure 3.3: Energy levels of the internal d.o.f. of the Ca^+ and Be^+ ions. The arrows indicate transitions between levels, which can be realised in our setup by resonant EM fields. For Ca, the ground state Zeeman splitting is pictured. Be, with a non-zero nuclear spin ($I = \frac{3}{2}$) shows a Hyperfine splitting of its levels. The energy splitting of the Zeeman and Hyperfine levels is given for a magnetic field strength $B = 119.64\text{G}$.

	Transition	λ [nm] / ω [Hz]	EM field	Lifetime	Notes
Ca⁺	$S_{1/2} \leftrightarrow P_{1/2}$	397nm	Laser	$\tau \sim 4\mu s$	dipole trans.
	$S_{1/2} \leftrightarrow D_{5/2}$	729nm	Laser	$\tau \sim 1.2s$	quadrupole trans.
	$ \downarrow\rangle \leftrightarrow \uparrow\rangle$	$\sim 4 - 330\text{MHz}$	RF, Raman		Zeeman qubit
Be⁺	$S_{1/2} \leftrightarrow P_{1/2}$	313.1nm	Laser		dipole trans.
	$ F=1\rangle_S \leftrightarrow F=2\rangle_S$	$\sim 1.25\text{GHz}$	RF, Raman		Hyperfine qubit
	$ F; m_F\rangle_S \leftrightarrow F; m_F \pm 1\rangle_S$	$\sim 100\text{MHz}$	RF, Raman		Hyperfine qubit

Table 3.1: Properties of the different two-level transitions of the two ions. The energy separations of the Hyperfine qubits are given for a magnetic field strength $B = 199.64\text{G}$.

	Wavelength λ [m]	Frequency ω [$2\pi \cdot \text{Hz}$]
Lasers	$\sim 150\text{nm} - 1\text{mm}$	$\sim 10^{12} - 10^{15}\text{GHz} = 1 - 3\text{THz}$
Microwave (MW)	$\sim 10^{-2}\text{m}$	$\sim 100\text{GHz}$
Radio Frequency (RF)	$\sim 10^3\text{m}$	$\sim 10\text{MHz}$

Table 3.2: Range for the frequency and wavelength of different EM fields, which can be used to address atomic transitions.

The $S_{1/2} \leftrightarrow P_{1/2}$ two-level system is connected by an *electric-dipole transition*. Therefore, the P -level is very unstable and the transition's lifetime is very short; the P -level immediately decays to the S ground-level. In contrast, the $S_{1/2} \leftrightarrow D_{5/2}$ transition of Ca⁺ is very stable (life-time $\tau \sim 1.2\text{s}$). This is due to the fact that the S - and D -levels have the same parity and are therefore coupled only by *electric quadrupole transitions*. Both transitions are in the optical range and can be addressed by lasers. Lasers allow very accurate spatial selectivity, which is a necessary condition for single-qubit operations and phonon momentum exchange (to cool the ions).

The low probability of the $S_{1/2} \rightarrow D_{5/2}$ excitation can be overcome by either using a laser of very narrow linewidth or a two-photon process with the P -level intermediately populated. In a laser of narrow linewidth, i.e. with a narrow spectrum, a higher number of photons is in resonance with the addressed transition. This increases the probability for the excitation. In a two-photon process, the lasers drive a transition via an auxiliary intermediate P state. The lasers are detuned from the $S \leftrightarrow P$ transition, in order to keep the population of the P level low.

The *Zeeman levels* of Ca⁺ and the *Hyperfine levels* of Be⁺ show good stability due to their small energy gap. As a drawback, the Zeeman level transitions have to be driven by an RF field or Raman pulses. If a Zeeman/Hyperfine level transition is driven by an RF field, this leads to a very bad spatial selectivity.

3.3 Qubit encoding

In the following, all possibilities for qubit encoding should be explored, regardless of whether they will be useful for the intended implementation or not.

The qubits can either be encoded in the internal or motional d.o.f. of the ions (c.f. the ion's state space (1.1) and Hamiltonian (1.3)). For the internal d.o.f., different two-level systems are available, as indicated in Figure 3.3.

The qubits should be encoded in stable states. Unstable states would lead to loss of information as well as incoherent scattering, which increases the entropy of the EM fields and affects the motional mode of the ions due to the recoil energy of the scattered photons.

For the intended implementation of the work extraction gate (c.f. Section 4) we are interested in qubits with special properties. In an optimal scheme, the *battery qubit* is encoded in a degenerate qubit. The *thermal qubit* should by definition be initialised by coupling it to a thermal bath, simulating the environment. These special types of qubits are explored in Subsections 3.3.1 and 3.3.2.

Internal two-level systems: According to Table 3.1, the following energy levels are stable enough to be suited for information encoding:

- Be⁺: Only the Hyperfine ground-states are stable. Transitions are allowed between states with a difference in angular momentum of $\Delta m_F = \pm 1$.
- Ca⁺: The Zeeman levels of both, the $S_{1/2}$ -ground states and the $D_{5/2}$ -states, are stable enough to encode information.

Motional two-level system: The motional d.o.f. can be considered as an (approximate) two-level system if it is driven by Raman pulses (π -pulses) $|0\rangle|n\rangle \rightarrow |1\rangle|n\rangle \rightarrow |0\rangle|n+1\rangle$. The excitation and the decay are both driven transitions and therefore well-controlled. They only occur between the chosen levels, all the other levels $|0\rangle|n\pm s\rangle$, $s \in \mathbb{N}$ are not populated.

3.3.1 Degenerate qubit (Battery qubit)

Single-ion qubit: The only way to implement a degenerate qubit in a single ion, is to encode it in Zeeman (ground-state) levels at zero magnetic field. *Zeeman states* are degenerate for zero magnetic field. But due to the high sensitivity of the ion's electronic structure to magnetic field noise, it is practically impossible to achieve degeneracy. One would have to perfectly compensate for all the magnetic field noise (e.g. the earth magnetic field), which would require very accurate and time-varying detection of the noise. This is not feasible in practice. Another way to protect an experiment from magnetic field noise is by shielding. A shielding can be realised with μ -metal. But it is very difficult to find an arrangement such that no additional induction between the plates occurs.

However, if we consider a qubit with non-degenerate computational basis (σ_z -eigenstates) 0, 1, the same qubit has degenerate eigenstates in the rotational \pm -basis. This possibility is used in Section 5.2.

Two-ion qubit: The combination of two *identical* qubits in two identical ions is described in a 4-dimensional Hilbertspace $\mathcal{H} = \mathbb{C}^2 \otimes \mathbb{C}^2$. A degenerate “logical” qubit can be encoded in the subspace, spanned by the two degenerate “physical” states $\{|01\rangle, |10\rangle\}$.

$$\begin{aligned}|0\rangle_L &= |0\rangle_P \otimes |1\rangle_P = |01\rangle_P \\|1\rangle_L &= |1\rangle_P \otimes |0\rangle_P = |10\rangle_P\end{aligned}\tag{3.1}$$

$|0\rangle_L, |1\rangle_L$ are degenerate logical qubits. Any single-qubit operation on the logical level (e.g. a bit-flip) corresponds to a two-ion gate on the physical level. This could require more complicated implementations.

3.3.2 Thermal Qubit

Definition (Thermal State): In principle any two-level state $\rho = p_0|0\rangle\langle 0| + p_1|1\rangle\langle 1|$, with population probabilities $p_0 > p_1$ and $p_0 + p_1 = 1$, corresponds to a thermal state at “virtual” temperature T [28]. In general this temperature does not agree with the real temperature of the system. This abstraction allows the following definitions of “real” and “virtual” thermal states.

- a) **“real” thermal state:** A state that is in contact with a thermal bath at some temperature T *thermalises* and reaches the corresponding equilibrium thermal distribution with population numbers $p_1 = e^{-i\Delta E/kT}, p_0 = 1 - p_1$. This is the natural definition of a thermal state where “real” and “virtual” temperature agree. The initialisation of such a state occurs without the employment of another energy source than the thermal energy of the environment.
- b) **“virtual” thermal state:** On a two-level system, an arbitrary distribution of the populations can be achieved on purpose by induced transitions. For an internal qubit such a state can be initialised either by optical pumping followed by spontaneous decay or as a fully induced three-level (Raman) transition. The final populations are obtained from the Rabi frequency, the pulse length and the decay rate.

In the *theoretical scheme*, the thermal qubit denotes a two-level system, whose population is initiated by intermediately coupling it to a thermal bath and letting it thermalise. In order to maintain coherence of the qubit, it needs to be isolated from the environment before and after the thermalisation process.

In *standard ion trap experiments*, thermalisation is a process that experimentalists want to avoid, since it means a loss of coherence of the ion’s state. Therefore a standard ion trap experiment is not designed for coupling and decoupling an ion’s state to the environmental thermal bath. A lot of effort is invested in order to isolate the ions, also thermally, from the environment.

The whole trap is kept at very low temperature and the ions are further cooled down by different laser cooling techniques, like Doppler cooling and sideband cooling. The low temperature improves the coherence of the ions’ internal states and brings the system into the Lamb Dicke regime (c.f. Section 1.1.4), which is a requirement for most ion manipulation schemes. An even harder restriction is required by most two-qubit gates, which use the motional state as ‘bus mode’ and only work with good fidelity for “cold” ions in their motional ground state (e.g. the Cirac&Zoller gate and the geometric phase gate, Section 2). At these cold temperatures the thermal population of the excited qubit level, according to the Boltzmann distribution, are close to zero, which is not optimal for the performance of our gate. This means the temperature in the trap itself is too low to consider it as a thermal bath.

Due to this low trap temperature and the protection of the experiment from coupling to the environment, we are left with the possibility of a “virtual” thermal state. Such a state can be

induced either by a laser, which directly addresses the internal or motional state of the ion, or by using the indirect sympathetic cooling method [11].

Thermal internal state:

- *Direct field-ion interactions:* A specific distribution of an internal state, in order to initialise a “virtual” thermal state, can be obtained by optical pumping or driving the carrier transition.
- *Indirect field-ion interaction:* The motional state can be modified indirectly by sympathetic cooling. Using sideband transformations, this (“real”) thermal motional state can be mapped onto the internal state by a sideband transition. By this process, the ion, in which the information is encoded, is not directly addressed by an EM field (e.g. laser).

Thermal motional state:

The motional state of an ion string can be considered as a thermal state. The coupling brings them in thermal equilibrium relative to each other: all ions are in the same thermal state and behave like a thermal bath. The ‘temperature’ of the thermal bath, i.e. the motional state of the string, can be controlled by lasers. In the following, three approaches to implement a thermal motional state are given:

- *Laser cooling (optical pumping):* A thermal distribution of the motional state can be obtained by laser cooling (optical pumping): an internal state is excited to an intermediate, unstable state $|0\rangle|n\rangle \rightarrow |1\rangle|n\rangle$ (e.g. the $S \leftrightarrow P$ transition), which decays spontaneously to all motional states $|0\rangle|n+s\rangle$ (not only two levels). This leads to a Boltzmann distribution for the populations of the motional state; i.e. a *thermal motional many-level state*. But a qubit requires a well-defined two-level system.
- *Anharmonic trap potential:* The application of an anharmonic trap potential changes the motional state (along the trap axis) from a h.o. into an anharmonic behaviour with linearly increasing separation of the energy levels. This allows to single out a two-level system: Either the difference between the first and second energy gap is big enough, such that the third level is not populated for thermal states at small enough temperatures. Or due to the different energy gaps the transformation between two states can be selectively addressed by a resonant em field.
- **Sympathetic cooling via a thermal bath:** The initialisation of a motional thermal state, as described above, requires internal state relaxation or sideband transformations. Both processes couple the motional state to the internal states, which destroys the coherence of the internal state [11]. If we want to run our gate several times sequentially, this can cause a problem, since we want to continue with the final qubit states of the previous gate. The problem of loss of coherence due to the coupling of internal and motional states can be circumvented by so-called *sympathetic cooling*: the ions, which carry no information serve as a thermal bath, to which the information carrying ions can be coupled and decoupled. These ‘bath’ ions can be laser cooled directly without affecting any information.

This phenomenon is used to simulate the coupling/decoupling of a motional qubit to a thermal bath: an ion (e.g. a Be^+ ion) with encoded qubit is placed in between two ions of a string of another type of ions (e.g. Ca^+ ions). The motional (i.e. thermal) state of the Ca^+ ions is controlled by external lasers. If the ions are coupled, the Be ion achieves the same motional state. This corresponds to the coupling of the Be ion to a thermal bath. To decouple the Be ion from the thermal bath, the separation between the ions must be increased in order to diminish the Coulomb interaction.

3.4 Tunable Quantities

(a) Settings that can be adjusted *before* the experiment but then must be taken as constant during the experiment.

- **Trap frequencies:** By changing the DC and RF trapping potentials the spectrum of the axial motional d.o.f. can be changed.

- *harmonic DC potential*: a change of the RF *trap frequency* $\omega_z \approx 0.1 - 3\text{MHz}$ increases/decreases the energy spacing of the h.o. spectrum

- *anharmonic DC potential*: The axial motion of the ions occur as anharmonic oscillator with non-equidistant energy separation. This allows to pick out a specific transition between two motional states, e.g. in order to consider a motional two-level system.

- The *trapping RF potential*, which determines the radial (transverse) motion of the trapped ions, can be adjusted to lift the degeneracy of the x- and y-direction.

- **External electric and magnetic fields:**

- The energy separation of *Zeeman* and *Hyperfine qubits* can be changed by adjusting the external magnetic field.

Note: The external magnetic field B and the trap frequency ω_z can be adjusted, such that the Zeeman ground levels of Beryllium fit the energy separation of two harmonic motional mode.

(b) Parameters that can be changed *during* the experiment

- **EM fields:**

- EM fields with different *intensity* and *frequency* can be turned on/off. An adjustment of the field intensity and detuning changes the *Rabi frequency* of the induced transition and hence the strength of the atom-light interaction.

- A gate can selectively be applied on a qubit by adjusting the *pulse length* and *phase* of the applied EM field.

- **External electric and magnetic fields:**

- external *magnetic fields* can be changed quickly in theory, but high fields are stored by inductive effects in the coils and therewith decay slowly

- external *electric fields* can easily and very quickly be changed

Part II

Work Extraction Gate

Chapter 4

Theoretical concept

To implement the gates, we will use electromagnetic fields (mostly lasers) to manipulate the ion's states. The interaction of the ions with the EM fields corresponds to a coupling of the ions to the environment: the ions are not anymore isolated and energy is exchanged between the ions and the EM fields.

As known from thermodynamics, both energy and entropy have to be considered as resources to extract work. We want to extract work by using only the battery qubit and the thermal energy as resources. In order to proof this, the total operation, performed on the qubit-system, has to be reversible and energy conserving.

Energy conservation is ensured if the energy, exchanged in the single gates, sum up to zero for the total (composite) gate. *Reversibility* excludes the use of field entropy as a resource. It is given if all field-atom interactions occur in a coherent way, such that the entropy of the EM fields is not changed ($\Delta S_{\text{EM}} = 0$). Photon absorption and induced emission are both coherent operations, whereas spontaneous emission (scattering) violates coherence.

4.1 Work extraction protocols

This project is embedded in theoretical work that aims to find protocols for extracting work from quantum systems.

We consider a system in which one bit of information is stored. As a classical example we can think of a so-called *Szillard engine* [1]. In quantum mechanics, such a system can be realised as a single qubit, with two degenerate eigenstates. If the qubit is in a known state, e.g. $|0\rangle$, the system carries one bit of information. Due to its function, we denote such a qubit as '*Szilard qubit*'.

The '*Szilard qubit*' is coupled to a 'storage' system, whose energy can be changed by performing work on it or extracting work from it. In a quantum mechanical frame, we can think of a system with discrete energy levels. The excitation of its state to a higher level corresponds to the storage of work. Both, the '*Szilard qubit*' and the storage system, are coupled to a thermal bath at a given temperature T and can therewith exchange an arbitrary amount of thermal energy with the environment.

The Landauer Principle connects the *2nd law of Thermodynamics* with information theory. It states, that a system, as described above, can perform a maximum amount of work of $\Delta W = kT \ln 2$ on the storage system.

Quantum mechanics has the advantage that it naturally provides discrete states and energy levels.

This simplifies the abstraction of the system and the implementation of a work extraction process. All investigations of the work extraction process are done within the frame of *resource theory of thermodynamics*. This restricts the set of allowed operations onto energy conserving unitaries and the unlimited exchange of energy with the thermal bath at given temperature T [26]. In this context, any state which is not a thermal state is considered as a resource. In this sense the only resource available for the work extraction is the ‘Szilard’ or information qubit.

Protocol to extract work from qubits: Several protocols to implement work extraction from quantum systems have been developed. This project is based on a specific protocol, developed in [26]. This gate acts on a system, which is similar to the one described above (c.f. Figure 4.1):

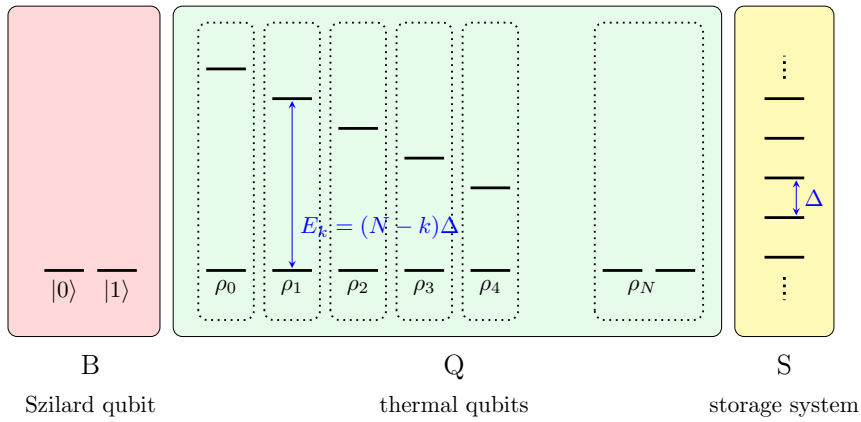


Figure 4.1: System, on which the work extraction protocol acts. In this system, the storage system shows a discrete, instead of continuous, spectrum with energy spacing Δ . The energy separations of the thermal qubits ρ_k are chosen, such that they fit a multiple of Δ ($E_k = kT \ln\left(\frac{1-p_k}{p_k}\right) = (N - k)\Delta$). Hence, in the k -th step of the protocol, the state of the storage system is lifted or lowered by $(N - k)\Delta$.

- (1) A *battery qubit* B with degenerate basis $\{|0\rangle_B, |1\rangle_B\}$ is transformed from an initially pure state to a mixed state. Its denotation as battery qubit indicates its function as a resource for the work extraction process. This is our ‘Szilard qubit’.
- (2) A *storage system* S , on which work is performed and which stores this energy. S is implemented in a quantum system with infinitely many equidistant energy levels $|n\rangle_S$ with energy separation Δ . Work is performed on the system by lifting the population from state $|n_0\rangle$ ($E = E_0$) to a state $|n_1\rangle$ of higher energy ($E_1 - E_0 = k\Delta$, $k \in \mathbb{N}$). The energy is then stored in the population of the (stable) excited state. Letting S decay ($|n_1\rangle \rightarrow |n_0\rangle$), we gain back the work $k\Delta$. The idea of considering work as lifting a (quantum) state to a higher energy level is discussed in [28].
- (3) A *storage system* S , on which work is performed and which stores this energy. S is implemented in a quantum system with a continuous degree of freedom x with corresponding energy states $|x\rangle_S$. Work is performed on the system by lifting the population from state $|x_0\rangle$ ($E = E_0$) to a state $|x_1\rangle$ of higher energy ($\Delta E = E_1 - E_0$). The energy is then stored in the population of the (stable) excited state. Letting S decay ($|x_1\rangle \rightarrow |x_0\rangle$), we gain back the work ΔE . The idea of considering work as lifting a (quantum) state to a higher energy level is discussed in [28].

- (4) The coupling to the thermal bath is realised by additional N *thermal qubits* Q_k , $k = 1, \dots, N$ with different energy separation, which are all in a thermal state with relation to the temperature T . The energy separation of qubit k is chosen such that the population of its excited state is given by $p_k = \frac{k}{2N}$. This requires an energy gap of $E_k = kT \ln\left(\frac{1-p_k}{p_k}\right)$. These qubits can interact with the battery qubit and storage system. The coupling of B and S to a thermal bath can be simulated by the interaction with arbitrary many of these thermal qubits.

Work extraction is achieved by applying the following unitary on the system, including B , Q_k and S :

$$\begin{aligned} \tilde{U}_k = & \sum_x \left(|00\rangle\langle x| \langle 11| \langle x - E_k|_{BQ_kS} + |11\rangle\langle x - E_k| \langle 00| \langle x|_{BQ_kS} \right) \\ & + \left(|01\rangle\langle 01|_{BQ_k} + |10\rangle\langle 10|_{BQ_k} \right) \otimes \mathbb{I}_S, \quad k = 1, \dots, N \end{aligned} \quad (4.1)$$

The total gate is implemented by the subsequent application of these operations, where in the k -th step the unitary \tilde{U}_k is applied on the thermal qubit k and the final states of the $(k-1)$ -th operation of the other two systems. In the asymptotic limit ($N \rightarrow \infty$), the average extracted work approaches the optimum ($\langle E \rangle_S = kT \ln 2$) and the energy spread, given by the variance divided by the average energy, vanishes: $\frac{\Delta E_S^2}{\langle E \rangle_S} \sim \frac{1}{\sqrt{N}}$.

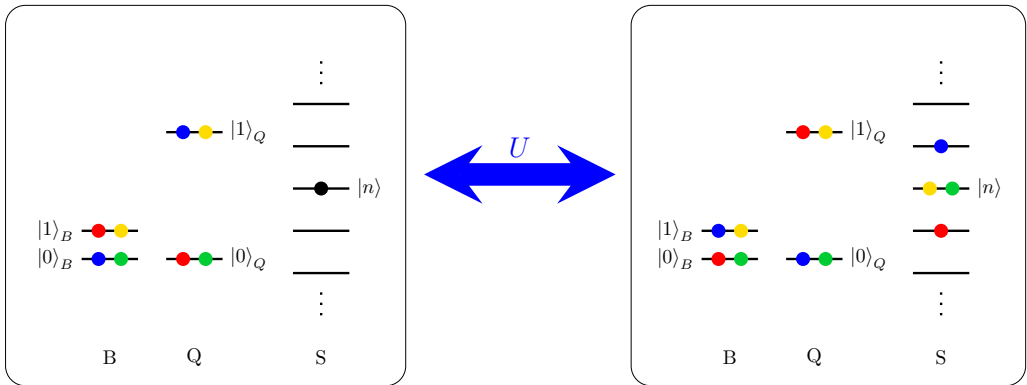


Figure 4.2: Sketch of the simplified work extraction gate. B : battery qubit, Q : thermal qubit, S : storage system. The coloured dots indicate the four different possible initial states (left box) and the corresponding action of the gate. The storage system is initially in the same state $|n\rangle$ for all internal states (indicated as black) but splits under the action of the gate, conditioned on the internal state. The green and yellow states remain unchanged, whereas from the blue state work can be extracted as visible in the last box.

4.2 Experimental implementation of a simplified gate

This project aims to experimentally implement a simplified version of the work extraction gate, described above. As experimental setup we chose ion traps, due to their promising progress towards quantum computation in the recent years.

The protocol, which we want to implement, describes one iteration step of the work extraction gate, described above. It corresponds to a single application of the gate, given in Equation 4.1. The gate has been adapted to a storage system S with discrete (instead of continuous) energy spectrum, which is easier to implement. Ideally such a system is realised by a harmonic oscillator,

4.2. EXPERIMENTAL IMPLEMENTATION OF A SIMPLIFIED GATE

which provides a large number of energy levels of constant separation ΔE . Furthermore, we allow a small non-degeneracy of the battery qubit B .

The unitary \tilde{U}_k in Equation 4.1 can be adapted in two ways, depending on the choice of energy gaps of the three systems (c.f. paragraph below):

$$\begin{aligned} U^{(a)} &= \sum_n \left(|01\rangle_{BQ} |n\rangle_S \langle 10|_{BQ} \langle n+1|_S + |10\rangle_{BQ} |n+1\rangle_S \langle 01|_{BQ} \langle n|_S \right) \\ &\quad + \left(|00\rangle_{BQ} \langle 00|_{BQ} + |11\rangle_{BQ} \langle 11|_{BQ} \right) \otimes \mathbb{I}_S \\ U^{(b)} &= \sum_n \left(|11\rangle_{BQ} |n\rangle_S \langle 00|_{BQ} \langle n+1|_S + |00\rangle_{BQ} |n+1\rangle_S \langle 11|_{BQ} \langle n|_S \right) \\ &\quad + \left(|10\rangle_{BQ} \langle 10|_{BQ} + |01\rangle_{BQ} \langle 01|_{BQ} \right) \otimes \mathbb{I}_S. \end{aligned} \quad (4.2)$$

Some straight-forward calculations show, that the action of these gates corresponds to a swap of the distributions of qubit B and Q : the initially pure battery qubit B ends in a thermal distribution whereas the thermal qubit Q ends in a pure ground-state qubit (which can be thermalised again).

$$\rho_B^{(i)} = (1 - \epsilon)|0\rangle\langle 0| + \epsilon|1\rangle\langle 1| \longrightarrow \rho_B^{(f)} = (1 - p)|0\rangle\langle 0| + p|1\rangle\langle 1| = \sigma_Q^{(i)} \quad (4.3)$$

$$\sigma_Q^{(i)} = (1 - p)|0\rangle\langle 0| + p|1\rangle\langle 1| \longrightarrow \sigma_Q^{(f)} = (1 - \epsilon)|0\rangle\langle 0| + \epsilon|1\rangle\langle 1| = \rho_B^{(i)} \quad (4.4)$$

The performance of this gate is far below the optimum, with an energy gain of $E_S \approx 0.28 \cdot kT \approx 0.40 \cdot kT \ln 2$ [1].

An optimal work extraction scheme could be achieved by the repeated implementation of U , while replacing the qubit Q after every step by a thermal qubit of smaller energy gap $\omega_{Q,k}$. In order to fulfil energy conservation, the difference in the energy separation of two thermal qubits in subsequent applications has to be equal to the energy gap of the storage system (or a multiple of it): $\omega_{Qk} - \omega_{Q,k+1} = n\omega_S$, $n \in \mathbb{N}$. In our experimental setup it appears to be difficult to change the energy separation of the thermal qubit while maintaining a constant separation in the battery qubit (c.f. Section 5.2).

One could also imagine a repeated application of $U^{(a,b)}$, while after every step the qubit Q is thermalised again (or replaced by a thermal qubit) and the battery qubit is replaced by a new one (in a well-known state). This motivates the denotation ‘‘battery qubit’’: a battery can be produced independently of the system and replaced in order to refresh the resource.

Energy conservation: In principle, this simplified system has to obey the same restrictions as the optimal system, allowing only energy conserving unitaries and the exchange of thermal energy with the heat bath. This requires total isolation of the system from any other energy source. The total gate $U^{(a,b)}$ fulfils energy conservation for following restrictions on the energy gaps of the three systems:

$$\begin{cases} U^{(a)} : & \Delta E_Q - \Delta E_B = \Delta E_S \\ U^{(b)} : & \Delta E_Q + \Delta E_B = \Delta E_S \end{cases} \quad (4.5)$$

The gate needs to be implemented as a circuit, composed by the elementary physical operations given in Section 2.2. All of these operations require the system to be coupled to an external EM field, e.g. a laser field.

The only gate that can be driven without the absorption of external energy, corresponds to the coupling of two states (internal or motional d.o.f.) with equal energy. As an example we can think of a rotation between two degenerate internal states or a redsideband transformation on an ion, where the internal energy gap ω_{eg} is equal to the frequency of the motional mode ω_m . This kind of

gates can be realised by coupling the ions to a standing wave EM field, which does not transfer any energy to the ion. But the EM field is nevertheless required, since otherwise the different states are not coupled: the interaction Hamiltonian, and therewith all terms that couple different states, vanishes.

All other gates, such as an arbitrary qubit rotation, absorbs or releases energy from the EM field. Equation 4.5 only ensures, that in the total circuit, the same amount of energy was absorbed as emitted. Intermediate energy absorption is still allowed.

The necessity of an EM field motivates the extension of our system to incorporate this external field.

As a *toy model*, we can think of a cavity that contains photons of the required resonant frequencies and our qubit systems B , Q and S . In some operations of the circuit, a photon would be absorbed. In other operations, a photon would be (coherently) emitted. Equation 4.5 ensures that at the end of the gate, the total energy of the cavity photons would be equal to the initial energy amount. But the cavity would in general contain photons of different frequencies than initially. (Considering laser beams instead of single photons, this means that a photon is absorbed from laser A and later a photon is emitted to a different laser mode B.)

Strict isolation and energy conservation would prohibit intermediate energy absorption and emis-

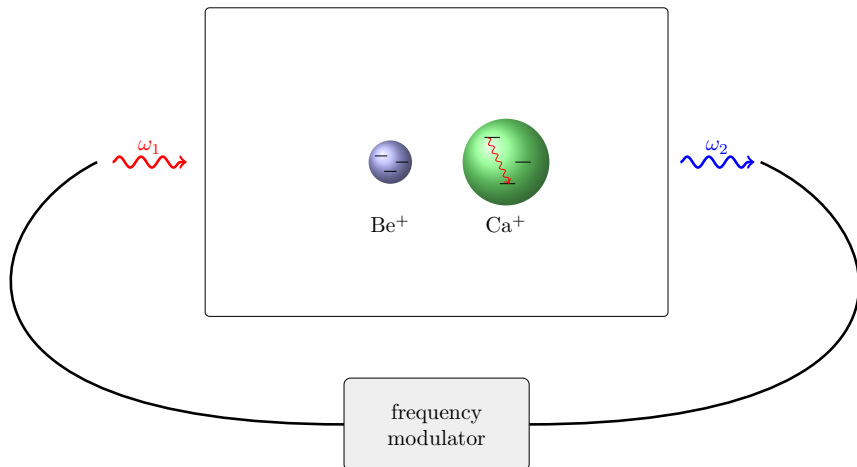


Figure 4.3: *Toy model*: The figure shows a cavity with ions, which are addressed by EM fields from the left (ω_1). In return, photons are coherently emitted by the ions in some of the gates (ω_2). The total energy from the incoming photons has to meet the total energy of the outgoing photons. If all ion-field interactions are coherent operations, the emitted photons can be transformed back to their initial mode in an energy conserving way.

sion by the qubits. Such an implementation could only be realised if the three systems B , Q and S could directly be coupled to each other and energy (and entropy) could directly be transferred between the systems. As a thought experiment one may think of a process, in which qubit Q relaxes to its ground state and emits a photon of energy ω . This photon could be absorbed again by the storage system S . Such a process requires a perfect control of single qubits and the ions and is therefore impractical.

The idea of strict energy conservation can be eased by following thought experiment (c.f. Figure 4.3): Energy conservation is fulfilled, as long as the final cavity photons can be *reversibly* converted back to the initial photons. This process is conceptually feasible, if no irreversible, i.e. no incoherent, processes are involved in the total circuit implementation. All operations presented in Section 2.2 are coherent processes (up to higher-order perturbative terms).

In our setting, we will consider classical EM fields, which consist of many photons, instead of single photons. For such a system, the requirement of coherent processes is equivalent to requiring entropy conservation for the EM field:

$$\Delta S_{\text{EM}} = 0.$$

In order to prove that the ions did absorb no energy from the lasers, it will be necessary to compare the incoming and outgoing laser intensities. This is experimentally very challenging, since the uncertainty in laser intensity is about $\pm 5\%$, which is much larger than the energy differences in atomic transitions. An amount of energy, equal to the extracted work, could just appear as noisy disturbance. It would therefore not be possible to experimentally check, whether energy was absorbed from the lasers or not.

4.3 Decomposition of the work extraction Gate

In this section, approaches to a mathematical decomposition of the work extraction gate are presented. It can be summarised that a mathematical decomposition into logical gates is not successful, since it leads to a very long and therewith inefficient circuit (high number of gates). Nevertheless, crucial evidence about the structure of the gate followed from the decomposition: the gate can be expressed in terms of a controlled sideband transformation. This idea could be implemented in the final circuit in Section 5.

Furthermore, the storage system is discussed, since the theoretical scheme has to be adapted from an ideal, infinite system to the bounded systems, available in the experiment.

Bounded Storage system S : In the experimental setting that we consider, it is not possible to find a storage system with an infinite number of energy levels as used in the theoretical concept. All systems are at least *bounded* at the bottom by a ground state. This causes problems when applying the unitary $U^{(a)}$ (4.2) to the storage ground state $|0\rangle_S$, since there is no $| -1 \rangle_S$ -level onto which the ground state can be lowered.

This can be solved by thinking of a *circular* storage system as circular; i.e. the ground state $|0\rangle_S$ is “lowered” to a given maximal state $|n_{max}\rangle$ and vice versa ($|0\rangle_S \leftrightarrow |n_{max}\rangle_S$). But this swap violates energy conservation. The operation can be kept in the “energy conserving regime” when restricting our system to the initial state $\sim |0\rangle_B$.

In the final implementation, the gate is adapted such that it acts as the identity operator on the boundary states $|0\rangle_S$ and $|n_{max}\rangle_S$.

4.3.1 Decomposition into CNOT gates:

- a) **Two-level storage system S :** In the simplest case, the storage system is considered to be a two-level system. The total initial system is given by the product state $\rho = \rho_B \otimes \rho_Q \otimes \rho_S$ with the thermal state $\rho_Q = (1-p)|0\rangle\langle 0|_Q + p|1\rangle\langle 1|_Q$, $p = \frac{1}{Z}e^{-\Delta E_Q \beta}$ and the almost pure battery qubit $\sigma_B = (1-\epsilon)|0\rangle\langle 0| + \epsilon|1\rangle\langle 1|$.

This system serves only as a “toy model”. In order to be able to distinguish the case of work extraction and work performance (i.e. raising or lowering of the storage system’s state), our storage system requires at minimum three levels ($n \geq 3$).

To achieve a unitary operation, we consider a circular system, as described above.

$$U^{(a)} : \begin{cases} |000\rangle_{BQS} \leftrightarrow |000\rangle_{BQS} \\ |010\rangle_{BQS} \leftrightarrow |101\rangle_{BQS} \\ |100\rangle_{BQS} \leftrightarrow |011\rangle_{BQS} \\ |110\rangle_{BQS} \leftrightarrow |110\rangle_{BQS} \end{cases}$$

$$U^{(a)} = (|01\rangle\langle 10| + |10\rangle\langle 01|)_{BQ} \otimes \sigma_x, S + (|00\rangle\langle 00| + |11\rangle\langle 11|)_{BQ} \otimes \mathbb{I}_S \quad (4.6)$$

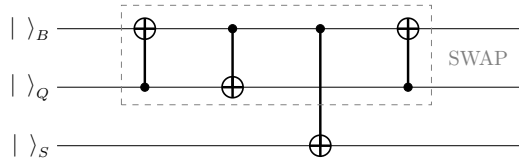


Figure 4.4: Work extraction gate for a two-level storage system S . The CNOT gate represents the σ_x operator.

If we consider only the battery B and the thermal Q qubit, the gate corresponds to a SWAP operation:

$$\begin{aligned} \sigma_B^{(i)} &= (1 - \epsilon)|0\rangle\langle 0| + \epsilon|1\rangle\langle 1| \longrightarrow \sigma_B^{(f)} = (1 - p)|0\rangle\langle 0| + p|1\rangle\langle 1| = \rho_Q^{(i)} \\ \rho_Q^{(i)} &= (1 - p)|0\rangle\langle 0| + p|1\rangle\langle 1| \longrightarrow \rho_Q^{(f)} = (1 - \epsilon)|0\rangle\langle 0| + \epsilon|1\rangle\langle 1| = \sigma_B^{(i)} \end{aligned}$$

- b) **n -dimensional storage system S :** The general n -qubit gate $U^{(a)}$ acts on all three systems. The third term accounts for the boundary states of our storage system ($n \in [0, N]$).

$$\begin{aligned} U^{(a)} &= \sum_{0 < n \leq N} (|01\rangle\langle 10|_{BQ} \otimes |n-1\rangle\langle n|_S) + \sum_{0 \leq n < N} (|10\rangle\langle 01|_{BQ} \otimes |n+1\rangle\langle n|_S) \\ &\quad + (|10\rangle\langle 10|_{BQ} \otimes |0\rangle\langle 0|_S + |01\rangle\langle 01|_{BQ} \otimes |N\rangle\langle N|_S) \\ &\quad + (|00\rangle\langle 00|_{BQ} + |11\rangle\langle 11|_{BQ}) \otimes \mathbb{I}_S \end{aligned} \quad (4.7)$$

By a simple decomposition, $U^{(1)}$ can be broken down to a controlled unitary $(n-1)$ -qubit gate V that acts only on two systems (e.g. Q and S) and is controlled by the third system B (c.f. Figure 4.5).

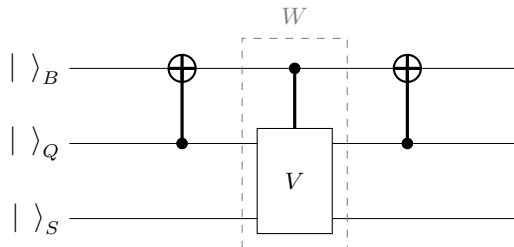


Figure 4.5: Simplified work extraction gate for a storage system of arbitrary dimension n .

$$U = (\text{CNOT}_{BQ} \otimes \mathbb{I}_S) \underbrace{(|0\rangle\langle 0|_B \otimes \mathbb{I}_{QS} + |0\rangle\langle 0|_B \otimes V)}_W (\text{CNOT}_{BQ} \otimes \mathbb{I}_S) \quad (4.8)$$

$$\begin{aligned}
 |00n\rangle &\xrightarrow{\text{CNOT}} |00n\rangle \xrightarrow{W} \mathbb{I}_B \otimes \mathbb{I}_{QS} |00n\rangle = |00n\rangle \xrightarrow{\text{CNOT}} |00n\rangle \\
 |01n\rangle &\longrightarrow |11n\rangle \rightarrow \mathbb{I}_B \otimes V |10n\rangle = |00n+1\rangle \longrightarrow |10n+1\rangle \\
 |10n\rangle &\longrightarrow |10n\rangle \rightarrow \mathbb{I}_B \otimes V |11n\rangle = |00n-1\rangle \longrightarrow |01n-1\rangle \\
 |11n\rangle &\longrightarrow |01n\rangle \rightarrow \mathbb{I}_B \otimes \mathbb{I}_{QS} |01n\rangle = |00n\rangle \longrightarrow |11n\rangle
 \end{aligned} \tag{4.9}$$

$$V = \left(\begin{array}{ccc|cc} 0 & & & & \\ \cdots & 0 & & D_+ & \\ & 1 & & & \\ \hline D_- & & 1 & 0 & \cdots & 0 \end{array} \right) : \left\{ \begin{array}{ll} |1\rangle|n\rangle_{QS} \rightarrow |0\rangle|n+1\rangle_{QS}, & 0 \leq n < N \\ |0\rangle|n\rangle_{QS} \rightarrow |1\rangle|n-1\rangle_{QS}, & 0 < n \leq N \\ |1\rangle|N\rangle_{QS} \rightarrow |1\rangle|N\rangle_{QS} & \\ |0\rangle|0\rangle_{QS} \rightarrow |0\rangle|0\rangle_{QS} & \end{array} \right\} \text{ boundary states} \tag{4.10}$$

with the off-diagonal matrices $D_- = \begin{pmatrix} 0 & & & \\ 1 & \cdots & 0 & \\ & \cdots & 1 & 0 \end{pmatrix}$, $D_+ = \begin{pmatrix} 0 & 1 & & \\ & \cdots & 0 & \\ & & 1 & 0 \end{pmatrix}$.

The non-zero entries on the diagonal of V account for the boundary states of the storage systems ($|n\rangle = |0\rangle$ or $|N\rangle$), which have to be treated as special cases, as indicated in equation 4.7.

Note, that V corresponds to a red sideband transformation (RSB) a hence we need to know how to implement a *controlled sideband transformation* W . For a bounded h.o.-system ($n \in [0, N]$) the sideband transformations are given by:

$$\begin{aligned}
 U_{BSB} &= \sum_{0 \leq n \leq N} (|0\rangle|n\rangle\langle 1|n+1\rangle + |1\rangle|n+1\rangle\langle 0|n\rangle) + |1\rangle|0\rangle\langle 1|0\rangle + |0\rangle|N\rangle\langle 0|N\rangle \\
 U_{RSB} &= \sum_{0 \leq n \leq N} (|0\rangle|n+1\rangle\langle 1|n\rangle + |1\rangle|n\rangle\langle 0|n+1\rangle) + |0\rangle|0\rangle\langle 0|0\rangle + |1\rangle|N\rangle\langle 1|N\rangle \\
 U_{BSB} &= \left(\begin{array}{ccc|cc} 0 & & & & \\ \cdots & 0 & & D_+ & \\ & 1 & & & \\ \hline D_- & & 1 & 0 & \cdots & 0 \end{array} \right), \quad U_{RSB} = \left(\begin{array}{ccc|cc} 0 & & & & \\ \cdots & 0 & & D_+ & \\ & 1 & & & \\ \hline D_- & & 1 & 0 & \cdots & 0 \end{array} \right)
 \end{aligned}$$

Using the two-ion MS gate, an implementation of such a controlled redsideband transition could be found, which is described in Section 5. This implementation was developed by directly decomposing $U^{(a)}$ into elementary *physical* gates (rotations, sideband transformations and the MS-gate).

Before following this more intuitive way, we tried to further decompose the gate into elementary *logical* gates. As universal set of gates we chose the rotations and the CNOT gate. In the following a brief sketch of our attempt is given:

A controlled gate is a special case of a multiplexed gate $A = A_0 \oplus A_1$. Such a multiplexed gate can be “decomplexed” into rotations and lower-dimensional gates, using the Cosine-Sine decomposition (Section 2.3). These gates can then be further decomposed into single- and two-qubit rotations [22]. For an arbitrary two-qubit gate, there exists an algorithm for its decomposition into single-qubit rotations and a geometric phase gate (CPhase) [23]. Either, this geometric phase gate can directly be implemented, or the CPhase gate can be expressed in terms of CNOT

gates and single-qubit rotations (c.f. Section 2.1). This procedure decomposes the gate $U^{(a)}$ into CNOTs and single-qubit rotations.

The resulting circuit would not be optimal in terms of the number of elementary gates (CNOTs and rotations), especially since the CNOT gate needs to be further decomposed, either into rotations and sideband transformations (Cirac&Zoller gate) or into rotations and two MS-gates (c.f. Section 2.2.2).

Chapter 5

Experimental Realisation

5.1 Implementation using the MS-gate

For the following gate implementation, the battery and the thermal qubit are encoded in internal states of two different ions, which are labelled as B and Q in correspondence with the encoded battery and thermal qubits. The storage system is given by a common motional mode of the two ions. For each ion we consider four internal states. The states $|0\rangle_{B,Q}, |1\rangle_{B,Q}$ denote the *computational qubits*. The states $|\tilde{0}\rangle_{B,Q}, |\tilde{1}\rangle_{B,Q}$ are introduced as *auxiliary qubits*.

The total gate is illustrated in Figure 5.1 according to Equation 5.1. The decomposition consists of a total of *six gates*: four two-ion Mølmer-Sørensen-gates (MS-gates), one red sideband (RSB) transition and one bit flip (π -pulse). Note, that we choose to implement the gate $U^{(a)}$ (c.f. Chapter 4, Equation 4.2), but the scheme can easily be adapted to the implementation of $U^{(b)}$. The corresponding gates are listed in the Appendix B.

$$\begin{aligned}
 U^{(a)} &= \sum_n \left(|01\rangle\langle 10|_{BQ} \otimes |n\rangle\langle n+1|_S + |10\rangle\langle 01|_{BQ} \otimes |n+1\rangle\langle n|_S \right) \\
 &\quad + \left(|00\rangle\langle 00|_{BQ} + |11\rangle\langle 11|_{BQ} \right) \otimes \mathbb{I}_S \\
 &= \left[U_\pi^{(MS,0)} \otimes \mathbb{I}_S \circ U_\pi^{(MS,1)} \otimes \mathbb{I}_S \right] \circ [\mathbb{I}_B \otimes R^+(\pi, 0)_{QS}] \circ [R(\pi, 0)_B \otimes \mathbb{I}_{QS}] \\
 &\quad \circ \left[U_\pi^{(MS,0)} \otimes \mathbb{I}_S \circ U_\pi^{(MS,1)} \otimes \mathbb{I}_S \right]
 \end{aligned} \tag{5.1}$$

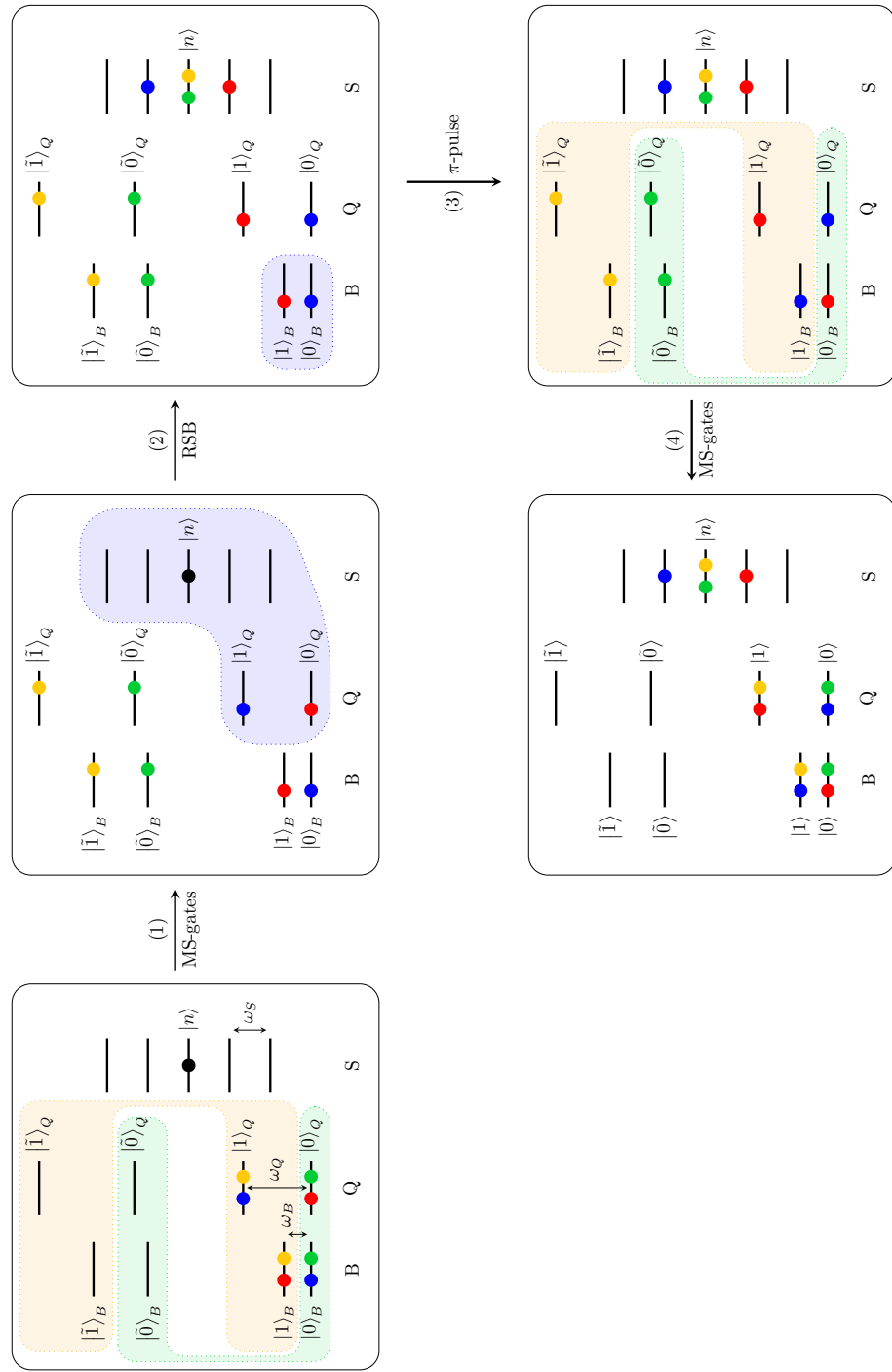


Figure 5.1: Implementation of the work-extraction gate using two ancilla qubits and the MS-gate. The colours indicate the four different possible initial states (first box) and the corresponding action of the gate. The storage system (motional state) is initially in the same state $|n\rangle$ for all internal states (indicated as black) but splits under the action of the gate, conditioned on the internal state. The green and yellow states remain unchanged, whereas from the blue state work can be extracted as visible in the last box. The coloured boxes enclose the states that are involved in the next step of the gate.

How to read the graphics:

Following states are indicated in the Figure:

- B and Q denote two ions; each of them with four energy levels indicated. The levels $|0\rangle$ and $|1\rangle$ are called *computational qubits*, $|\tilde{0}\rangle$ and $|\tilde{1}\rangle$ are *ancilla or auxiliary qubits*.
- S depicts a common motional mode of the two ions.

The coloured dots on the energy levels indicate the four different possible initial states (first box: e.g. the initial state $|00\rangle_{BQ}$ is indicated by the green dots). The storage system (motional state) is initially in the same state $|n\rangle$ for all internal states (indicated as black) but splits under the action of the gate, conditioned on the internal state.

The dashed lines enclose the states which are involved in the next step of the gate; e.g. in step two the qubit $|0\rangle, |1\rangle$ of ion Q and the common motional mode S are involved.

Gate implementation: In the following, the four individual steps of the gate implementation are described. It is important to note that the two ions B and Q are exchangeable, i.e. both can play the role of the control qubit in the second step (RSB transition). This could simplify the experimental implementation of the scheme.

1) MS-gates: Two MS-gates, applied on the joint system of the battery and the thermal qubit, excite the states $|00\rangle_{BQ}$ to $|\tilde{0}\tilde{0}\rangle_{BQ}$ and $|11\rangle_{BQ}$ to $|\tilde{1}\tilde{1}\rangle_{BQ}$ (Figure: yellow and green state). Guaranteed that the states $|\tilde{0}\rangle_B, |\tilde{1}\rangle_Q$ are initially unoccupied, all the other states of the joint system remain unchanged (blue and red state). The MS-gates can be performed using the common “stretching”-mode of the two ions.

$$U_{\pi}^{(MS,0)} : \begin{cases} |00\rangle_{BQ} \leftrightarrow |\tilde{0}\tilde{0}\rangle_{BQ} \\ |0\tilde{0}\rangle_{BQ} \leftrightarrow |\tilde{0}0\rangle_{BQ} \end{cases}, \quad U_{\pi}^{(MS,1)} : \begin{cases} |11\rangle_{BQ} \leftrightarrow |\tilde{1}\tilde{1}\rangle_{BQ} \\ |1\tilde{1}\rangle_{BQ} \leftrightarrow |\tilde{1}1\rangle_{BQ} \end{cases}$$

After the MS-gates, any controlled operation, which is conditioned on *two* qubits being in the excited $|1\rangle$ -state (or $|0\rangle$ -state), can be reduced to a normal controlled operation, which is conditioned only on *one* ion being in the $|1\rangle$ -state ($|0\rangle$ -state).

2) An RSB transition of ion Q *coherently* changes the motional state and flips the computational qubit of the ion Q :

$$R^+(\pi, 0) : |0\rangle_Q |n\rangle_S \leftrightarrow |1\rangle_Q |n-1\rangle_S \quad (\theta = \pi, \text{ at zero phase } \phi = 0)$$

3) Bit-flip on ion B : The computational qubit of ion B has to be flipped by applying a π -pulse on its carrier transition.

$$R(\pi, 0) : |0\rangle_B \leftrightarrow |1\rangle_B \quad (\theta = \pi, \text{ at zero phase } \phi = 0)$$

4) reverse the two MS-gates: (as in 1))

5.2 Encoding of the 3 systems

In the following I want to list the most important properties required for the different subsystems B , Q , S and give some proposals for their experimental implementation, which respect the theoretical

and experimental restrictions. The optimal encoding scheme is a trade-off between different criteria concerning the energy gaps and the ions' mass. For more details about the ions and qubit encoding I refer to Sections 3.2 and 3.3.

- **Ions of different weight:** In order to achieve a measurable amount of extracted work, we will apply our gate $U^{(a)}$ several times. After each application we need to reset the battery and the thermal qubit. This reset requires energy, which does not count for the energy balance, since we can think of it as taking fresh qubits. However, it is important to not disturb the storage system S in this reset process.

The reset, i.e. the preparation of an intended qubit state, can be done by several optical pumping steps. In each step, photons are scattered. Every such photon transfers a recoil energy of $E_{rec} \sim \eta^2 \sim 1/m_{ion}$ to the ion (c.f. Section 1.1.4). This perturbs the motional modes of the ion string, which concerns also the storage system.

The preparation of a pure state requires more optical pumping steps than the preparation of a thermal state. Therefore we choose Ca as the heavier ion for encoding the pure battery qubit B .

- **Energy gaps:** Energy conservation requires $\omega_B - \omega_Q = \omega_S$, with ω_i the energy difference of the computational qubit i and the motional mode frequency $\omega_m \sim 4 - 400\text{MHz}$. (For the implementation of $U^{(b)}$ it has to be adapted to $\omega_B + \omega_Q = \omega_S$). If we require a battery qubit B close to degeneracy, we also need a thermal qubit Q with a very small energy gap. This restricts the encoding of qubit Q to Zeeman or Hyperfine qubits. For optical qubits, like the $\{|S\rangle, |D\rangle\}$ two-level system of Ca, it is impossible to achieve energy conservation.
- **Selectivity of the transitions:** All induced transitions (MS-gates, RSB and π -pulse) should be driven on frequencies that are far detuned from the other transitions in both ions, in order to ensure good selectivity. In the Be ion, this is achieved by choosing both levels of the auxiliary qubit within the same hyperfine manifold ($\tilde{\omega}_B \sim 100\text{MHz}$) and the computational levels in different manifolds ($\omega_B \sim 1.25\text{GHz}$).

If the energy gap of a transition is in the RF regime and close to the motional mode, problems could occur with the resolution of the intended excitation. This problem could occur for transitions between Hyperfine levels within the same manifold ($\omega_m \sim \omega \approx 100\text{MHz}$).

Based on the above criteria two encoding schemes were developed. The first one considers two different qubits in two identical ions (Ca). This simplifies the application of the MS gate, but the energy separation of the battery and thermal qubit are similar. The second approach benefits of an alternating string by using one Ca and one Be ion (i.e. different qubits in two different ions). In both schemes, the **Storage system** S is encoded in the motional COM-mode, due to following reasoning: To achieve a large number of (equidistant) states, we need to encode the storage system in the motional state. It is important to choose for the MS-gate and the storage system independent oscillation modes (e.g. the breathing mode and the COM mode). Since the Ca ion is much heavier, the common COM-motion corresponds approximately to the motion of the Ca ion. On contrary, the light mass of the Be ion allows a much higher recoil energy by a state-dependent force, applied on the Beryllium.

To mediate interactions between the two ions for the MS-gates, the stretching mode is used.

5.2.1 Different qubits in two Ca ions

a) Two Ca ions in an inhomogeneous B-field:

Consider two Ca ions in an inhomogeneous B-field ($\vec{\nabla} \vec{B} \neq 0$). A non-zero field gradient leads to a different Zeeman splitting in two ions at different positions. If the battery and thermal qubit are encoded in the Zeeman S - and D -levels, they have different energy separation. The qubit encoding is described in Table 5.1.

Computational Qubit:

$$\begin{aligned} |0\rangle &= \left|S_{1/2}, m_s = -1/2\right\rangle \\ |1\rangle &= \left|S_{1/2}, m_s = +1/2\right\rangle \end{aligned}$$

$$\omega_B = \omega_{01} \sim 300\text{MHz}$$

Auxiliary Qubit:

$$\begin{aligned} |\tilde{0}\rangle &= \left|D_{5/2}, m_j = -1/2\right\rangle \\ |\tilde{1}\rangle &= \left|D_{5/2}, m_j = +1/2\right\rangle \end{aligned}$$

$$\tilde{\omega}_B = \omega_{\tilde{0}\tilde{1}} \sim 200\text{MHz}$$

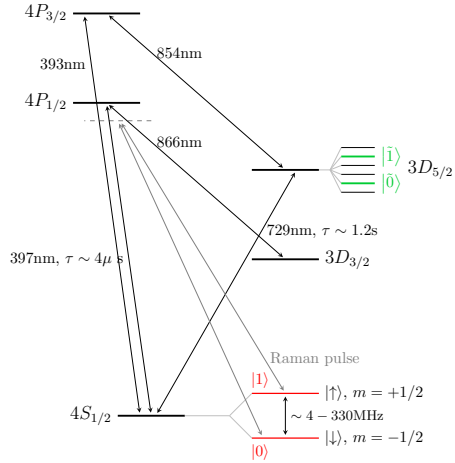


Table 5.1: Encoding of the computational and auxiliary qubit levels in a Ca^+ ion

The MS-gates act on the optical transitions $|S\rangle_{\uparrow,\downarrow} \leftrightarrow |D\rangle_{m_1,m_2}$, where the selective transition is guaranteed by polarised beams. The energy separations of these transitions only differ by the difference in their Zeeman shifts: $\omega_1 \approx \omega_{SD}^{(1)} + \delta, \omega_2 \approx \omega_{SD}^{(2)} - \delta$ with $\frac{\omega_{SD}^{(1)} - \omega_{SD}^{(2)}}{\omega_{SD}^{(1)}} \approx \frac{2\text{MHz}}{200\text{THz}} \approx 10^8$. This difference might be small enough to assume identical coupling of the two qubits ($\Omega_1 \approx \Omega_2 = \Omega$) and approximate the system with two identical qubits.

- ⊕ MS-gate can be applied on two identical ions
- ⊕ Due to $\omega_B \approx \omega_Q$, the frequency of the COM motional mode $\omega_m = \omega_S = \omega_Q - \omega_B$ is small and can still be treated as a perturbation on the internal energy structure.
- ⊖ Non-degenerate battery qubit B

b) Degenerate battery qubit B , encoded in σ_x -eigenstates:

Consider two qubits, encoded in the ground-state Zeeman levels of two Ca ions. In the computational basis $\{|0\rangle, |1\rangle\}$, the qubit energy separation is equal to the Zeeman energy splitting. However, in the rotational basis $|\pm\rangle = \frac{1}{\sqrt{2}}(|0\rangle \pm |1\rangle)$, the two qubit states are degenerate. This can be used to encode a degenerate battery qubit.

For both Ca ions we choose the four levels, indicated in Table 5.1. In order to transform into the rotational basis for the battery qubit, we enclose the circuit, given in Equation 5.1, by two Hadamard gates on the computational qubit of the battery ion B .

- ⊕ MS-gate can be applied on two identical ions
- ⊖ Degenerate battery qubit B
- ⊖ Large motional gap $\omega_m = \omega_S \approx \omega_Q$ ⊖ For the application of the RSB and the bit flip, the ions must be separated in order to ensure, that only one ion is addressed by the EM field.

5.2.2 Different ions

A very clear distinction between the two qubits is achieved when encoding the qubits in two ions of different species: one Be ion with four states encoded in the Hyperfine ground levels and one Ca ion with a qubit encoded in the Zeeman ground states and two auxiliary states in the D-level

Zeeman states. The different mass and laser-ion couplings complicate the two-ion interaction, i.e. the MS gate. The transitions, involved in an MS-gate, are in a totally different energy range: $\omega_1 \approx \omega_{Be} + \delta \approx 1.25\text{GHz}$, $\omega_2 \approx \omega_{Ca} - \delta \approx 200\text{THz}$. The small energy gaps in the RF range ($E_{0\bar{0}} \approx E_{1\bar{1}} \approx 1.25\text{GHz}$), might even make the application of an MS-gate impossible.

Battery Qubit B : Ca^+ ion

Ideally, the battery qubit would be degenerate. Since this is hard to achieve (c.f. Section 3.3.1), we admit a small, non-zero energy gap. This energy gap needs to be small, compared to the energy separation of the thermal qubit and the storage system (motional mode): $\omega_B \ll \omega_S, \omega_Q$. In Ca, energy conservation is only achievable for one encoding scheme, described in Table 5.1.

Thermal Qubit Q : Be^+ Hyperfine levels

For Hyperfine qubits one has to take care, that all required transitions are allowed (i.e. $\Delta m_F = \pm 1$). The two encoding schemes, described in Tables 5.2 and 5.3, allow all transitions that are driven in the gate: $|0\rangle \leftrightarrow |\tilde{0}\rangle \leftrightarrow |1\rangle \leftrightarrow |\tilde{1}\rangle$.

The energy separations between levels of the same Hyperfine manifold are in the range of $70 - 100\text{MHz} \leq \omega_m$, similar to the motional frequency ω_m . The two manifolds are separated by $\sim 1.25\text{GHz} \gg \omega_m$, which is much larger than the motional frequency. Therefore, the two levels of the computational qubit need to be chosen within the same manifold, such that energy conservation of the gate is achievable due to $\omega_B \approx \omega_m$.

Note, that for the implementation of gate $U^{(b)}$, different transitions would need to be allowed: $|0\rangle \leftrightarrow |\tilde{0}\rangle \leftrightarrow |\tilde{1}\rangle \leftrightarrow |1\rangle$. These require a different encoding scheme.

A “virtual” thermal state can be prepared by optical pumping.

(i) Version 1: (Table 5.2)

- \oplus The transitions $|0\rangle \leftrightarrow |\tilde{0}\rangle$ and $|1\rangle \leftrightarrow |\tilde{1}\rangle$, which are used in the MS-gates, are not resonant with the motional modes.
- \ominus The RSB transition (step 2 of the implementation) would probably induce a bit flip in the computational and auxiliary qubit, due to $\omega_Q \approx \tilde{\omega}_Q$.

Computational Qubit:

$$|0\rangle = |S_{1/2}; F = 2, m_F = -1\rangle \\ |1\rangle = |S_{1/2}; F = 2, m_F = 0\rangle$$

$$\omega_Q = \omega_{01} \sim 87\text{MHz}$$

Auxiliary Qubit:

$$|\tilde{0}\rangle = |S_{1/2}; F = 1, m_F = 0\rangle \\ |\tilde{1}\rangle = |S_{1/2}; F = 1, m_F = 1\rangle$$

$$\tilde{\omega}_Q = \omega_{\tilde{0}\tilde{1}} \sim 100\text{MHz}$$

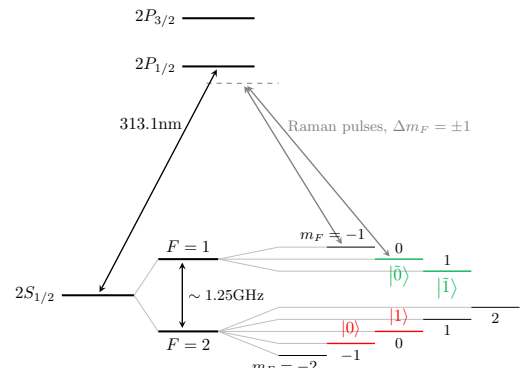


Table 5.2: Encoding of the computational and auxiliary qubit levels for the *thermal* qubit Q in Be^+ (**Version 1**)

(ii) **Version 2:** (Table 5.3)

- ⊕ Good selectivity of the RSB, since the computational and auxiliary qubits have very different energy separations $\omega_Q \neq \tilde{\omega}_Q$.
- ⊖ The Be-transition in the MS-gate, which induces $|1\rangle|1\rangle \leftrightarrow |\tilde{1}\rangle|\tilde{1}\rangle$, is close to the motional frequency: $|1\rangle \xrightarrow{\omega(1\tilde{1})} |\tilde{1}\rangle$, $\omega(1\tilde{1}) \approx 100\text{MHz} \approx \omega_m$

Computational Qubit:

$$\begin{aligned}|0\rangle &= |S_{1/2}; F = 2, m_F = -1\rangle \\|1\rangle &= |S_{1/2}; F = 2, m_F = 0\rangle\end{aligned}$$

$$\omega_Q = \omega_{01} \sim 1.25\text{GHz}$$

Auxiliary Qubit:

$$\begin{aligned}|\tilde{0}\rangle &= |S_{1/2}; F = 1, m_F = 0\rangle \\|\tilde{1}\rangle &= |S_{1/2}; F = 2, m_F = 1\rangle\end{aligned}$$

$$\tilde{\omega}_Q = \omega_{\tilde{0}\tilde{1}} \sim 87\text{MHz}$$

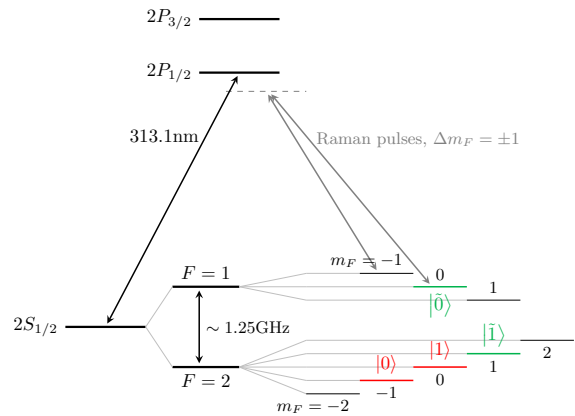


Table 5.3: Encoding of the computational and auxiliary qubit levels for the *thermal* qubit Q in Be^+ (**Version 2**)

5.3 The MS-gate for two ions of different species

Originally the *MS-gate* was implemented for two identical qubits in two ions of the same species [14], [15], [16]. It is still an open question, whether the MS-gate can be implemented for two clearly distinguishable qubits, either in two ions of the same species (two Ca ions) or in two ions of different species (Be and Ca) as described in the previous Section 5.2.

Assumptions and approximations: In order to derive the dominant terms of the interaction Hamiltonian in the MS-gate, several assumptions and approximations are made [16]. In Table 5.4 the most crucial assumptions are listed. A check mark (\checkmark) on the left denotes, that the assumption is either valid or the violation of it does not affect problematically the implementation of the MS-gate. A question mark stands for an assumption that could either not be validated so far or for a violated assumption, whose consequences are not yet clear.

- \checkmark For two identical ions, the MS-gate does not depend on the motional state of the ions, especially the Rabi frequency is a constant ($\tilde{\Omega} \neq \tilde{\Omega}(n)$). It is straightforward to show that this still holds for two ions of different species.
- \checkmark equal *Rabi frequency* $\Omega_1 = \Omega_2 = \Omega$ (i.e. identical coupling strength to laser field) and *Lamb-Dicke parameters* $\eta_1 = \eta_2 = \eta$ (i.e. identical recoil for both ions).
The above parameters are not identical, but this does not affect crucially the Hamiltonian.
- \checkmark *Lamb-Dicke Limit:* $(n + 1)\eta \ll 1$: This allows the expansion $e^{i\eta(\hat{a} + \hat{a}^\dagger)} \approx 1 + i\eta(\hat{a} + \hat{a}^\dagger) + \mathcal{O}(\eta^2)$.
Due to the different mass of the two ions, the Lamb-Dicke parameters differ ($\eta_1 \neq \eta_2$). But since both ions are excited by a separate laser, in contrast to the original MS-gate, where both lasers address both ions, the lasers can be tuned accurately in order to keep the L-D parameters low.
- ? *Rotating wave approximation (RWA):* The RWA is used to neglect fast rotating terms in the interaction Hamiltonian.
Each ion is manipulated by one laser. The two lasers differ in frequency and beam direction, so the initial “kick”, which is given to the ion when starting the gate, is different for the two ions. This means the two ions will start with random relative “motional phase” (in phase space). This can cause problems, since we need to drive a closed path in phase space for both ions. This problem is easy to calibrate out for two identical ions, by testing their maximally entangled state.
- \checkmark *Weak field regime:* $\eta\Omega \ll \nu - \delta$ ($\delta = \pm(\omega_{1,2} - \omega_{eg})$): detuning We can keep our system in the weak field regime by carefully adjusting the intensity, beam direction and detuning of the EM fields.

Table 5.4: Assumptions, which are used in the derivation of the interaction Hamiltonian that determines the MS-gate.

Chapter 6

Outlook

6.1 Open questions

The adaptation of the theoretical concept of the work extraction gate to the physical setup leads to some fundamental problems. The following two points are independent of the proposed gate implementation in Section 5.1 and need to be investigated also for different approaches:

- (i) For the battery qubit we require an energy gap that is smaller than the energy of the motional mode, used for the storage system: $\omega_B \ll \omega_S$.
This could cause fundamental problems: If the energy separation of an internal qubit is close to the separation of the motional mode or even smaller ($\omega_0 \leq \omega_m$) this could lead to unintended coupling of the motional modes to the internal states of the atom. This would render the approximations in the derivation of the interaction Hamiltonian in Section 1.1.4 invalid, since the motional mode can not be treated anymore as perturbation.
- (ii) In order to implement the optimal work extraction protocol (c.f. Section 4), the gate $U^{(a)}$ would have to be implemented repeatedly with different energy separation for the thermal qubit in each repetition. If, as proposed in the encoding schemes above, the battery and thermal qubit are encoded in Hyperfine and Zeeman levels of the ions, the energy separation can be adjusted by lowering the external magnetic field. But since both qubits are sensitive on such a change, it would be difficult to change only the energy separation of the thermal qubit (ΔE_Q) without changing the separation of the battery qubit (ΔE_B).

6.2 Different approaches for the gate implementation

In this section, two other approaches are sketched, which could lead maybe to more optimal gate implementations:

- 1) *Phase gate for degenerate σ_x -eigenstates:* A degenerate battery state could be achieved by driving continuously the carrier transition of two qubits in two ions. The resulting Hamiltonian corresponds to a σ_x phase gate in the rotational basis $|\pm\rangle$ (eigenstates of σ_x).
- 2) *Controlled raising/lowering of the motional state by state-dependent forces:* This idea is based on the principle of the geometric phase gate, where a state-dependent force acts with opposite sign on the two internal qubit states of an ion. If the Raman beams, which establish the force, are tuned close to the collective stretching mode of the ion string, the motional mode (i.e. the storage system) would be changed only if the two ions are in different internal state. Therewith the manipulation of the storage system is directly controlled by both qubits.
To develop further this idea, the idea of the geometric phase gate would need to be adapted carefully.

In the following these two approaches are described in more detail.

6.2.1 Phase gate for degenerate σ_x -eigenstates

The gate implementation, proposed in Section 5.1, shows two main drawbacks: First of all, it is still an open question, whether the MS-gate can be implemented for two ions of different species. And for Hyperfine qubits, as will be used in the Be ion, the MS-gate is experimentally challenging [20]. Secondly, there is no possibility to choose a degenerate single-ion battery qubit in our setup. These two issues could be avoided by transforming to a degenerate basis, consisting of the eigenstates $|\pm\rangle$ of the σ_x -operator. In [20], a σ_z -phase gate for this basis was shown. It was implemented for a Hyperfine qubit in Beryllium.

Gate implementation: The qubits are encoded in two hyperfine states of two ${}^9\text{Be}^+$ ions: $|g\rangle = |F = 2, m_F = 1\rangle$, $|e\rangle = |F = 1, m_F = 0\rangle$.

For these qubits, two transitions are induced: The *carrier transition* and one *sideband transition* (in [20] the RSB is chosen). The carrier transition is driven by a *resonant microwave field* ($\omega_C = \omega_0$). The sideband transition is realised as a *Raman transition*. The two lasers are chosen such that their frequency difference is detuned by δ from the first red sideband of some collective motional mode ω_m : $\Delta\omega_L = \omega_0 + \omega_m + \delta$. All fields address both ions.

Transforming to a rotating frame (i.e. interaction picture) w.r.t. the free atom Hamiltonian

$$H_A = \hbar\omega_0 (\sigma_x \otimes \mathbb{I} + \mathbb{I} \otimes \sigma_x) + \hbar\omega_m (\hat{a}^\dagger + \hat{a})$$

and *neglecting far off-resonant terms*, the interaction Hamiltonian shows two terms [20]

$$H = H_C + H_{\text{RSB}} = \sum_{i=1,2} \left(\hbar\Omega_C \hat{\sigma}_i^\dagger e^{i\phi} + \hbar\Omega_{\text{RSB}} \hat{\sigma}_i^\dagger \hat{a}_m^\dagger e^{-i\delta t} e^{i\phi'} + h.c. \right). \quad (6.1)$$

The first term couples the qubit states by the carrier transition at Rabi frequency Ω_C . The second term couples the motional and internal d.o.f. where oscillations occur at Rabi frequency Ω_{RSB} . The phases, indicated by ϕ and ϕ' will be neglected in the following for simplicity.

For $\Omega_C \gg \Omega_{\text{RSB}}$ we can transform into the rotational frame w.r.t. Ω_C :

$$\begin{aligned} U &= e^{i\Omega_C t(\sigma_x \otimes \mathbb{I} + \mathbb{I} \otimes \sigma_x)} \\ \tilde{H} &= U H U^\dagger + i\hbar (\partial_t U) U^\dagger \end{aligned} \quad (6.2)$$

This calculations are easily done when *transforming to the σ_x -eigenstates* $|\pm\rangle = \frac{1}{\sqrt{2}}(|e\rangle \pm |g\rangle)$. The resulting Hamiltonian contains terms, which are oscillating at frequency $\sim \Omega_C$. For $\Omega_C \ll \delta$, these terms can be neglected by applying another time the RWA and we are left with an effective Hamiltonian that describes a σ_z -phase gate in the rotational $|\pm\rangle$ -basis:

$$H \approx i\hbar \frac{\Omega_{\text{RSB}}}{2} \sum_{i=1,2} \underbrace{(|+)\langle +|_i - |-\rangle\langle -|_i)}_{\sigma_z \text{ in rotational basis } |\pm\rangle} (\hat{a}^\dagger e^{-i\delta t} + \hat{a} e^{i\delta t}). \quad (6.3)$$

This Hamiltonian represents an entangling phase gate in the σ_x -basis.

In general, one distinguishes between σ_z - and σ_ϕ -phase gates [7]. The operator denotes the basis, in which the gate acts as a phase gate: either the computational basis $\{|g\rangle, |e\rangle\}$, or considering $\sigma_\phi = \cos \phi \sigma_x + \sin \phi \sigma_y$, the $|\pm\phi\rangle = \frac{1}{\sqrt{2}}(|+e^{i\phi}\rangle + |e^{i\phi}\rangle)$ -basis, which lies in the equatorial plane of the Bloch sphere. The MS-gate, as used in our proposal, also corresponds to such a σ_ϕ -gate [14]. This supports the idea of replacing the MS-gate in the decomposition in Section 5.1 by such a dressed-state σ_x -gate.

6.2.2 Controlled raising / lowering of the motional state by state-dependent forces

In this implementation, the storage system S is represented by the common *stretching mode* of the ion string. Hence, work-extraction is equal to the excitation of the stretching mode by adding one (or several) phonon(s). Conversely, the storage system can perform work by emitting one (or several) phonon(s), which lowers its vibrational state.

The battery and the thermal qubit are represented by their states $|\uparrow\rangle_i, |\downarrow\rangle_i, i = B, Q$. By applying the gate $U^{(a)}$, work should be extracted for the battery and thermal qubit being in the common state $|\uparrow\downarrow\rangle_{BQ}$. For $|\downarrow\uparrow\rangle_{BQ}$, the storage system itself should perform work and for the two other states nothing should happen:

$$\left\{ \begin{array}{l} |\Psi\rangle_{BQ} = |\uparrow\downarrow\rangle_{BQ} : \text{work extraction, i.e. excitation of } S \\ |\Psi\rangle_{BQ} = |\downarrow\uparrow\rangle_{BQ} : S \text{ performs work, i.e. lowering of the state of } S \\ |\Psi\rangle_{BQ} = |\uparrow\uparrow\rangle_{BQ} \\ |\Psi\rangle_{BQ} = |\downarrow\downarrow\rangle_{BQ} \end{array} \right\} : \text{no action}$$

Like for the geometric phase gate, we consider a state-dependent force that acts in opposite direction on an ion with internal state $|\uparrow\rangle$ as for an ion in state $|\downarrow\rangle$. Such a force can be established by two Raman beams. The beams are tuned such that their frequency difference is close to $\omega_m = \omega_{\text{stretch}}$.

Consider an ion string consisting of two ions ($N = 2$) in the motional ground state and assume the ions are initially in the state $|\Psi\rangle = |\uparrow\downarrow\rangle$. At time $t = 0$, the laser beams are switched on for a pulse time of $t = \pi/\delta$. The force vectors, acting on the two ions, point in opposite directions

(c.f. Figure 6.2.2) and the stretching mode (our storage system S) is excited. After this pulse, the ion string is in the first excited state of the stretching mode, i.e. it absorbed one phonon of energy ω_{stretch} . After a time $t = \frac{2\pi}{\omega_{\text{stretch}}}$, the ions return to their equilibrium position. If another pulse is applied now, the ion and the force are in phase and the pulse should have no other effect on the string than adding another phonon of the same energy, i.e. to excite the motional mode to its second state.



Now consider the same scenario as above, but with the ions in the initial state $|\Psi\rangle = |\downarrow\uparrow\rangle$. As before, a force pulse excites the stretching mode. The only difference is, that for $|\Psi\rangle = |\downarrow\uparrow\rangle$ the oscillation is initiated by a motion of the ions towards each other, whereas for $|\Psi\rangle = |\uparrow\downarrow\rangle$ the ions first moved away from each other. Both oscillations can be described by a sine-function at frequency ω_{stretch} but shifted by a relative phase of $\phi = \pi$:

$$\begin{aligned} |\Psi\rangle = |\downarrow\uparrow\rangle : \quad x(t) &= x_0 \sin(\omega_{\text{stretch}} t) \\ |\Psi\rangle = |\uparrow\downarrow\rangle : \quad x(t) &= x_0 \sin(\omega_{\text{stretch}} t + \pi), \end{aligned}$$

where x_0 denotes the amplitude of the oscillation. When summing up these two functions, they annihilate each other.

Very naively, I apply this idea to a sequence of gates: On a two-ion string like above, two force pulses at times $t = 0$ and $t = \frac{2\pi}{\omega_{\text{stretch}}}$ are applied. Additionally, in between these pulses the two qubits are flipped ($|\uparrow\rangle \leftrightarrow |\downarrow\rangle$).

Applying the interference idea, the first pulse would raise the state of system S (corresponding to work extraction), whereas the second pulse would lower the state again (corresponding to work performance by the system S). Therewith, the lowering of the stretching mode could be implemented.

Open questions: The idea, sketched above, is not yet very elaborated. Many open questions remained, such as the following:

In the geometric phase gate the laser pulses are applied exactly for a period of $T = 2\pi/\delta$, such that the motional state is back in its initial state after the pulse. For the above proposal, we would need to apply a shorter pulse in order to change the motional state. Is this possible, i.e. how long would a laser pulse need to be?

What happens for the internal states being in a superposition of $|\downarrow\downarrow\rangle$, $|\downarrow\uparrow\rangle$, $|\uparrow\downarrow\rangle$, $|\uparrow\uparrow\rangle$?

Chapter 7

Conclusion

With the circuit, presented in Chapter 5.1, we could find a decomposition of the work extraction gate, which can in principle be implemented. The implementation can be performed, using only two ions. Therewith, the experimental realisation does not require a very sophisticated setup (e.g. long ion string, shuttling of ions etc.).

With a total number of six gates, the efficiency of the circuit is good, especially compared to the circuits, which are found when mathematically decomposing the gate operator.

The need for the adaptation of the theoretical conditions on a work extraction scheme to the constraints of a physical system, helped us to gain a better understanding of the energy and entropy conservation in our system. As an example, total isolation of our three-part system is required in theory. By restricting the allowed interactions of the ions on reversible (i.e. coherent) processes, this condition could be relaxed. The total system was extended such that the EM field could be included.

Part III

Appendix

Appendix A

Notation

Operators:

$\sigma_- = \sigma := |g\rangle\langle e|$, $\sigma_+ = \sigma^\dagger$
 \hat{a}, \hat{a}^\dagger
 \hat{c}, \hat{c}^\dagger

lowering, raising operators for internal d.o.f.
annihilation, creation operator of the motional modes of the ion
annihilation, creation operator of the electromagnetic field in the quantum-mechanical description

Frequencies:

$\omega_0 = \omega_{eg}$
 ω_L
 $\omega_i, i \in \{x, y, z\}$

corresponding to the energy difference of the internal d.o.f.
frequency of the applied laser field
frequencies of the three motional modes (harmonic oscillators) of the ion corresponding to the three spatial directions

Quantum Optics:

Ω
 η

Rabi frequency
Lamb-Dicke parameter

Appendix B

Variations of the MS-gate

The Figures in this Chapter show four different versions of the gate implementation. Figure shows the most promising implementation, which is discussed in Chapter 5.1.

The gates, denoted by Version A and B show implementations of the two different gates $U^{(a)}$ and $U^{(b)}$. Subfigures a) and b) differ in the second and third step. In both subfigures a), a π -pulse on the redsideband (RSB), followed only by a π -pulse on the Carrier transition on qubit $|\tilde{\psi}\rangle_B$. In subfigures b) a state-dependent force is applied, which only excites the motional mode and does not change the internal state. Hence, both ancilla qubits need to be flipped.

	Implemented Gate:	Energy conservation:
Version A:	$U^{(a)}: 01\rangle n\rangle \leftrightarrow 10\rangle n+1\rangle$	$\omega_Q - \omega_B = \omega_S$
Version B:	$U^{(b)}: 00\rangle n+1\rangle \leftrightarrow 11\rangle n\rangle$	$\omega_Q + \omega_B = \omega_S$

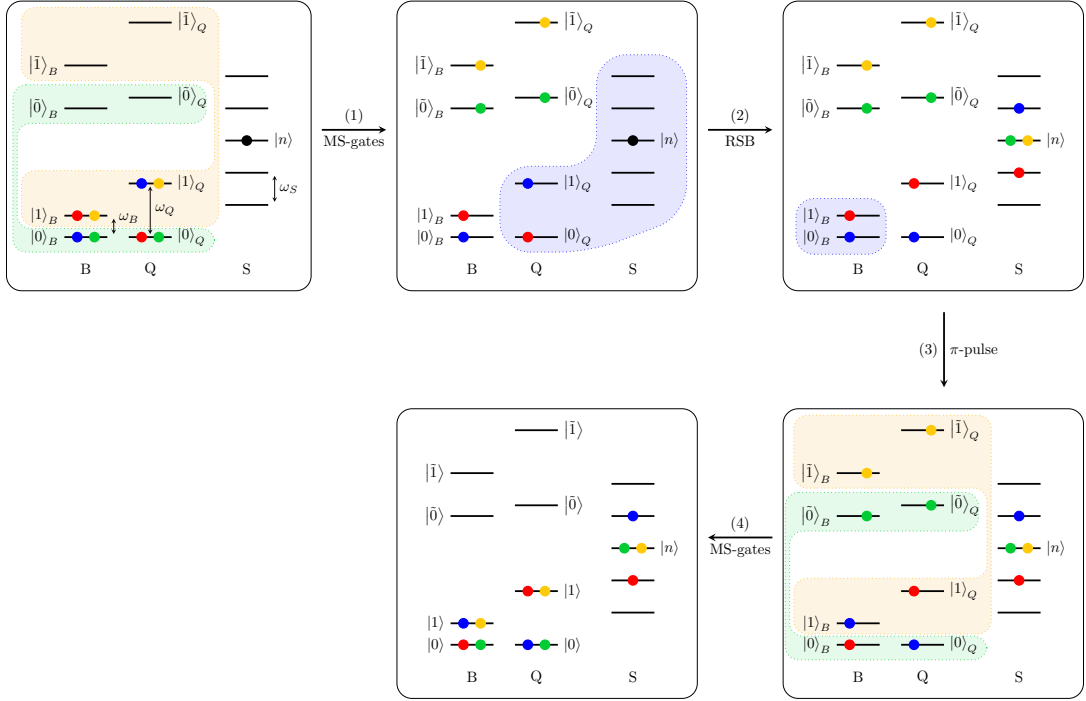
How to read the graphics: Following states are indicated in the Figure:

- B and Q denote two ions; each of them with four energy levels indicated. The levels $|0\rangle$ and $|1\rangle$ are called *computational qubits*, $|\tilde{0}\rangle$ and $|\tilde{1}\rangle$ are *ancilla* or *auxiliary qubits*.
- S depicts a common motional mode of the two ions.

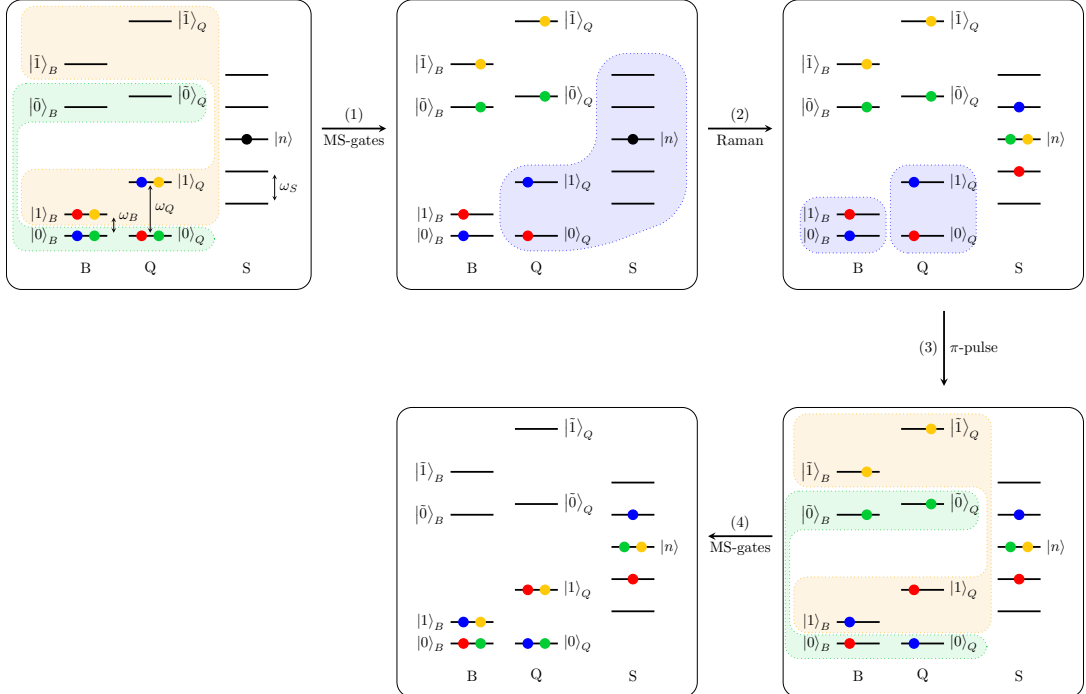
The coloured dots on the energy levels indicate the four different possible initial states (first box: e.g. the initial state $|00\rangle_{BQ}$ is indicated by the blue dots) and the corresponding action of the gate. The storage system (motional state) is initially in the same state $|n\rrangle$ for all internal states (indicated as black) but splits under the action of the gate, conditioned on the internal state.

The dashed lines enclose the states which are involved in the next step of the gate; e.g. in step two the qubit $|0\rangle, |1\rangle$ of ion Q and the common motional mode S are involved.

The arrow denoted with “Raman” means the action of a state-dependent force, driving the transition $|0\rangle|n+1\rangle \leftrightarrow |1\rangle|n\rangle$.

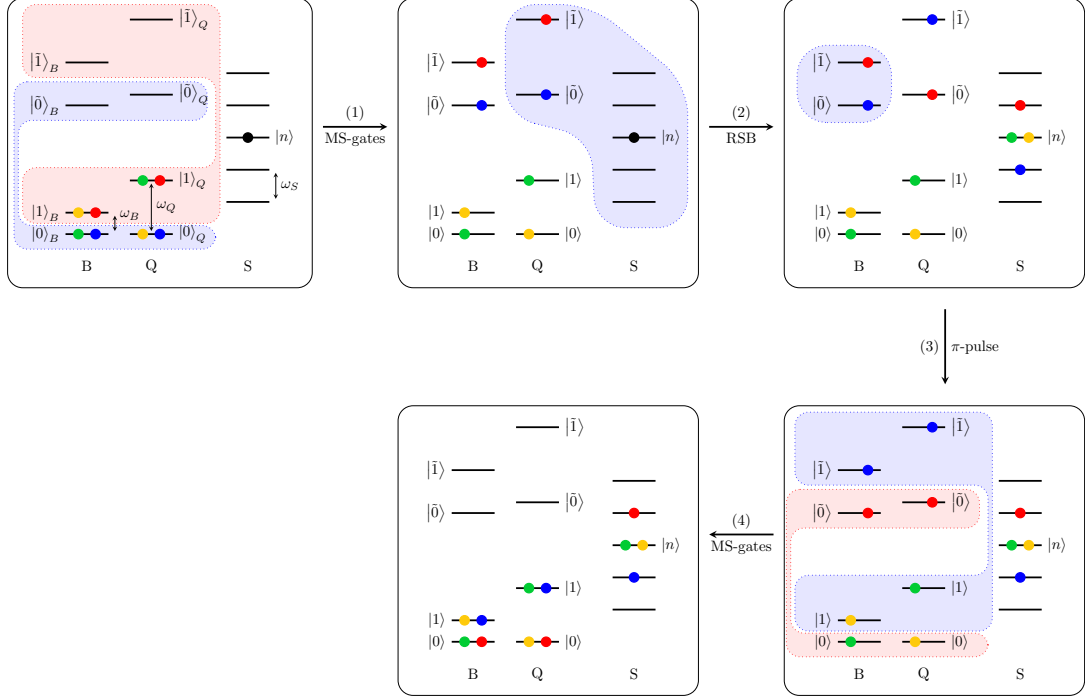


(a) In the second step a π -pulse on the *red sideband transition (RSB)* is implemented: (1) MS-gates / (2) $|\bar{0}\rangle|n\rangle \leftrightarrow |\bar{1}\rangle|n-1\rangle$ / (3) bit flip (π -pulse) / (4) MS-reverse

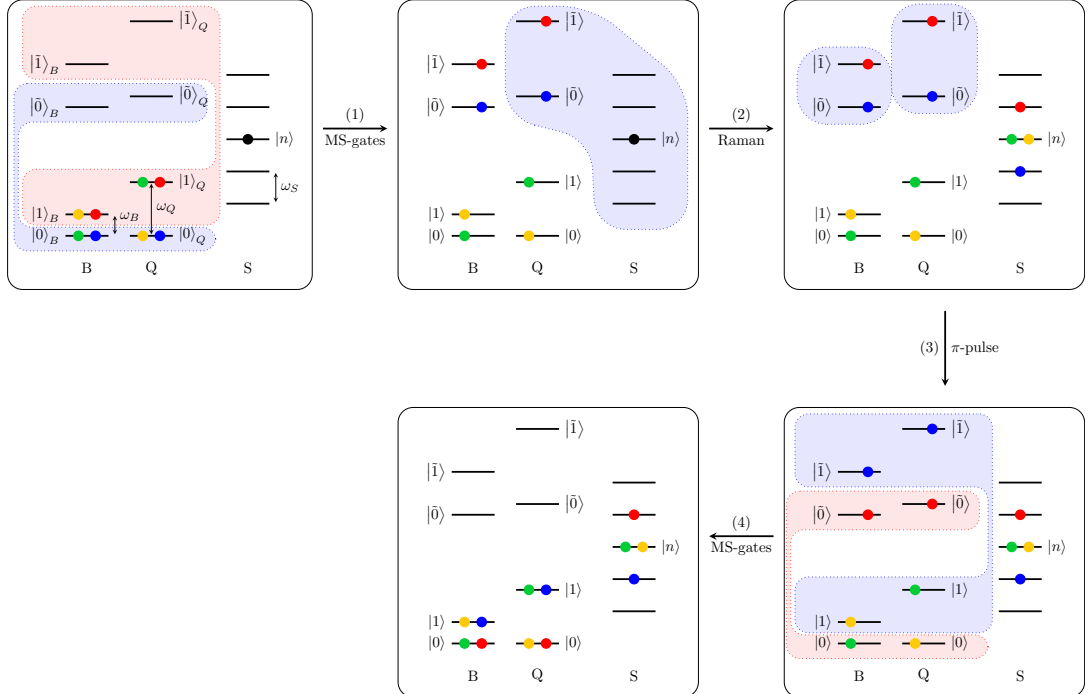


(b) In the second step a *state-dependent force (Raman pulses)* drives only the motional state. Both qubits need to be flipped (1) MS-gates / (2) Raman transitions: $|\bar{0}\rangle|n\rangle \leftrightarrow |\bar{0}\rangle|n-1\rangle$, $|\bar{1}\rangle|n\rangle \leftrightarrow |\bar{1}\rangle|n+1\rangle$ / (3) 2 x bit flip (π -pulses) / (4) MS-reverse

Figure B.1: **Version A:** Implementation of the gate: $U^{(a)}: |01\rangle|n\rangle \leftrightarrow |10\rangle|n+1\rangle$. Energy conservation requires $\omega_Q - \omega_B = \omega_S$.



(a) In the second step a *π -pulse* on the *redsideband transition (RSB)* is implemented: (1) MS-gates / (2) $|\bar{0}\rangle|n\rangle \leftrightarrow |\bar{1}\rangle|n-1\rangle$ / (3) bit flip (π -pulse) / (4) MS-reverse



(b) In the second step a *state-dependent force (Raman pulses)* drives only the motional state. Both qubits need to be flipped (1) MS-gates / (2) Raman transitions: $|\bar{0}\rangle|n\rangle \leftrightarrow |\bar{0}\rangle|n-1\rangle$, $|\bar{1}\rangle|n\rangle \leftrightarrow |\bar{1}\rangle|n+1\rangle$ / (3) 2 x bit flip (π -pulses) / (4) MS-reverse

Figure B.2: **Version B:** Implementation of the gate: $U^{(b)}: |00\rangle|n+1\rangle \leftrightarrow |11\rangle|n\rangle$. Energy conservation requires $\omega_Q + \omega_B = \omega_S$.

Appendix C

Additional Information

C.1 Geometric Phase gate

Classical driven harmonic oscillator: The Hamiltonian of the system corresponds to a *forced* or *driven harmonic oscillator*, driven by an EM force $\vec{F}(t) = -q\vec{E}(t) = -qE_0\hat{n}\cos(\omega t)$. This leads to following potential term in the Hamiltonian $H = \hbar\omega_m(\hat{a}^\dagger\hat{a} + 1/2) + V(t)$

$$\begin{aligned} V(t) &= \vec{F}\vec{r}_i = -qE_0\hat{z}\cos(\omega t + \phi) \\ &= -qE_0z_0(\hat{a}^\dagger + \hat{a})\frac{(e^{i(\omega t+\phi)} + e^{-i(\omega t+\phi)})}{2} \\ &\approx \frac{qE_0z_0}{2}(\hat{a}e^{i(\omega t+\phi)} + \hat{a}^\dagger e^{-i(\omega t)}), \end{aligned} \quad (\text{C.1})$$

where r_i is the position of the ion and in the last step the RWA (c.f. Section 1.1.4) was applied. In the interaction picture, corresponding to a frame rotating at the field frequency ω , this gives:

$$V_I(t) = \frac{qE_0z_0}{2}(\hat{a}e^{i\delta t} + \hat{a}^\dagger e^{-i\delta t})$$

Since $V_I(t)$ does not commute for different times the exponential solution to the time-dependent Schrödinger equation is only fulfilled for infinitesimal time steps Δt , which lead to infinitesimal displacements $\Delta\alpha(t) = \frac{i}{\hbar}qE_0z_0e^{i\delta t}\Delta t$

$$|\Psi(t)\rangle = e^{-iV_I(0)\Delta t/\hbar}|\Psi(0)\rangle = e^{(\Delta\alpha\hat{a}^\dagger + \Delta\alpha^*\hat{a})}|\Psi(0)\rangle.$$

A finite displacement is given by $\alpha(t) = \int_0^t \Delta\alpha(t)dt = \frac{-qE_0z_0}{2\hbar\delta}(1 - e^{i\delta t})$, from which the period $T = 2\pi/\delta$ for a closed looped in phase space follows. For a finite path α the evolution operator, denoted as *displacement operator*, can be derived using the Baker-Hausdorff relation

$$U(t=0, t) = e^{-iV_I(0)t/\hbar}e^{i\phi} \quad \text{with } \phi = \text{Im} \oint \alpha^* d\alpha.$$

The phase ϕ arises from the non-commuting potential. After a whole period, the displacement operator becomes equal to the identity up to the phase factor: $U(0, T) = \mathbb{I}e^{i\phi}$. The phase depends on the area in phase space, encircled by the path α . It can be tuned to a desired value by adjusting the intensity and the detuning of the EM field (lasers).

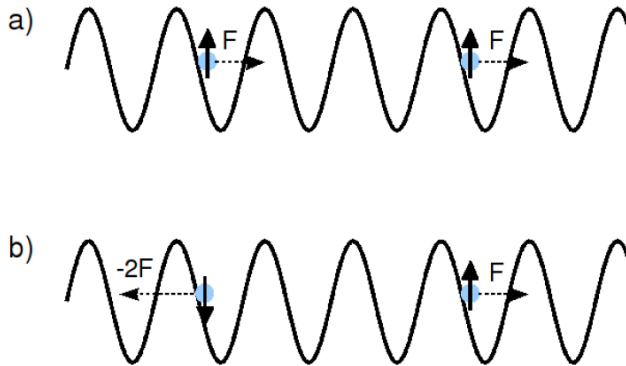


Figure C.1: [6] The oscillating EM field, created by the two interfering lasers, acts on the two ions. The ion-ion distance is adjusted to the field wavelength. a) Both ions are in the same internal state: no motional excitation. b) The ions are in different internal state: the 'breathing' mode is excited.

Idea: The basic idea of the gate is, to produce a force with an external EM field (laser), that acts on the motional mode of the ions and displaces the corresponding harmonic oscillator state in phase space. In a classical picture of a mechanical h.o., this corresponds to a *driven harmonic oscillator*, which is generated by applying a periodic force with slightly off-resonant frequency (detuning δ). This leads to a periodic damping and acceleration of the h.o. After a period $T = \frac{2\pi}{\delta}$ the h.o. has returned back to its initial state in phase space.

The same holds for a quantum mechanical h.o.: The applied force is detuned by δ from the h.o. frequency ω_m . Within a period $T = \frac{2\pi}{\delta}$ the h.o. state describes a *closed path in phase space*. After the gate was applied, the motional mode has returned to its initial state, up to an *acquired phase factor*. This phase distinguishes the quantum mechanical from the classical case. It arises due to the non-commutative characteristics of the time-evolution operator, generated by the force.

So far, a qubit, encoded in the internal state of an ion, would simply acquire a global phase during the gate. But if we apply a *state-dependent force*, which acts with different strength on the ion depending on its internal state, the two qubit states acquire different phase factors and a phase gate can be realised. The same idea is used for a controlled phase gate on two qubits: The applied force is chosen such that it acts differently on the ions, depending on the *common two-qubit state*. The frequency of this periodic force displacement is tuned close to the frequency of a common motional mode of the ion string (COM or stretch mode). The resonant frequency corresponds to the harmonic oscillator mode, which is displaced in phase space.

Implementation: The basic idea of the gate is, to produce a force with an external EM field (laser), that acts on the motional mode of the ions and displaces the corresponding harmonic oscillator state in phase space.

Therefore an EM field is produced by two Raman laser beams of different frequencies, which simultaneously illuminate both ions and interfere at the ions' positions. The interference leads to an oscillation of the superposed laser field and therewith an oscillation of the force, acting on the ions (c.f. Figure C.1). The trap frequency is adjusted such that the ion-ion distance is a multiple of the wavelength of the oscillating laser field (c.f. Figure C.1). Therewith both ions experience the same field strength.

The oscillation frequency is equal to the frequency difference of the two lasers $\Delta\omega := \omega_1 - \omega_2$.

By adjusting the individual beams $\Delta\omega$ can be tuned close to the frequency of the motional mode ω_m , which should be driven by the field: $\Delta\omega := \omega_1 - \omega_2 = \omega_m + \delta$, $\delta \ll \omega_m$.

The individual Raman lasers are detuned from an internal transition in the ion ($\omega_i = \omega_{eg} + \Delta$, $i = 1, 2$). As an example, consider qubits that are encoded in the $S_{1/2}$ -level of Be^+ . The individual lasers address the $S_{1/2} \leftrightarrow P_{1/2}$ transition (c.f. paragraph below). State-dependency of the force can be achieved by a good choice of this transition.

Experimental realisations & references:

- (i) *Hyperfine qubits in Be^+* [17]: The qubits $\{| \uparrow \rangle, | \downarrow \rangle\}$ are encoded in two Hyperfine levels of the $S_{1/2}$ -ground state of two beryllium ions. The laser beams, generating the EM field, are tuned such that the two qubit states experience opposite force vectors ($F_\uparrow = -2F_\downarrow$). Therewith a geometric phase gate, using the common stretch mode as driven h.o., is implemented. If the two ions are in the same internal state, both ions experience the same force. But since the field is far off-resonance from the COM mode, it has no effect on the ions. If the two ions are in different internal states, they experience opposite force and the stretch mode is excited, i.e. the corresponding h.o. is displaced in phase space and a phase is acquired.

By adjusting the laser intensities and pulse duration a phase factor of $e^{i\phi} = e^{i\pi/2}$ can be achieved. This leads to a **controlled phase gate (CPhase)** composed with individual $\pi/2$ -phase shifts on the $|\uparrow\rangle$ -states:

$$U_{T=\frac{2\pi}{\delta}} = \underbrace{\begin{pmatrix} 1 & 0 & 0 & 0 \\ 0 & e^{i\pi/2} & 0 & 0 \\ 0 & 0 & e^{i\pi/2} & 0 \\ 0 & 0 & 0 & e^{i\pi} \end{pmatrix}}_{U_{CPhase}} \underbrace{\begin{pmatrix} 1 & 0 & 0 & 0 \\ 0 & 1 & 0 & 0 \\ 0 & 0 & 1 & 0 \\ 0 & 0 & 0 & e^{-i\pi} \end{pmatrix}}_{:} \begin{cases} |\downarrow\downarrow\rangle \rightarrow |\downarrow\downarrow\rangle \\ |\downarrow\uparrow\rangle \rightarrow e^{i\pi/2} |\downarrow\uparrow\rangle \\ |\uparrow\downarrow\rangle \rightarrow e^{i\pi/2} |\uparrow\downarrow\rangle \\ |\uparrow\uparrow\rangle \rightarrow e^{-i\pi} (e^{i\pi/2} |\uparrow\rangle)(e^{i\pi/2} |\uparrow\rangle) \end{cases}. \quad (\text{C.2})$$

- (ii) *Optical qubits in Ca^+* [18]: The qubits are encoded in one of the Zeeman $S_{1/2}$ -levels and a Zeeman $D_{5/2}$ -level: $\{|0\rangle = |S_{1/2}\rangle |1\rangle = |D_{5/2}\rangle\}$. The two Raman beams, establishing the periodic force, are tuned to the $S_{1/2} \leftrightarrow D_{5/2}$ transition: $\omega_i = \omega_{SD} \pm \Delta$. The frequency difference of the two beams is tuned close to the COM mode frequency ($\Delta\omega = \omega_{\text{COM}} + \delta$). Due to the interaction with the resonant laser beams, the two involved energy levels experience a shift (ac Stark shift or differential light shift, c.f. [7], [18]). The beams can be tuned such that the two levels are shifted by the same amount but in opposite direction. This shift determines the strength of the ion-field interaction and therewith the strength of the force, acting on the ion.

Due to the opposite sign of the force, the COM motional mode is only excited, if the two ions are both in the same state. If the two ions are in different states, they would experience different force exciting the stretch mode. But since the effective EM field is far detuned from the corresponding mode $\Delta\omega \ll \omega_{\text{stretch}}$ it is not excited.)

$$U_{t=2\pi/\delta} = \begin{pmatrix} e^{i\pi/2} & 0 & 0 & 0 \\ 0 & 1 & 0 & 0 \\ 0 & 0 & 1 & 0 \\ 0 & 0 & 0 & e^{i\pi/2} \end{pmatrix} : \begin{cases} |SS\rangle \rightarrow e^{i\pi/2} |SS\rangle \\ |SD\rangle \rightarrow |SD\rangle \\ |DS\rangle \rightarrow |DS\rangle \\ |DD\rangle \rightarrow e^{i\pi/2} |DD\rangle \end{cases} \quad (\text{C.3})$$

Appendix D

Calculations

D.1 Derivation of the general qubit rotation matrix

$$R(\theta, \phi) = \exp i\theta/2(e^{i\phi}\hat{\sigma}_+ + e^{-i\phi}\hat{\sigma}_-) \quad (\text{D.1})$$

The matrix form of $R(\theta, \phi)$ can be derived by using following theorem:

$$A \in \mathbb{C}^{n \times n} \text{ with } A^2 = \mathbb{I}: \quad e^{ixA} = \cos(x)\mathbb{I} + i \sin(x)A, \forall x \in \mathbb{R} \quad (\text{D.2})$$

The raising- and lowering operators are given by

$$\begin{aligned} \hat{\sigma}_+ &:= |e\rangle\langle g| = \begin{pmatrix} 0 & 0 \\ 1 & 0 \end{pmatrix} \\ \hat{\sigma}_- &:= |g\rangle\langle e| = \begin{pmatrix} 0 & 1 \\ 0 & 0 \end{pmatrix} \end{aligned} \quad (\text{D.3})$$

where we used the vector basis $|g\rangle = \begin{pmatrix} 1 \\ 0 \end{pmatrix}, |e\rangle = \begin{pmatrix} 0 \\ 1 \end{pmatrix}$.

Therefrom it can be calculated:

$$A := e^{i\phi}\hat{\sigma}_+ + e^{-i\phi}\hat{\sigma}_-$$

$$\begin{aligned} A^2 &= e^{2i\phi}\hat{\sigma}_+^2 + \underbrace{(\hat{\sigma}_+\hat{\sigma}_- + \hat{\sigma}_-\hat{\sigma}_+)}_{|e\rangle\langle e| + |g\rangle\langle g| = \mathbb{I}} + e^{-2i\phi}\hat{\sigma}_-^2 = \mathbb{I} \\ \hat{\sigma}_+^2 &= \hat{\sigma}_-^2 = 0 \\ \hat{\sigma}_+\hat{\sigma}_- &= |e\rangle\langle g| |g\rangle\langle e| = |e\rangle\langle e| \\ \hat{\sigma}_-\hat{\sigma}_+ &= |g\rangle\langle e| |e\rangle\langle g| = |g\rangle\langle g| \end{aligned} \quad (\text{D.4})$$

$$R(\theta, \phi) = \exp i\theta/2(e^{i\phi}\hat{\sigma}_+ + e^{-i\phi}\hat{\sigma}_-) = \cos \theta/2 \mathbb{I} + i \sin \theta/2 (e^{i\phi}\hat{\sigma}_+ + e^{-i\phi}\hat{\sigma}_-) \quad (\text{D.5})$$

$$\Rightarrow R(\theta, \phi) = \begin{pmatrix} \cos \theta/2 & ie^{-i\phi} \sin \theta/2 \\ ie^{i\phi} \sin \theta/2 & \cos \theta/2 \end{pmatrix}, \quad (\text{D.6})$$

D.2 Derivation of the interaction Hamiltonian for two-level systems

D.2.1 Rotating-wave approximation (RWA):

In general, the rotating-wave approximation (RWA) discards terms that are oscillating at high frequency (compared to the dominating terms) and replaces them by their zero time-average value. This amounts to a coarse-grained time-evolution.

Application for two-level systems: Consider an atomic two-level system of energy gap ω_{eg} and an EM mode of frequency ω_L . The interaction of the atomic system with the EM field is described by the interaction Hamiltonian H_{AF} (1.13). This Hamiltonian can be expanded into terms that are oscillating at different frequencies $\pm(\omega_L - \omega_{eg} \pm s\omega_m)$, $s \in \mathbb{N}$. Assume, that the EM field is in resonance with one of these terms, e.g. $\omega_L \approx \omega_{eg}$. Then the first order terms $\sim e^{\pm i(\omega_L - \omega_{eg})t}$ become time-independent, whereas the higher order terms oscillate at the corresponding frequency difference $0 \ll \Delta = \omega_L - \omega_{eg} \pm s\omega_m$, $s > 0$ and remain time-dependent. On the time-scale of the dominant, time-independent term, the contribution of the rapidly oscillating terms can be neglected.

D.2.2 Interaction Picture:

$$\tilde{H} := UHU^\dagger + i\hbar(\partial_t U)U^\dagger$$

with the transformation: $U := e^{iH_A t/\hbar} = e^{i(\omega_0|e\rangle\langle e| + \omega_z(\hat{a}^\dagger \hat{a} + 1/2))t}$

$$\begin{aligned} H_A &= \hbar\omega_0 |e\rangle\langle e| + \hbar\omega_z(\hat{a}_z^\dagger \hat{a}_z + 1/2) \\ H_{AF} &= \frac{\hbar\Omega}{2} \left(\hat{\sigma}^\dagger e^{-i(\omega_L t - \vec{k}\vec{r})} + \hat{\sigma} e^{i(\omega_L t - \vec{k}\vec{r})} \right) \\ &= \frac{\hbar\Omega}{2} \left(\hat{\sigma}^\dagger e^{-i(\omega_L t - \eta(\hat{a} + \hat{a}^\dagger))} + \hat{\sigma} e^{i(\omega_L t - \eta(\hat{a} + \hat{a}^\dagger))} \right), \quad \eta := k_z z_0 \end{aligned} \quad (\text{D.7})$$

$$\begin{aligned} H &= H_A + H_{AF} \\ &= \hbar\omega_0 |e\rangle\langle e| + \hbar\omega_z(\hat{a}_z^\dagger \hat{a}_z + 1/2) + \frac{\hbar\Omega}{2} \left(\hat{\sigma}^\dagger e^{-i(\omega_L t - \vec{k}\vec{r})} + \hat{\sigma} e^{i(\omega_L t - \vec{k}\vec{r})} \right) \end{aligned}$$

The creation and annihilation operators act as following on the Fock states of the EM field

$$\hat{a} |n\rangle = \sqrt{n} |n-1\rangle, \quad (\text{D.8})$$

$$\hat{a}^\dagger |n\rangle = \sqrt{n+1} |n+1\rangle, \quad (\text{D.9})$$

$$\hat{a}^\dagger \hat{a} |n\rangle = n |n\rangle, \quad \hat{a}^\dagger \hat{a} |n\rangle = \sum_{n=-\infty}^{\infty} n |n\rangle \langle n|. \quad (\text{D.10})$$

In the following the different terms of $\tilde{H} = U H_A U^\dagger + U H_{AF} U^\dagger + i\hbar(\partial_t U)U^\dagger$ are computed:

(a) *Time derivative:*

$$\begin{aligned} i\hbar(\partial_t U)U^\dagger &= i\hbar \left(i\omega_0 |e\rangle \langle e| + i\omega_z (\hat{a}^\dagger \hat{a} + 1/2) \right) e^{i\omega_0 t |e\rangle \langle e|} e^{i\omega_z (\hat{a}^\dagger \hat{a} + 1/2)} e^{-i\omega_0 t |e\rangle \langle e|} e^{-i\omega_z (\hat{a}^\dagger \hat{a} + 1/2)} \\ &= -\hbar \left(\omega_0 |e\rangle \langle e| + \omega_z (\hat{a}^\dagger \hat{a} + 1/2) \right) = -H_A \end{aligned}$$

(b) *Atom Hamiltonian H_A :*

$$\begin{aligned} U H_A U^\dagger &= e^{i\omega_0 t |e\rangle \langle e|} \hbar \omega_0 |e\rangle \langle e| e^{-i\omega_0 t |e\rangle \langle e|} \otimes e^{i\omega_z (\hat{a}^\dagger \hat{a} + 1/2)} \hbar \omega_z (\hat{a}^\dagger \hat{a} + 1/2) e^{-i\omega_z (\hat{a}^\dagger \hat{a} + 1/2)} \\ &= \hbar \omega_0 e^{i\omega_0 t} |e\rangle \langle e| e^{-i\omega_0 t} \otimes \hbar \omega_z \left(e^{i\omega_z \hat{a}^\dagger \hat{a}} \sum_n n |n\rangle \langle n| e^{-i\omega_z \hat{a}^\dagger \hat{a}} + 1/2 \right) \\ &= \hbar \omega_0 |e\rangle \langle e| \otimes \hbar \omega_z \left(\sum_n n \underbrace{e^{i\omega_z \hat{a}^\dagger \hat{a}} |n\rangle \langle n|}_{e^{i\omega_z n} |n\rangle} \underbrace{e^{-i\omega_z \hat{a}^\dagger \hat{a}}}_{\langle n| e^{-i\omega_z n}} + 1/2 \right) \\ &= \hbar \omega_0 |e\rangle \langle e| \otimes \hbar \omega_z (\hat{a}^\dagger \hat{a} + 1/2) \\ &= H_A \end{aligned}$$

$$\Rightarrow U H_A U^\dagger + i\hbar(\partial_t U)U^\dagger = 0$$

(c) *Interaction Hamiltonian H_{AF} :*

$$H_{AF} = \frac{\hbar\Omega}{2} \left(\hat{\sigma}^\dagger e^{-i(\omega_L t - \vec{k}\vec{r})} + \hat{\sigma} e^{i(\omega_L t - \vec{k}\vec{r})} \right) = \frac{\hbar\Omega}{2} \left(\hat{\sigma}^\dagger e^{-i(\omega_L t - \eta(\hat{a} + \hat{a}^\dagger))} + \hat{\sigma} e^{i(\omega_L t - \eta(\hat{a} + \hat{a}^\dagger))} \right) \text{ with the Lamb-Dicke parameter } \eta := k_z z_0.$$

$$\Rightarrow H_{AF} \sim e^{\pm i(\omega_L t - \eta(\hat{a} + \hat{a}^\dagger))} \sim e^{\pm i\eta(\hat{a} + \hat{a}^\dagger)}$$

For a small parameter η (i.e. within the Lamb-Dicke regime), the exponential function can be expanded to first order in $\eta \ll 1$ as:

$$H_{AF} \sim e^{\pm i\vec{k}\vec{r}} = e^{\pm i\eta(\hat{a}^\dagger + \hat{a})} \simeq 1 \pm i\eta(\hat{a}^\dagger + \hat{a}) + \mathcal{O}(\eta^2)$$

(i) *motional d.o.f.:*

$$U := e^{iH_A t / \hbar} = e^{i(\omega_0 |e\rangle \langle e| + \omega_z (\hat{a}^\dagger \hat{a} + 1/2))t} \sim e^{i\omega_z t (\hat{a}^\dagger \hat{a})}$$

$$\begin{aligned}
 e^{i\omega_z t(\hat{a}^\dagger \hat{a})} H_{\text{AF}} e^{-i\omega_z t(\hat{a}^\dagger \hat{a})} |n\rangle &\sim e^{i\omega_z t \hat{a}^\dagger \hat{a}} e^{\pm i\eta(\hat{a}^\dagger + \hat{a})} e^{-i\omega_z t \hat{a}^\dagger \hat{a}} |n\rangle \\
 &\simeq e^{i\omega_z t \hat{a}^\dagger \hat{a}} \left(1 \pm i\eta(\hat{a}^\dagger + \hat{a})\right) e^{-i\omega_z t \hat{a}^\dagger \hat{a}} |n\rangle \\
 &= \left(e^{i\omega_z t \hat{a}^\dagger \hat{a}} e^{-i\omega_z t \hat{a}^\dagger \hat{a}} \pm e^{i\omega_z t \hat{a}^\dagger \hat{a}} i\eta(\hat{a}^\dagger + \hat{a}) e^{-i\omega_z t \hat{a}^\dagger \hat{a}}\right) |n\rangle \\
 &= |n\rangle \pm e^{i\omega_z t \hat{a}^\dagger \hat{a}} (i\eta(\sqrt{n+1}|n+1\rangle + \sqrt{n}|n-1\rangle)) e^{-i\omega_z t n} \\
 &= |n\rangle \pm i\eta \left(e^{i\omega_z t(n+1)} \sqrt{n+1}|n+1\rangle + e^{i\omega_z t(n-1)} \sqrt{n}|n-1\rangle\right) e^{-i\omega_z t n} \\
 &= |n\rangle \pm i\eta e^{i\omega_z t n} e^{-i\omega_z t n} \left(e^{i\omega_z t} \sqrt{n+1}|n+1\rangle + e^{-i\omega_z t} \sqrt{n}|n-1\rangle\right) \\
 &= \left(1 \pm i\eta(\hat{a}^\dagger e^{i\omega_z t} + \hat{a} e^{-i\omega_z t})\right) |n\rangle.
 \end{aligned}$$

(ii) internal d.o.f.: $H_{\text{AF}} \sim \hat{\sigma}^\dagger e^{-i\omega_L t} + \hat{\sigma} e^{i\omega_L t}$ with $\hat{\sigma} := |g\rangle\langle e|$

$$\begin{aligned}
 e^{i\omega_0 t|e\rangle\langle e|} H_{\text{AF}} e^{-i\omega_0 t|e\rangle\langle e|} &\sim \left(e^{-i\omega_L t} e^{i\omega_0 t|e\rangle\langle e|} \hat{\sigma}^\dagger e^{-i\omega_0 t|e\rangle\langle e|} + e^{i\omega_L t} e^{i\omega_0 t|e\rangle\langle e|} \hat{\sigma} e^{-i\omega_0 t|e\rangle\langle e|}\right) \\
 &= e^{-i\omega_L t} \underbrace{e^{i\omega_0 t|e\rangle\langle e|}}_{=e^{i\omega_0 t \cdot 1}|e\rangle} \underbrace{\langle g| e^{-i\omega_0 t|e\rangle\langle e|}}_{=\langle g| e^{-i\omega_0 t \cdot 0}=|g\rangle} + e^{i\omega_L t} \underbrace{e^{i\omega_0 t|e\rangle\langle e|}}_{=e^{i\omega_0 t \cdot 0}|g\rangle=|g\rangle} \underbrace{\langle e| e^{-i\omega_0 t|e\rangle\langle e|}}_{=\langle e| e^{-i\omega_0 t \cdot 1}} \\
 &= e^{-i(\omega_L - \omega_0)t} |e\rangle\langle g| + e^{i(\omega_L - \omega_0)t} |g\rangle\langle e| \\
 &= \hat{\sigma}^\dagger e^{-i(\omega_L - \omega_0)t} + \hat{\sigma} e^{i(\omega_L - \omega_0)t}
 \end{aligned}$$

$$\begin{aligned}
 \Rightarrow U H_{\text{AF}} U^\dagger &\approx \frac{\hbar\Omega}{2} \left(\hat{\sigma}^\dagger e^{-i(\omega_L - \omega_0)t} + \hat{\sigma} e^{i(\omega_L - \omega_0)t}\right) \otimes \mathbb{I}_{\text{motional}} \\
 &\quad + \frac{\hbar\Omega}{2} [\hat{\sigma}^\dagger e^{-i(\omega_L - \omega_0)t} \otimes i\eta \left(a_z^\dagger e^{i\omega_z t} + a_z e^{-i\omega_z t}\right) \\
 &\quad - \hat{\sigma} e^{i(\omega_L - \omega_0)t} \otimes i\eta \left(a_z^\dagger e^{i\omega_z t} + a_z e^{-i\omega_z t}\right)] + \mathcal{O}(\eta^2)
 \end{aligned} \tag{D.11}$$

(d) Total Hamiltonian:

$$\begin{aligned}
 \tilde{H} &= \underbrace{i\hbar(\partial_t U)U^\dagger + U H_{\text{A}} U^\dagger}_{=0} + U H_{\text{AF}} U^\dagger = U H_{\text{AF}} U^\dagger \\
 &= \frac{\hbar\Omega}{2} \left(\hat{\sigma}^\dagger e^{-i((\omega_L - \omega_0)t - \phi_L)} e^{i\eta(\hat{a}^\dagger e^{i\omega_z t} + \hat{a} e^{-i\omega_z t})} + \text{h.c.}\right) \\
 &\approx \frac{\hbar\Omega}{2} \left(\hat{\sigma}^\dagger e^{-i((\omega_L - \omega_0)t - \phi_L)} + \hat{\sigma} e^{i((\omega_L - \omega_0)t - \phi_L)}\right) \otimes \mathbb{I}_{\text{motional}} \\
 &\quad + \frac{\hbar\Omega}{2} \left[\hat{\sigma}^\dagger e^{-i((\omega_L - \omega_0)t - \phi_L)} \otimes i\eta \left(\hat{a}^\dagger e^{i\omega_z t} + \hat{a} e^{-i\omega_z t}\right) - \hat{\sigma} e^{i((\omega_L - \omega_0)t - \phi_L)} \otimes i\eta \left(\hat{a}^\dagger e^{i\omega_z t} + \hat{a} e^{-i\omega_z t}\right)\right] \\
 &\quad + \mathcal{O}(\eta^2) \\
 &\approx \frac{\hbar\Omega}{2} \left(\hat{\sigma}^\dagger e^{-i((\omega_L - \omega_0)t - \phi_L)} + \hat{\sigma} e^{i(\omega_0 - \omega_L)t}\right) \otimes \mathbb{I}_{\text{motional}} \\
 &\quad + \frac{\hbar\Omega}{2} [i\eta \hat{\sigma}^\dagger \otimes \left(\hat{a}^\dagger e^{-i((\omega_L - \omega_0 - \omega_z)t - \phi_L)} + \hat{a} e^{i((\omega_L - \omega_0 + \omega_z)t - \phi_L)}\right) \\
 &\quad - i\eta \hat{\sigma} \otimes \left(\hat{a}^\dagger e^{i((\omega_L - \omega_0 + \omega_z)t - \phi_L)} + \hat{a} e^{i((\omega_L - \omega_0 - \omega_z)t - \phi_L)}\right)] \\
 &\quad + \mathcal{O}(\eta^2)
 \end{aligned} \tag{D.12}$$

Bibliography

- [1] Philipp Kammerlander, *Work extraction from pure qubits*, Semester Thesis, ETH Zurich, (May 2012)
- [2] Daniel A. Steck, *Quantum and Atom Optics*, Oregon Center for Optics and Department of Physics, University of Oregon , (2012), available online at <http://steck.us/teaching>, (revision 0.8.3, 25 May 2012)
- [3] C. F. Walls, Gerard J. Milburn, *Quantum Optics*, Springer Verlag Berlin Heidelberg, (2008)
- [4] S. Kryszewski, *Quantum Optics - Lecture Notes for Students*, Gdańsk (2004-2011)
- [5] Serge Haroche and Jean-Michel Raimond, *Exploring the Quantum - Atoms, Cavities and Photons*, Oxford University Press, (2006)
- [6] Hartmut Häffner, *Quantum computing with trapped ions*, Dept. of Physics, University of California, Berkeley, CA 94720, USA
- [7] Roee Ozeria, *Tutorial: The trapped-ion qubit tool box*, arXiv:1106.1190v1, (2011)
- [8] D. J. Wineland, *Quantum information processing and quantum control with trapped atomic ions*, Phys. Scr. T137, (2009) 014007, (Online at stacks.iop.org/PhysScr/T137/014007)
- [9] D. Leibfried, R. Blatt, C. Monroe, D. Wineland, *Quantum dynamics of single trapped ions*, Reviews of modern Physics, Vol. 75, (2003)
- [10] D. J. Wineland et al. *Quantum information processing with trapped ions*, arXiv:quant-ph/0212089v2, (2003)
- [11] M. D. Barrett, B. DeMarco, T. Schaetz, D. Leibfried, J. Britton, J. Chiaverini, W. M. Itano, B. Jelenkovic, J.D. Jost, C. Langer, T. Rosenband, D. J. Weinland, *Sympathetic cooling of ${}^9Be^+$ and ${}^{24}Mg^+$ for quantum logic*, arXiv:quant-ph/0307088v1, (2008)
- [12] J. I. Cirac, P. Zoller, *Quantum Computations with Cold Trapped Ions*, Phys. Rev. Lett. 77, 71, (1994)
- [13] J.F. Poaytos, J. I. Cirac, P. Zoller, *Quantum Gates with “Hot” Trapped Ions*, Phys. Rev. Lett. 81, (1998)
- [14] K. Mølmer, A. Sørensen, *Multiparticle Entanglement of Hot Trapped Ions*, Phys. Rev. Lett. 82, 1835, (1999)
- [15] A. Sørensen, K. Mølmer, *Quantum Computation with Ions in Thermal Motion*, Phys. Rev. Lett. 82, 1971, (1999)
- [16] A. Sørensen, K. Mølmer, *Entanglement and quantum computation with ions in thermal motion*, Phys. Rev. Lett. A, Volume 62, (2000)
- [17] D. Leibfried et al., *Experimental demonstration of a robust, high-fidelity geometric two ion-qubit phase gate*, Nature, Vol. 422, (2003)
- [18] K. Kim et al. *Geometric phase gate on an optical transition for ion trap quantum computation*, Phys. Rev. A 77, (2008)
- [19] P J Lee et al, *Phase control of trapped ion quantum gates*, IOPscience, J. Opt. B: Quantum Semiclass. Opt. 7 S371, (2005)
- [20] T.R. Tan, J. P. Gaebler, R. Bowler, Y. Lin, J. D. Jost, D. Leibfried[†], and D. J. Wineland, *Demonstration of a dressed-state phase gate for trapped ions*, arXiv:1301.3786v1, (2013)

BIBLIOGRAPHY

- [21] M. A. Nielsen, I. L. Chuang, *Quantum Computation and Quantum Information*, Cambridge University Press, (2001)
- [22] *Elementary gates for quantum computation*, Phys. Rev. A, Volume 52, Number 5, (1995)
- [23] *Realization of a programmable two-qubit quantum processor* D. Hanneke, J.P. Home, J.D. Jost, J.M. Amini, D. Leibfried and D. J. Wineland, Nature Physics, Vol 6, (2010)
- [24] Peter Selinger, *Quantum circuits of T-depth one*, arXiv:12010.0974v1, (2012)
- [25] V.V. Shende, S. S. Bullock, I. L. Markov, *Synthesis of Quantum Logic Circuits*, arXiv:quant-ph/0406176v5, (2006)
- [26] P. Skrzypczyk, A. J. Short, S. Popescu, *Extracting work from quantum systems*, arXiv:1302.2811v1, (2013)
- [27] Lidia del Rio, Johan Åberg, Renato Renner, Oscar Dahlsten and Vlatko Vedral, *The thermodynamic meaning of negative entropy*, Nature 474, 61-63, (02 June 2011)
- [28] Nicolas Brunner, Noah Linden, Sandu Popescu and Paul Skrzypczyk, *Virtual qubits, virtual temperatures, and the foundations of thermodynamics*, Phys. Rev. E, 85:051117, (May 2012)